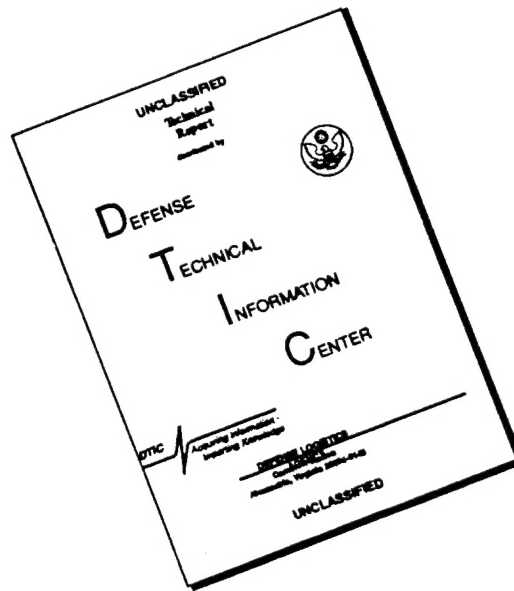




# DISCLAIMER NOTICE



THIS DOCUMENT IS BEST QUALITY AVAILABLE. THE COPY FURNISHED TO DTIC CONTAINED A SIGNIFICANT NUMBER OF PAGES WHICH DO NOT REPRODUCE LEGIBLY.

## GENERAL INSTRUCTIONS FOR COMPLETING SF 298

The Report Documentation Page (RDP) is used in announcing and cataloging reports. It is important that this information be consistent with the rest of the report, particularly the cover and title page. Instructions for filling in each block of the form follow. It is important to *stay within the lines* to meet *optical scanning requirements*.

**Block 1. Agency Use Only (Leave blank).**

**Block 2. Report Date.** Full publication date including day, month, and year, if available (e.g. 1 Jan 88). Must cite at least the year.

**Block 3. Type of Report and Dates Covered.** State whether report is interim, final, etc. If applicable, enter inclusive report dates (e.g. 10 Jun 87 - 30 Jun 88).

**Block 4. Title and Subtitle.** A title is taken from the part of the report that provides the most meaningful and complete information. When a report is prepared in more than one volume, repeat the primary title, add volume number, and include subtitle for the specific volume. On classified documents enter the title classification in parentheses.

**Block 5. Funding Numbers.** To include contract and grant numbers; may include program element number(s), project number(s), task number(s), and work unit number(s). Use the following labels:

<b>C</b> - Contract	<b>PR</b> - Project
<b>G</b> - Grant	<b>TA</b> - Task
<b>PE</b> - Program Element	<b>WU</b> - Work Unit Accession No.

**Block 6. Author(s).** Name(s) of person(s) responsible for writing the report, performing the research, or credited with the content of the report. If editor or compiler, this should follow the name(s).

**Block 7. Performing Organization Name(s) and Address(es).** Self-explanatory.

**Block 8. Performing Organization Report Number.** Enter the unique alphanumeric report number(s) assigned by the organization performing the report.

**Block 9. Sponsoring/Monitoring Agency Name(s) and Address(es).** Self-explanatory.

**Block 10. Sponsoring/Monitoring Agency Report Number.** (If known)

**Block 11. Supplementary Notes.** Enter information not included elsewhere such as: Prepared in cooperation with...; Trans. of...; To be published in.... When a report is revised, include a statement whether the new report supersedes or supplements the older report.

**Block 12a. Distribution/Availability Statement.** Denotes public availability or limitations. Cite any availability to the public. Enter additional limitations or special markings in all capitals (e.g. NOFORN, REL, ITAR).

**DOD** - See DoDD 5230.24, "Distribution Statements on Technical Documents."

**DOE** - See authorities.

**NASA** - See Handbook NHB 2200.2.

**NTIS** - Leave blank.

**Block 12b. Distribution Code.**

**DOD** - Leave blank.

**DOE** - Enter DOE distribution categories from the Standard Distribution for Unclassified Scientific and Technical Reports.

**NASA** - Leave blank.

**NTIS** - Leave blank.

**Block 13. Abstract.** Include a brief (*Maximum 200 words*) factual summary of the most significant information contained in the report.

**Block 14. Subject Terms.** Keywords or phrases identifying major subjects in the report.

**Block 15. Number of Pages.** Enter the total number of pages.

**Block 16. Price Code.** Enter appropriate price code (*NTIS only*).

**Blocks 17. - 19. Security Classifications.** Self-explanatory. Enter U.S. Security Classification in accordance with U.S. Security Regulations (i.e., UNCLASSIFIED). If form contains classified information, stamp classification on the top and bottom of the page.

**Block 20. Limitation of Abstract.** This block must be completed to assign a limitation to the abstract. Enter either UL (unlimited) or SAR (same as report). An entry in this block is necessary if the abstract is to be limited. If blank, the abstract is assumed to be unlimited.

# **PRELIMINARY PERFORMANCE CHARACTERIZATION OF A HIGH-CURRENT Cs-Ba TACITRON\***

Douglas Brent Morris, Captain, United States Air Force

M.S., Nuclear Engineering, University of New Mexico, 1996

Preliminary performance characterization of a high-current Cs-Ba tacitron has been completed. Characterization includes analysis of the effects of emitter temperature, cesium reservoir pressure, and barium reservoir pressure on the I-V performance of the device. In particular, these operating parameters' effects on the forward voltage drop and maximum conduction current are presented in detail. Preliminary grid-controlled modulation and voltage hold-off capabilities are also outlined.

Analysis shows that the high-current Cs-Ba tacitron performs similar to previously tested cylindrical and planar Cs-Ba tacitrons. Current densities of nearly  $10 \text{ A/cm}^2$  were consistently achieved with forward voltage drops of less than 2 V at conduction currents of greater than 250 A. Preliminary modulation data (low collector bias limited) show modulation frequencies of up to 12 kHz at current densities of about  $3 \text{ A/cm}^2$ , voltage drops of less than 5 V, and conduction currents of up to 80 A. The device has demonstrated preliminary voltage hold-off of greater than approximately 125 V (power supply limited). These preliminary operating characteristics in conjunction with the tacitron's inherent tolerance of temperature and radiation make it a potential switching mechanism for not only space nuclear power applications, but for other terrestrial high-temperature and/or high radiation applications.

---

\* Total thesis length is 100 pages.

## REFERENCES

- Alcock, C.B., V.P. Itkin, and M.K. Horrigan (1984), "*Vapor Pressure Equations for the Metallic Elements*," Canadian Metallurgical Quarterly, **23**, No. 3, 309-313.
- Ambrus, J. W. Wright, and D. Bunch (1984), "*Review of the Tri-Agency Space Nuclear Reactor Power System Technology Program*," 19th Intersociety Energy Conversion Engineering Conference.
- Angelo, J.A. and D. Buden (1985), *Space Nuclear Power*, Orbit Book Co., Malabar, FL.
- Baksht, F.G., V.B. Kaplan, A.A. Koskin, A.M. Martsinovskii, F.N. Rasulov, N.N. Sveshnikova, V.I. Serbin, and V.G. Yur'ev (1978a), "*Stationary Conducting State of A Grid-Controlled Switching Element: I*," Sov. Phys. Tech. Phys., **23**, 1301.
- Baksht, F.G., V.B. Kaplan, A.A. Koskin, A.M. Martsinovskii, F.N. Rasulov, N.N. Sveshnikova, V.I. Serbin, and V.G. Yur'ev (1978b), "*Stationary Conducting State of A Grid-Controlled Switching Element: II*," Sov. Phys. Tech. Phys., **23**, 1308.
- Baksht, F.G., G.A. Dyuzhev, A.M. Martsinovskii, B.Ya. Moyzhes, G.Ye. Pikus, E.B. Sonin, V.G. Yur'ev (1978c), *Thermionic Converters and Low-Temperature Plasmas*, English edition edited by L.K. Hansen, Rasor Associates, Inc., Published by Technical Information Center/U.S. Department of Energy.
- Booz-Allen & Hamilton, Inc. (1995), "*TOPAZ International Program: Lessons Learned in Technology Cooperation With Russia*," produced, designed, & researched under BMDO Contract #SDI1084-93-C-0010, Stephenson Printing, Springfield, VA.
- Burkes, T.R. (1987), "*A Critical Analysis and Assessment of High Power Switches: 1987*," Final Report for subcontract DAAK21-82-C-0011, submitted to Naval Surface Weapons Center, Dahlgren, VA 22448-5000.
- Chen, F.F. (1984), *Introduction to Plasma Physics and Controlled Fusion*, Plenum Press, New York, NY.
- Child, C.D. (1911), "*Discharge from Hot CaO*," Physical Review, **32**, 492.
- Cobine, J.D. (1958), *Gaseous Conductors: Theory and Engineering Applications*, Dover Publications, Inc., New York.
- Djachiachvili, I. and M.S. El-Genk (1994), "*Investigation of Triangular Aperture Grid for Plasma Switch Devices*," 21st International Power Modulation Symposium, June 28-30, Costa Mesa, CA, 1994.

Pirrie, C.A., P.D. Culling, H. Menown, and N.S. Nicholls (1988), "*Performance of a Compact Four Gap Thyatron in a High Voltage Repetition Rate Circuit*," IEEE Power Modulation Symposium, Hilton Head Island, SC, 141.

PL/VTPP (1995), "*Space Power System Component Testing: High-Current Tacitron Characterization*," SubTask Statement 09/00, Contract #F29601-94-C-0139, Phillips Laboratory Space & Missiles Technology Directorate, Power and Thermal Management Division (PL/VTP), Kirtland AFB, NM.

Preece, W.H. (1885), "*On Peculiar Behavior of Glow-Lamps When Raised to High Incandescence*," Proc. Roy. Soc. (London), Ser. A, **38**, 219.

Prince, D.C. (1925), "*The Inverter*," General Electric Review, **28**, 676.

Sarjeant, W.J. and R.E. Dollinger (1989), *High-Power Electronics*, TAB Professional and Reference Books, Blue Ridge Summit, PA.

U.S. Congress (1986), "*Space Nuclear Power, Conversion, and Energy Storage for the Nineties and Beyond*," Hearings Before the Subcommittee on Energy Research and Production of the Committee on Science and Technology, U.S. House of Representatives, Ninety-Ninth Congress, First Session, Government Publications Office, Washington, D.C..

Wernsman, B. and M.S. El-Genk (1996), Private Communication on "Cs-Ba Tacitron: Effects of Control Grid Design on Tube Switching Performance," Final Draft Report of work sponsored by the Ballistic Missile Defense Organization, the U.S. Air Force Phillips Laboratory, and the Department of Energy's University Research Program under research contracts #F29601-C-91-0031 and #DEFG02-92ER75708, respectfully (*To be published as an U.S. Air Force Phillips Laboratory Technical Report*).

Wernsman, B. and M.S. El-Genk (1994), "*Operation Characteristics of a Planar Cs-Ba Tacitron*," *Review of Scientific Instruments*, April 1994.

- Dvornikov, V.D., S.T. Latushkin, V.A. Krestov, L.M. Tikhomirov, and L.I. Yudin (1972), "*Powerful Tacitrons and Certain of Their Characteristics in the Nanosecond Range*," (Translated from Priory I Tekhnika Eksperimenta, No. 4, 108), Plenum Publishing Corporation, New York, NY (1973).
- Dvornikov, V.D., S.T. Latushkin, L.I. Yudin, and V.M. Komarov (1974), "*A Pulse Generator Based on Tacitrons*," (Translated from Priory I Tekhnika Eksperimenta, No. 2, 107), Plenum Publishing Corporation, New York, NY (1975).
- El-Genk, M.S., C.S. Murray, and S. Chaudhuri of ISNPS; V. Kaibyshev, A. Borovskikh, I. Djachiachvili, and Y. Taldonov of KIAE (1991), "*Experimental Evaluation of Cs-Ba Thermionic Switch/Inverter -- Tacitron*," Proceedings of the IECEC, Boston, MA, 4-9 August.
- El-Genk, M.S., B. Wernsman, and J. Luke (1994), "*Recent Advances In Cs-Ba Tacitron Technology*," University of New Mexico, NM.
- Fry, T.C. (1921), "*The Thermionic Current Between Parallel Plane Electrodes: Velocities of Emission Distributed According to Maxwell's Law*," Physical Review, **17**, 441.
- Goldberg, S. & J. Rothstein (1961), "*Hydrogen Thyatrons*," Advance in Electronics and Electron Physics, **14**, Academic Press.
- Hatsopoulos, G.N. and E.P. Gyftopoulos (1973), *Thermionic Energy Conversion-Volume 1: Processes and Devices*, MIT Press, Boston, MA.
- Henderson, B.W. (1992), "*Tacitron Research Upgrades Under Way*," Aviation Week and Space Technology, **136**, No. 20, p. 26.
- Hemenway, C.L. R.W. Henry, and M. Caulton (1962), *Physical Electronics*, John Wiley & Sons, Inc., New York.
- Hull, A.W. (1929), "*Hot-Emitter Thyatrons*," General Electric Review, **32**, 213.
- Johnson, E.O. (1951), "*Controllable Gas Diode*," Electronics, 107.
- Johnson, E.O. & W.M. Webster (1952), "*The Plasmatron, A Continuously Controllable Gas-Discharge Developmental Tube*," Proc. Inst. Rad. Eng., 645.
- Johnson, E.O., J. Olmstead, and W.M. Webster (1954), "*The Tacitron, A Low-Noise Thyatron Capable of Current Interruption by Grid Action*," Proc. Inst. Rad. Eng., 1350.
- Kaibyshev, V.Z., G.A. Kuzin, and M.V. Mel'nikov (1972), "*Use of the Thermionic Converter for Regulation of Current in Electric Circuits*," Sov. Phys. Tech. Phys., **17**, 1006.

- Kaibyshev, V.Z. and G.A. Kuzin (1975) "*Effect of a Third Electrode on a Low-Voltage Arc*," Sov. Phys. Tech. Phys., **20**, 203.
- Kaplan, V.B., A.N. Makarov, A.M. Martsinovskii, A.V. Novikov, V.I. Serbin, B.I. Tsirkel, and V.G. Yur'ev (1977a), "*Novel Low-Voltage High-Temperature Switching Element for DC-to-AC Conversion I: Effect of Grid on a Low-Voltage Cesium Arc*," Sov. Phys. Tech. Phys., **22**, 159.
- Kaplan, V.B., A.N. Makarov, A.M. Martsinovskii, A.V. Novikov, V.I. Serbin, B.I. Tsirkel, and V.G. Yur'ev (1977b), "*Novel Low-Voltage High-Temperature Switching Element for DC-to-AC Conversion II: Kinetics of the Quenching of the Discharge and Modulation in a Three-Electrode System*," Sov. Phys. Tech. Phys., **22**, 166.
- Kaplan, V.B., A.M. Martsinovskii, A.S. Mustafaev, V.I. Sitnov, A.Ya. Ender, and V.G. Yur'ev (1979), "*Spontaneous Current Cutoff in a High-Current Low Pressure Cesium -Barium Discharge*," Sov. Phys. Tech. Phys., **24**, 325.
- King, R.W. (1923), "*Thermionic Vacuum Tubes and Their Applications*," Bell System Technical Journal, **1**, 31.
- Langmuir, I. (1913), "*The Effect of Space Charge and Residual Gases on Thermionic Currents in High Vacuum*," Physical Review (2), **2**, 450.
- Luke, J.R. (1994), "*A Transient Model of a Cesium -Barium Diode*," Masters Thesis, Chemical & Nuclear Engineering Department of the University of New Mexico, Albuquerque, NM.
- Masten, G.B., I. Djachiachvili, D.B. Morris, and J.M. Gahl (1995a), "*Operating Characteristics of a High-Current Demountable Cs-Ba Tacitron*," 10th IEEE Pulsed Power Conference, Albuquerque, NM, 10-13 July, 1995.
- Masten, G.B., I. Djachiachvili, D.B. Morris, and J.M. Gahl (1995b), "*Preliminary Performance Results of a High-Current Cs-Ba Tacitron in a Simple Inverter*," 10th IEEE Pulsed Power Conference, Albuquerque, NM, 10-13 July, 1995.
- Murray, C.S. and M.S. El-Genk (1993), "*Experimental and Theoretical Studies of a High-Temperature Cesium-Barium Tacitron, with Application to Low Voltage-High Current Inversion*," Dissertation and Final Report No. UNM-ISONPS-1-1994, Institute for Space & Nuclear Power Studies, University of New Mexico, NM.
- ORION (1994), "*Development of High-Current Discharge Gas-Emission Additive Tacitron Power Conditioning Unit*," Task Area II of Subcontract S94-013, ORION International Technologies, Albuquerque, NM.

Douglas Brent Morris

Candidate

Chemical and Nuclear Engineering

Department

This thesis is approved, and it is acceptable in quality  
and form for publication on microfilm:

Approved by the Thesis Committee:

[Signature], Chairperson

[Signature]

[Signature]

[Signature]

Accepted:

[Signature]

Dean, Graduate School

APR 22 1996

Date

**PRELIMINARY PERFORMANCE CHARACTERIZATION  
OF A HIGH-CURRENT Cs-Ba TACITRON**

*D. Brent Morris*

**ABSTRACT OF THESIS**

Submitted in Partial Fulfillment of the  
Requirements for the Degree of

*Master of Science in Nuclear Engineering*

The University of New Mexico  
Albuquerque, New Mexico

*May 1996*

## **DEDICATION**

For my wife, Natalie, and my boys, Tarren and Conrey.

## ACKNOWLEDGMENTS

I would like to thank my thesis advisor, Dr. Norm Roderick, and committee members; Dr. John Gahl, Dr. Mohammed El-Genk, and Dr. Gordon Masten for allowing me the opportunity to research this area. The work has been interesting and a great challenge for me, both in the lab and on the word processor and I appreciate their time and input.

I would like to especially thank my good friend and mentor, Dr. Gordon Masten, for his tireless patience and seemingly endless consultation. He helped motivate me to perform the work, guided me while doing so, and educated me through his expertise on anything and everything. During much of his tutelage, he was between jobs and provided his time to me most charitably.

Thanks to the personnel of the U.S. Air Force Phillips Laboratory, Space and Missiles Technology Directorate, Power and Thermal Management Division (PL/VTP) for allowing me to conduct this research in their laboratory facility. Also, thanks to John Merrill and Matt Clark of ORION International Technologies Inc. for their support.

I would also like to thank Ben Wernsman and Jim Luke of the Institute for Space and Nuclear Power Studies at the University of New Mexico for providing their insight on tacitron operation and performance expectations. In addition, Iouri Djachiachvili donated several days of his time to assist me in operating the grid driver he built as part of the original high-current tacitron characterization effort. Without him, the modulation data reported herein may not have been completely collected or understood.

Thanks to the U.S. Air Force Academy and the Air Force Institute of Technology for their sponsorship of my graduate studies at the University of New Mexico. In particular, thanks to Maj Jeff McHarg, Director of Physics Research at the Air Force Academy, for providing essential components on a moment's notice.

Finally, and most importantly, I would like to thank my wife, Natalie, for giving me the support I needed to complete this project. Her understanding and patience was soothing and helped steer me to a successful completion. She, more than anyone, has helped me to overcome the obstacles and barriers I have encountered in this project, as she does everyday in my life.

**PRELIMINARY PERFORMANCE CHARACTERIZATION  
OF A HIGH-CURRENT Cs-Ba TACITRON**

*D. Brent Morris*

*B.S.E., Nuclear Science in Engineering, Arizona State University, 1990*

**THESIS**

Submitted in Partial Fulfillment of the  
Requirements for the Degree of

*Master of Science in Nuclear Engineering*

The University of New Mexico  
Albuquerque, New Mexico

*May 1996*

## **PRELIMINARY PERFORMANCE CHARACTERIZATION OF A HIGH-CURRENT Cs-Ba TACITRON**

D. Brent Morris

B.S.E., Nuclear Science in Engineering, Arizona State University, 1990

M.S., Nuclear Engineering, University of New Mexico, 1996

Preliminary performance characterization of a high-current Cs-Ba tacitron has been completed. Characterization includes analysis of the effects of emitter temperature, cesium reservoir pressure, and barium reservoir pressure on the I-V performance of the device. In particular, these operating parameters' effects on the forward voltage drop and maximum conduction current are presented in detail. Preliminary grid-controlled modulation and voltage hold-off capabilities are also outlined.

Analysis shows that the high-current Cs-Ba tacitron performs similar to previously tested cylindrical and planar Cs-Ba tacitrons. Current densities of nearly  $10 \text{ A/cm}^2$  were consistently achieved with forward voltage drops of less than 2 V at conduction currents of greater than 250 A. Preliminary modulation data (low collector bias limited) show modulation frequencies of up to 12 kHz at current densities of about  $3 \text{ A/cm}^2$ , voltage drops of less than 5 V, and conduction currents of up to 80 A. The device has demonstrated preliminary voltage hold-off of greater than approximately 125 V (power supply limited). These preliminary operating characteristics in conjunction with the tacitron's inherent tolerance of temperature and radiation make it a potential switching mechanism for not only space nuclear power applications, but for other terrestrial high-temperature and/or high radiation applications.

## TABLE OF CONTENTS

LIST OF FIGURES .....	xi
LIST OF TABLES .....	xiii
LIST OF ACRONYMS .....	xiv
1. INTRODUCTION.....	1
2. OBJECTIVE .....	6
3. LITERATURE SURVEY - SWITCHING ELEMENTS.....	8
3.1 Introduction.....	8
3.2 Thermionic Emission.....	8
3.3 Thermionic Vacuum Tubes .....	11
3.3.1 Conduction Current.....	11
3.3.2 Operating Characteristics .....	14
3.3.3 Applications .....	15
3.3.4 Summary.....	16
3.4 Thyratrons .....	16
3.4.1 Operating Characteristics .....	18
3.4.2 Applications .....	19
3.4.3 Summary.....	19
3.5 Plasmotrons .....	20
3.5.1 Operating Characteristics .....	20
3.5.2 Applications .....	22
3.5.3 Summary.....	23

3.6 Tacitrons.....	23
3.6.1 Hydrogen Tacitron.....	23
3.6.1.1 Applications.....	25
3.6.1.2 Summary.....	25
3.6.2 Cs Tacitron.....	26
3.6.2.1 Applications.....	28
3.6.2.2 Summary.....	29
3.6.3 Cs-Ba Tacitron.....	29
3.6.3.1 Recent Work.....	32
3.6.3.2 Applications.....	34
3.6.3.3 Summary.....	34
4. HIGH-CURRENT CESIUM-BARIUM TACITRON.....	37
4.1 Test Facility Description.....	37
4.1.1 Vacuum System.....	37
4.1.2 Control Rack.....	40
4.1.3 Data Acquisition and Control System.....	40
4.1.4 Instrumentation.....	43
4.1.5 Cs and Ba Reservoirs.....	43
4.1.6 Power Racks.....	45
4.1.7 High Current Cs-Ba Tacitron (Masten et al. 1995a, b).....	47
4.2 Operational Characteristics.....	53
4.2.1 Experimental Procedures.....	53

4.2.2 Forward Voltage Drop .....	55
4.2.2.1 Effect of Emitter Temperature .....	55
4.2.2.2 Effect of Cs Pressure .....	60
4.2.2.3 Effect of Ba Pressure .....	61
4.2.2.4 Effect of the Grid .....	65
4.2.2.5 High-Current Devices Comparison .....	66
4.2.2.6 Optimal Performance Parameters .....	67
4.2.3 Current Modulation .....	70
4.2.3.1 Extinguishing .....	70
4.2.3.2 Modulation Performance .....	71
4.2.4 Voltage Hold-Off .....	78
5. SUMMARY AND CONCLUSIONS .....	81
6. FUTURE WORK .....	86
7. REFERENCES .....	88
APPENDIX A - Cesium and Barium Vapor Pressures in the Reservoir and Gap .....	92
APPENDIX B - Approximate Tacitron Circuit Design Parameters .....	96
APPENDIX C - Tacitron and Thyatron Switching Efficiencies .....	98

## LIST OF FIGURES

Figure 3.1.	Essential Components (Inside Dashed Box) and Processes of a Thermionic Converter. <i>Adapted from Hatsopoulos &amp; Gyftopoulos (1973).</i>	10
Figure 3.2.	Illustration of a Typical Vacuum Tube ( $V \sim$ Applied Filament Voltage).	12
Figure 3.3.	Basic Thyatron Configuration. <i>Adapted from Goldberg &amp; Rothstein (1961).</i>	17
Figure 3.4.	Plasmatron Circuit Arrangement for Triode Operation. <i>Adapted from Johnson &amp; Webster (1952).</i>	21
Figure 3.5.	Dependence of Emission Current Density on Electrode Temperature.	31
Figure 3.6.	Cylindrical Cs-Ba Tacitron ( <i>Murray &amp; El-Genk 1993</i> ).	35
Figure 3.7.	Planar Cs-Ba Tacitron ( <i>Wernsman &amp; El-Genk 1996</i> ).	36
Figure 4.1.	Photograph of the High-Current Cs-Ba Tacitron Facility ( <i>From Left to Right: Data Acquisition System, Control Rack, Vacuum Stand, Power Rack 1, and Power Rack 2.</i> )	38
Figure 4.2.	Vacuum Chamber Feedthrough Designations.	39
Figure 4.3.	'Main Menu' Screen of Data Acquisition & Control System.	42
Figure 4.4.	External Cs Pipeline & Reservoirs with Thermocouples.	44
Figure 4.5.	Photograph of the High-Current Cs-Ba Tacitron.	49
Figure 4.6.	Schematic of the High-Current Cs-Ba Tacitron.	50
Figure 4.7.	Photograph of the tungsten emitter heater assembly.	51
Figure 4.8.	Photograph of Components of the High-Current Cs-Ba Tacitron ( <i>From Left to Right: Emitter Heater, Emitter Cup, Grid, and Collector</i> ).	51
Figure 4.9.	Hexagonal Grid Geometry of the High-Current Cs-Ba Tacitron.	52
Figure 4.10.	Effect of Emitter Temperature on the Forward Voltage Drop, $V_{CE}$ , for Device 1 at $T_{Cs} = 155^\circ\text{C}$ ( $P_{Cs} = 11\text{ mTorr}$ ), $T_{Ba} = 575^\circ\text{C}$ ( $P_{Ba} = 1.4\text{ mTorr}$ ) ( <i>Data sweeps are h110114, h100329, and h110127 for curves 1, 2, and 3, respectively.</i> )	57

Figure 4.11. Effect of Emitter Temperature on the Forward Voltage Drop, $V_{CE}$ , for Device 2 at $T_{Cs} = 130\text{ }^{\circ}\text{C}$ ( $P_{Cs} = 3.1\text{ mTorr}$ ), $T_{Ba} = 600\text{ }^{\circ}\text{C}$ ( $P_{Ba} = 2.9\text{ mTorr}$ ) (Data sweeps are h103056, h103053, and h110133 for curves 1, 2, and 3, respectfully.).	58
Figure 4.12. Effect of Cesium Pressure on the Forward Voltage Drop, $V_{CE}$ , for Device 2 at $T_E = 1050\text{ }^{\circ}\text{C}$ , $T_{Ba} = 600\text{ }^{\circ}\text{C}$ ( $P_{Ba} = 2.9\text{ mTorr}$ ) (Data sweeps are h103056, h110119, and h103019 for curves 1, 2, and 3, respectfully.).	63
Figure 4.13. Effect of Barium Pressure on the Forward Voltage Drop, $V_{CE}$ , for Device 2 at $T_E = 1250\text{ }^{\circ}\text{C}$ , $T_{Cs} = 130\text{ }^{\circ}\text{C}$ ( $P_{Cs} = 3.1\text{ mTorr}$ ) (Data sweeps are h110140, h110133, and h103044 for curves 1, 2, and 3, respectfully.).	64
Figure 4.14. Average Forward Voltage Drop and Ignition Voltages for the High-Current Cs-Ba Tacitrons as Diodes Over Experiment Duration (Each Device Under Identical Conditions.).	68
Figure 4.15. Optimal I-V Performance of the High-Current Cs-Ba Tacitrons as Diodes (Data sweeps are h110127 for Device 1 & h103029 for Device 2.).	69
Figure 4.16. Modulation Test 1108-005 of the High-Current Cs-Ba Tacitron (Grid (Fine) and Collector (Bold) Voltage Waveforms are at the Top of the Figure, While Grid (Fine) and Collector (Bold) Current Waveforms are at the Bottom.).	74
Figure 4.17. Modulation Test 1108-006 of the High-Current Cs-Ba Tacitron (Grid (Fine) and Collector (Bold) Voltage Waveforms are at the Top of the Figure, While Grid (Fine) and Collector (Bold) Current Waveforms are at the Bottom.).	75
Figure 4.18. Modulation Test 1117-010 of the High-Current Cs-Ba Tacitron (Grid (Fine) and Collector (Bold) Voltage Waveforms are at the Top of the Figure, While Grid (Fine) and Collector (Bold) Current Waveforms are at the Bottom.).	76
Figure 4.19. Modulation Test 1117-012 of the High-Current Cs-Ba Tacitron (Grid (Fine) and Collector (Bold) Voltage Waveforms are at the Top of the Figure, While Grid (Fine) and Collector (Bold) Current Waveforms are at the Bottom.).	77
Figure 4.20. Preliminary Voltage Hold-Off Measurements of the High-Current Cs-Ba Tacitron (Applied Pulses are 88 V (Fine) and 125 V (Bold) Peak Amplitude).	80

## LIST OF TABLES

Table 3-1	First Ionization Potentials of Gases Used in Grid-Controlled Switches .....	26
Table 4-1	Heater Operation Sequence and Current Limits .....	46
Table 4-2	System Operating Temperatures .....	53
Table 4-3	Effects of Emitter Temperature on Device 1 at $T_{Cs} = 155\text{ }^{\circ}\text{C}$ ( $P_{Cs} = 11$ mTorr) and $T_{Ba} = 575\text{ }^{\circ}\text{C}$ ( $P_{Ba} = 1.4$ mTorr) .....	59
Table 4-4	Effects of Emitter Temperature on Device 2 at $T_{Cs} = 130\text{ }^{\circ}\text{C}$ ( $P_{Cs} = 3.1$ mTorr) and $T_{Ba} = 600\text{ }^{\circ}\text{C}$ ( $P_{Ba} = 2.9$ mTorr) .....	60
Table 4-5	Effects of Barium Pressure on Device 2 at $T_E = 1250\text{ }^{\circ}\text{C}$ and $T_{Cs} = 130\text{ }^{\circ}\text{C}$ ( $P_{Cs} = 3.1$ mTorr) .....	62
Table 4-6	Modulation Parameters From Preliminary Tests of the High-Current Demountable Cs-Ba Tacitron ( <i>Device 1 Only</i> ) .....	72
Table 4-7	Modulation Parameters From Preliminary Tests of the High-Current Demountable Cs-Ba Tacitron .....	73

## LIST OF ACRONYMS

DARPA	Defense Advanced Research Projects Agency
DAS	Data Acquisition and Control System
DoD	Department of Defense
DOE	Department of Energy
ISNPS	Institute for Space and Nuclear Power Studies (Chemical & Nuclear Engineering Department of UNM)
KIAE	Kurchatov Institute of Atomic Energy (Moscow, Russia)
kWe	Kilowatt Electric Power
NASA	National Aeronautics and Space Administration
SCR	Silicon-Controlled Rectifier
SDI	Strategic Defense Initiative
SDIO	Strategic Defense Initiative Organization
SNAP-10A	System for Nuclear Auxiliary Power
TFE	Thermionic Fuel Element
TOPAZ	Thermionic Experiment with Conversion in the Active Zone (Russian)
UNM	University of New Mexico (Albuquerque, NM)
USAFA	United States Air Force Academy (Colorado Springs, CO)
U.S.	United States
PL/VTP	U.S. Air Force Phillips Laboratory, Space & Missiles Technology Directorate, Power & Thermal Management Division (Kirtland AFB, Albuquerque, NM)

## 1. INTRODUCTION

In the United States during the early 1980s, a renewed interest in space power was born because of President Ronald Reagan's Strategic Defense Initiative (SDI). The initiative, to develop a space-based ballistic missile defense, would require large power sources for space use. The Department of Defense (DoD) and the National Aeronautics and Space Administration (NASA) identified space nuclear power (SNP) as a technology that could meet the needs of the president's initiative as well as other future high-powered space missions (U.S. Congress 1986).

A tri-agency organization consisting of the Department of Energy (DOE), NASA, and the Defense Advanced Research Projects Agency (DARPA), was formed in 1983 to develop a 100 kWe SNP source. This program would eventually become known as SP-100 (Ambrus et al. 1984).

During power conversion concept selection for SP-100, thermoelectric energy conversion was chosen. Thermoelectrics involves a direct means of converting thermal energy into electricity by using two different semiconductor materials. If the ends of the materials are kept at different temperatures, then electricity can be produced by the migration of 'holes' and electrons (depending on the material) from the hot end to the cold end of the thermoelectric device. Thermionic power conversion, which was also considered, involved a cathode being heated to the point when electrons are 'boiled off' its surface across a small gap to a cooler collecting anode - another direct means of producing electricity from thermal energy (Angelo & Buden 1985). In-core thermionic conversion was recognized as having great potential for future high-power needs, but was

not selected for SP-100 because of uncertainties in meeting near-term performance and lifetime goals (Booz-Allen & Hamilton 1995). After all, America's only SNAP reactor to be launched into space, the SNAP-10A, employed thermoelectric conversion and little research had been done in the U.S. in thermoelectrics, let alone, thermionic energy conversion, in the twenty-plus years since its launch.

It is believed that thermionic energy conversion has some significant advantages over thermoelectric conversion, mainly in terms of higher conversion efficiencies and high heat rejection temperatures. The Soviet Union realized these advantages of thermionics and began designing, developing, and testing thermionic SNAP systems from the 1960s through the 1980s. The Soviet research was conducted through two separate and simultaneous thermionics programs based on multi-cell and single-cell concepts. Details of the Soviet research in thermionics were unknown to the west until the late 1980s.

The Soviet research culminated in two complete reactor systems. One design employed multi-cell thermionic fuel elements (TFEs). Generally, a TFE consists of a heat source, emitter and collector regions separated by a small interelectrode gap, and cooling supply. The core of the TOPAZ multi-cell reactor, as it came to be called by the Soviets, was made up of many channels of conversion elements. Each channel consisted of several individual TFEs, appearing much as batteries within a hand-held flashlight. The Soviet Union launched two of their multi-cell TOPAZ reactors into space in 1987 (Cosmos 1818 in February 1987 and Cosmos 1867 in July 1987). The multi-cell reactors were designed to produce 5-6 kWe for one year of operational life (Booz-Allen & Hamilton 1995).

The Soviet single-cell reactor core consisted of many single-cell TFE channels. Unlike the multi-cell design, each core channel consisted of just one long conversion element, i.e. TFE. The Soviets performed extensive ground tests on their single-cell thermionic reactors including lifetime nuclear and flight qualification tests, but never launched one. The single-cell reactors were designed to provide 5-6 kWe for an operational lifetime of up to three years. It would be these single-cell reactors that the Russians would offer to sell to the U.S. during the 1989 Space Nuclear Power Symposium in Albuquerque, New Mexico. It was also this offer that spurred great interest by the U.S. to purchase former Soviet space power technology and work with the Russians jointly in pursuing advances in other technological areas (Booz-Allen & Hamilton 1995).

The first purchase of Soviet technology by the U.S. was during the summer of 1989 when the Strategic Defense Initiative Organization (SDIO), negotiated a contract with the Kurchatov Institute of Atomic Energy (KIAE) to acquire a tacitron switch. The KIAE was one of the main organizations involved with the development of the single-cell reactor design, or TOPAZ-II as the U.S. would eventually name it. Tacitrons are high-power thermionic switches that are inherently radiation hard. The tacitron switching element was developed in the U.S. during the 1950s (Johnson et al. 1954), but its developmental use was overcome by the advent of semiconductor switches. The Soviet Union continued their own studies of tacitron technology for a wide range of uses while the U.S. interest in tacitron research waned. One important use the Soviets realized was the use of a tacitron switch in conjunction with a SNP system. A tacitron could be used to convert high-current/low-voltage dc power from a SNP supply to a low-current/high-voltage ac signal.

Because the tacitron is inherently radiation and temperature hard, it can be used in the vicinity of the SNP system to reduce line losses from power source to payload. In addition mission payload mass could be significantly reduced - an important consideration when launching anything into space. The SDIO also realized this potential of the tacitron and saw the acquisition of the Russian tacitron as a precursor to future purchases with the KIAE (Booz-Allen & Hamilton 1995 and Henderson 1992).

Since its acquisition, several Russian tacitrons have been extensively tested at the University of New Mexico's (UNM) Institute for Space and Nuclear Power Studies (ISNPS) and at the U.S. Air Force Phillips Laboratory at Kirtland AFB, NM. Tests have included characterization and optimization of performance and operating parameters, grid aperture and design effects, inverter operation, and switching efficiencies (El-Genk et al. 1994). In 1994, the Phillips Laboratory Space and Missiles Technology Directorate, Power and Thermal Management Division (PL/VTP) contracted with KIAE to develop a high-current tacitron device. Up to this time, all the U.S. research conducted on the Russian tacitron was conducted on low-current devices (less than 50 A). The PL/VTP was interested in developing space power-related technologies for application in U.S. space systems, specifically high-power energy conversion and power management and distribution. Under the contract, the KIAE was to develop two high-current tacitron devices designed to modulate average currents in the range of 100 to 200 A which would be tested at the Phillips Laboratory by PL/VTP and a third-party contractor. The tests planned were current-voltage characterization, modulation performance, and operating characteristics in inverter mode. The intent of the tests was to demonstrate proof-of-

principle power conditioning capability for a 6 kWe direct energy conversion space power source; that is, an equivalent to a TOPAZ-II thermionic SNP system (ORION 1994 & PL/VTPP 1995). Unfortunately, however, program delays and funding cuts prevented the completion of the testing goals to the full extent.

Air Force funding ceased in June 1995 for the high-current tacitron program at the Phillips Laboratory. At that time, the U.S. Air Force Academy (USAFA) requested that PL/VTP allow this graduate student, who's masters program was being sponsored by the USAFA, to continue testing of the high-current tacitron devices in the existing lab space of PL/VTP. It was agreed that testing would continue on the high-current tacitrons until laboratory space was needed for another program. In addition, testing could only be continued with the stipulation that no other PL/VTP resources would be expended for testing except those already in place; such as facility space, existing hardware, and utilities.

## 2. OBJECTIVE

The objectives of this research are to experimentally investigate the operating characteristics of the high-current tacitron devices: each device's performance under various operating parameters of emitter temperature, cesium pressure, and barium pressure is analyzed and compared and the optimal performance characteristics of the high-current tacitron devices are compared to previous tactiron testing results at the ISNPS and the Phillips Laboratory. Performance characterization comparisons of the high-current device and the previously tested Cs-Ba tacitrons should yield some insight into the possibility of tacitron scaling for desired operating regimes.

The effects of emitter temperature, cesium, and barium pressures on the I-V characteristics of the high-current tacitrons are analyzed. Variations in these parameters are used to determine forward voltage drop values, and maximum current densities during tacitron operation as a diode. Preliminary current modulation testing is investigated in order to examine to what extent the high-current tacitron can generate current pulses and at what repetition rates under the extinguishing mode (i.e. fully grid-controlled). In addition, preliminary voltage hold-off characteristics are examined during the breakdown mode. The aim of these objectives is general characterization of the high-current tacitron, its switching potential, and how its performance compares to previous tacitron devices.

Results from operational characteristics testing of the high-current tacitron are compared to characterization data for lower-current tacitron devices tested at the ISNPS and the Air Force Phillips Laboratory. The high-current tacitron can be considered the next generation of Russian tacitron switching elements. Its optimal performance

characteristics, including current density, forward voltage drop, and current modulation are used as a baseline for this comparison.

To understand the premise that the high-current tacitron is indeed suited as a high-power switch for space nuclear power applications, conventional electronic switching devices are also outlined in Chapter 3. The high-current tacitron, its experimental facility, the experimental procedures, and its operational characteristics are described in Chapter 4. Chapter 5 provides a summary and concluding remarks while future work is proposed in Chapter 6.

### 3. LITERATURE SURVEY - SWITCHING ELEMENTS

#### **3.1 Introduction**

The high-current tacitrons characterized in this thesis were developed in order to be used as a prototypic inverter for space-based nuclear power applications. Specifically, the high-current tacitrons were to be used to invert the power produced by a TOPAZ-II, or TOPAZ-II derivative thermionic space nuclear power system. Because there has never been a tacitron built like the high-current tacitron, its potential as a high-power switch for space-based applications can only be measured through extensive characterization testing. The results from testing can then be compared to other electronic switches in order to determine the high-current tacitron's functionality as a switch. Murray and El-Genk (1993) extensively outlined several hot-cathode switching elements and their functionality as space-based switches for nuclear power sources. They concluded that the Cs-Ba tacitron was best suited as part of a power conditioning unit for thermionic space nuclear power systems. Murray and El-Genk (1993) also stated that the operational characteristics of the tacitron are most similar to the plasmatron and thyatron. In order to better understand the operational characteristics of the Cs-Ba high-current tacitron, the operational characteristics of the plasmatron, thyatron, and earlier developed tacitrons will be explored.

#### **3.2 Thermionic Emission**

The electronic devices discussed herein can all be considered derivatives of thermionic converters employing thermionic emission. Thermionic emission is a phenomenon where

upon charged particles 'boil off' a heated metal surface. Discussion of thermionic converters involves two influences of performance characteristics: emission phenomena and transport phenomena. Emission phenomena are related to the processes by which charged particles are emitted from or collected at the electrode surfaces of a thermionic converter. Emission phenomena are dictated by the type of electrode material, thermodynamic properties and crystallographic structure of the surface, and the materials adsorbed to the electrode surface. In general, transport phenomena are analyzed in order to understand their affect on thermionic conversion and how best to reduce their unwanted attributes. Specifically, the accumulated negative space charge effect in the interelectrode gap is the most significant transport phenomenon. The negative space charge is created by electrons in transit between the electrodes as seen in Figure 3.1. The conduction current through the converter can be greatly inhibited unless the electrostatic effects of the negative space charge are reduced (Hatsopoulos & Gyftopoulos 1973).

The method of space charge reduction defines the type of thermionic converter. Vacuum thermionic converters have very small interelectrode gaps in order to reduce the number of electrons in transit between the electrodes; thus, reducing the negative space charge effect. Vapor or gas-filled thermionic converters have a rarefied gas in the interelectrode gap. The negative space charge in these converters is neutralized by positive ions produced through ionization of the vapor. Cesium is the vapor generally used because it has the lowest ionization potential of any element. In a cesiated thermionic converter, cesium is supplied to the interelectrode gap where the vapor is

partially ionized by thermal processes at the emitter surface and partially by means of impact phenomena in the gap (Hatsopoulos & Gyftopoulos 1973).

Another way to produce positive ions is to include a third electrode in the thermionic converter. The third electrode can ionize the vapor through the process of atom adsorption-ion desorption (thermionic emission) from its surface; ion emission from an ion-emitting material coated on the electrode; or by ionizing the vapor through impact by electrons emitted from or collected by the third electrode (Hatsopoulos & Gyftopoulos 1973). However, the first two processes listed above are undesirable in a switch.

It should be noted that throughout this text, when describing the electrodes of thermionic switches, the words cathode and anode can be equivalently replaced with emitter and collector, respectfully, and vice versa.

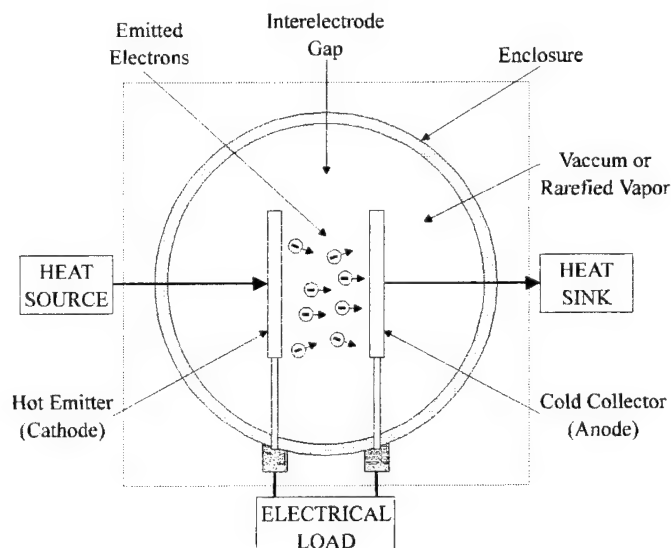


**Figure 3.1. Essential Components (Inside Dashed Box) and Processes of a Thermionic Converter. Adapted from Hatsopoulos & Gyftopoulos (1973).**

### **3.3 Thermionic Vacuum Tubes**

Thomas Edison is credited with discovering thermionic conversion in 1885 by observing that electric current could flow between heated and 'cold' electrodes (Preece 1885). Edison's discovery led to the development of several kinds of thermionic vacuum tubes employing the process of thermionic emission described previously.

A typical vacuum tube is shown in Figure 3.2. Vacuum tubes contain a cathode (emitter) filament, a bent-wire grid and a plate anode (collector). Upon application of a potential to the filament, the cathode heats and emits electrons for the desired current emission. The grid in such vacuum tubes is used to maintain the device in the 'off' mode by retarding the transient electrons. The current emission is retarded by applying a large negative potential on the grid. The full current emission can then be resumed by removing the potential, thus increasing the anode current - the 'on' mode.

#### **3.3.1 Conduction Current**

The electron current emitted from a hot metal surface is dependent on the temperature and the work function of the metal. The work function is related to the affinity of the metal to lose electrons. That is, the work function of a metal is defined as the amount of energy necessary to remove electrons from the surface. The saturated thermionic emission current (in A/cm<sup>2</sup>) can be represented by the Richardson-Dushman equation (Hatsopoulos & Gyftopoulos 1973).

$$J_s = A \cdot T^2 \cdot \exp\left(-\frac{\phi}{kT}\right) \quad (3.1)$$

where,  $A$  is a physical constant equal to  $120 \text{ A/cm}^2\text{-K}^2$ ,  $T$  is the emitter temperature in K,  $\phi$  is the emitter work function in eV, and  $k$  is Boltzmann's Constant ( $k = 8.62 \times 10^{-5} \text{ eV/K}$ ). In an analogous manner, the saturation ion emission current can be found if the metal cathode is in contact with a rarefied vapor:

$$j_s = \frac{e \cdot p_g}{\sqrt{2 \cdot \pi \cdot m_g \cdot k \cdot T_g} \left( 1 + 2 \cdot \exp \left( \frac{V_i - \phi}{kT} \right) \right)} \quad (3.2)$$

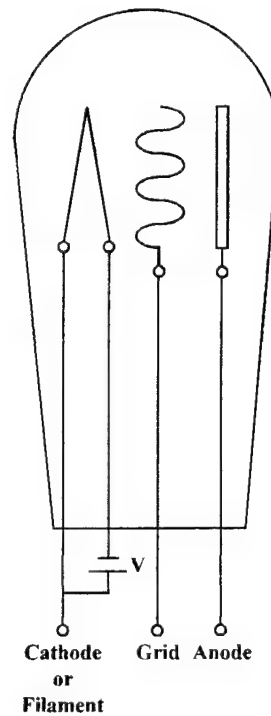


**Figure 3.2.** Illustration of a Typical Vacuum Tube ( $V \sim$  Applied Filament Voltage).

where,  $e$  is the electronic charge ( $e = 1.6021 \times 10^{-19}$  coulomb);  $p_g$ ,  $m_g$ ,  $T_g$ , and  $V_i$  are the pressure, mass, temperature, and first ionization energy, respectfully, of the vapor atoms.

Child (1911) and Langmuir (1913) both independently derived an equation to calculate the conduction current. The equation they derived is known as the “3/2 Power Law” for the amount of current that can be transferred across a distance  $d$  and is given by:

$$j = 2.33 \cdot 10^{-6} \cdot \frac{V^{\frac{3}{2}}}{d^2} \quad (3.3)$$

where  $V$  is the potential between emitter and collector. Murray and El-Genk (1993) give the electron emission current for a sample thermionic tube with a tungsten emitter ( $\phi = 5$  eV) at  $T_E = 1998$  K, as  $0.12 \text{ mA/cm}^2$ . They further state that for an anode voltage of  $V = 500$  V and a spacing of  $d \approx 0.86$  cm at the conditions above the space charge limited conduction current would be  $35.2 \text{ mA/cm}^2$ . In this case the thermionic tube becomes temperature saturated, because charge transport is now limited by the emitter temperature,  $T_E$ . If the emitter work function is reduced by the introduction of oxides on the emitter surface, the emission current density is increased. For example, if the tungsten work function from the example above is decreased to 3.5 eV, then the emission current increases to  $740 \text{ A/cm}^2$  and the tube has reached voltage saturation because charge transport is limited by the emitter-collector potential,  $V$ . For this reason, the amount of conduction current is governed by the voltage hold-off (the maximum anode voltage that can be applied) and the temperature and work function of the emitter.

Langmuir (1913) and Fry (1921) investigated how to increase the conduction current given in Equation (3.3). They found the current could be increased if the emitted electrons had some initial velocity when entering the grid-anode region. The electrons will have an initial velocity in the grid-anode region if the grid is positively biased. In this case, Equation (3.3) may take on a different exponential value. Equation (3.3) assumes the electrons have no initial velocity. Murray and El-Genk (1993) and King (1923) conclude that Equation (3.3) is a good approximation for the conduction current under a wide range of circumstances. For example, if for the same conditions above, a grid potential of +20 V is applied, the conduction current increases to 120 mA from 35.2 mA/cm<sup>2</sup> (Hull 1929).

### **3.3.2 Operating Characteristics**

Early triode thermionic vacuum tubes went by several names, such as the audion, vacuum tube, triode, and plotron, but each operated in similar fashion (King 1923). The conduction current of these tubes could be initiated by removing the negative grid bias. Turn-on time is limited by the time it takes to change from the 'off' mode negative grid bias to the 'on' mode positive grid bias needed to obtain the desired collector current. Similarly, the turn-off time of the device is the time needed to go from positively biasing the grid to negatively biasing the grid. Upon negatively biasing the grid, the flow of electrons from the emitter is retarded in the emitter-grid region. In either case, Murray and El-Genk (1993) state that the turn-on and turn-off times are on the order of tenths of microseconds.

The forward voltage drop, or voltage where conduction begins, for a vacuum tube can be disadvantageously high. Large voltage drops are common for thermionic vacuum tubes

because of the high negative space charge effect associated with operation in vacuum. The forward voltage drop depends greatly on the collector current which limits a tube's current conduction capability. Murray and El-Genk (1993) state that the forward voltage drop in thermionic vacuum tubes can be on the order of 1 kV and this is the reason that vacuum tubes are limited to high voltage applications ( $> 10$  kV) or very low current applications ( $< 1$  mA).

### 3.3.3 Applications

These early devices were used mainly as amplifiers and oscillators and could be used as rectifiers to convert an ac signal into dc. King (1923) states that the thermionic "valve" could be used as a switch:

If the plate circuit of the valve is inserted in a high tension circuit, the flow of current in the circuit may readily be stopped by cutting off the filament heating supply, thus making unnecessary the breaking of any contacts in the high tension circuit. In case the transmission of current in both directions is necessary, two valves may be used.

King also states that DeForest developed the three electrode vacuum tube that used a grid to control the flow of current. This grid control could stop the flow of electrons, thus turning the device off. These are two of the first references that a thermionic converter could be used as a switching element.

In 1925, Prince created an inverter using two thermionic vacuum tubes called pliotrons. Up to this time, dc signals could only be "inverted" to ac by using rotating machines. Each pliotron was supplied with 15 V at a power of approximately 10 kW resulting in a switching efficiency of nearly 90 % with a forward voltage drop of about 1.5 kV.

### **3.3.4 Summary**

The simple devices known as thermionic vacuum tubes are suited for high voltage or low current applications because of their inherent large forward voltage drops. These thermionic tubes employ thermionic emission as their operating process: electrons are boiled off a hot cathode across a gap to an anode. A biased grid (positively or negatively) between cathode and anode is used to turn the device on or off. Thermionic vacuum tubes can be used to invert dc signals to ac signals, but are not functionally applicable for space applications. The forward voltage drop can be decreased by the introduction of a rarefied vapor inside the tube. The vapor becomes ionized and decreases the negative space charge effect, making the forward voltage drop lower. This method was employed in the 1920s in the next generation of thermionic tubes known as thermionic vapor/gas tubes.

### **3.4 Thyratrons**

The thyatron was one of the first commercial thermionic vapor tubes. Under normal operation, when a gas is introduced to a thermionic vacuum tube it is ionized in the gap between the cathode and anode. The ions neutralize the negative space charge effect which increases the conduction current through the tube. As can be seen in Figure 3.3, typical thyratrons are planar in arrangement and have cathode and/or grid baffles placed between the cathode and grid. These baffles serve to avoid a direct 'line-of-sight' path for electrons between the cathode and anode through the grid apertures. If there was no baffle, then occasional stray electrons emitted from the cathode will pass through the grid into the grid-anode region. An electron multiplication 'avalanche' could develop causing an electrical breakdown of the gas within the tube (Sarjeant & Dollinger 1989).

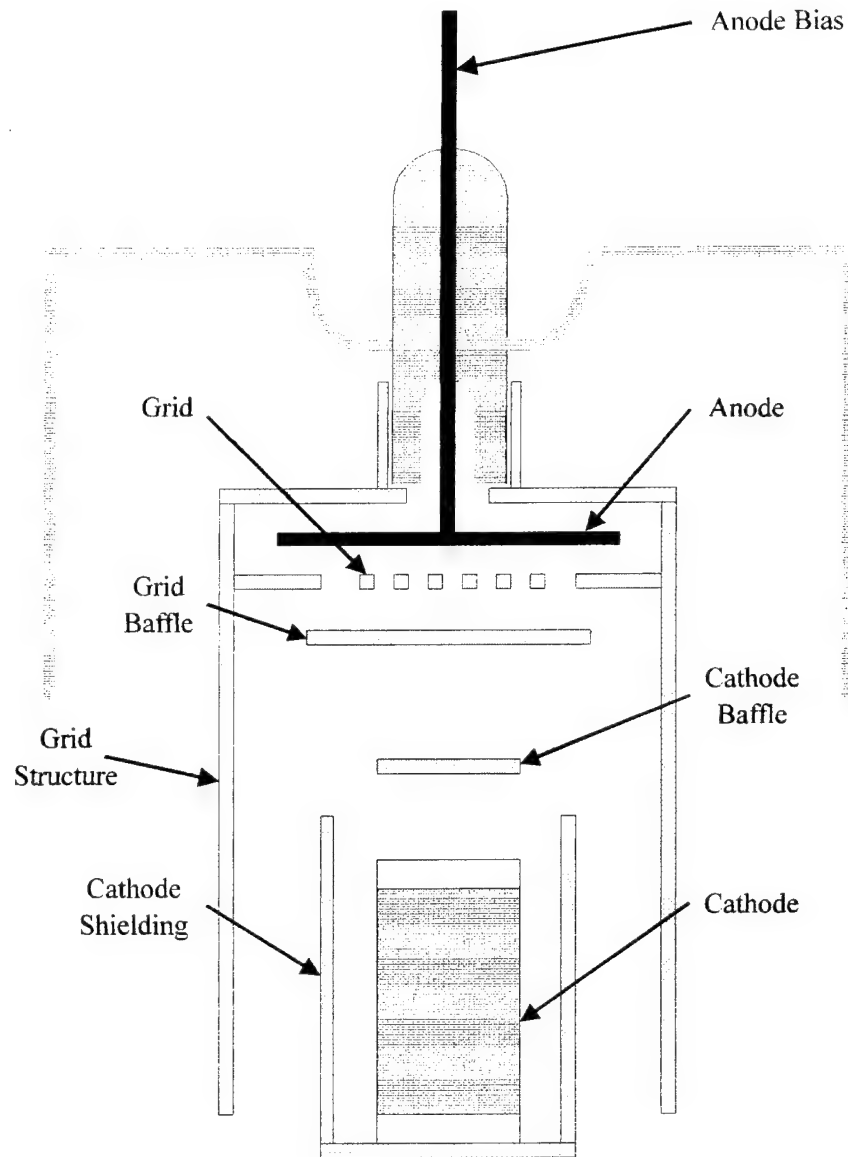


**Figure 3.3. Basic Thyatron Configuration.** *Adapted from Goldberg & Rothstein (1961).*

The baffles also prevent spurious ignitions and allow the tube to hold off voltage at a zero potential, rather than requiring the grid to be maintained at a constant negative bias (Burkes 1987). Spacing of the electrodes is determined by the Paschen breakdown curve for the particular vapor. It was F. Paschen in 1889 that discovered that the 'sparking' (hold-off) voltage is a function of the product of the vapor pressure and electrode separation only. For a device using a gas for the conduction medium, this relationship has come to be known as Paschen's Law (Cobine 1958). The electron collision frequency is lowest on the left side of the breakdown curve, making it unlikely that a random breakdown will occur in the device and reducing grid biasing requirements. Typically, the cathode is placed several mean free paths from the grid at the Paschen minimum (Sarjeant & Dollinger 1989). Murray and El-Genk (1993) give a good derivation of Paschen's Law in addition to the Townsend criterion for breakdown to occur.

Grid apertures in thyratrons are relatively large and gas operating pressures are in the tens of mTorr. At these pressures, for example, a single-gap hydrogen thyatron can generally hold off 40 kV and conduct several kA of pulse current at a forward voltage drop of roughly 100-150 V (Burkes 1987).

#### **3.4.1 Operating Characteristics**

If the thyatron grid is negatively biased, then as in a vacuum tube, the tube is in the off-state. The device is turned on when the grid potential is removed. Otherwise, turning the device on (i.e. ignition) occurs when the cathode temperature is raised to the point where current emission from the cathode is sufficiently high, or by applying a positive bias to the grid. Once ignited, the grid has no influence on the anode conduction current. The

conduction current is only limited by the load impedance and emission ability of the cathode. The grid can no longer control the arc, modulate, limit, or extinguish the current (Murray & El-Genk 1993).

The extinguishing mechanism for this type of thyatron device is the anode bias. Removing the anode bias ceases the discharge. If the anode potential is applied again before ions and electrons recombine to neutralize the plasma (de-ionization), then the plasma may re-ignite. This de-ionization time is the turn-off time of the device. Repeatedly applying and removing the anode bias produces the thyatron's ability to modulate current. Burkes (1987) reports that the plasma recovery process limits the peak pulse rates to about  $10^5$  Hz.

### **3.4.2 Applications**

Predominantly, hydrogen is the gas used in thyatrons because of its benign nature, material compatibility, availability, and high mobility which allows rapid turn-on times. Most recent thyatron designs conduct very high currents ( $> 40$  kA) at high anode potentials ( $> 60$  kV) with current densities ranging from tens to hundreds of amps per square centimeter (Pirrie et al. 1988 and Burkes 1987). This developmental preference has steered the use of thyatrons to high power applications instead of applications with space nuclear power systems.

### **3.4.3 Summary**

Thyatrons are triode gas tubes which are not completely grid-controlled. The grid, depending on the thyatron design, is used either to maintain the device in the off-state

with a negative bias, or to turn the device on with a positive bias. A positive bias serves two purposes: to accelerate the electrons emitted from the cathode and to promote ionization of the plasma. Thyratrons are most applicable to high-voltage and very high power applications.

### **3.5 Plasmatrons**

In the early 1950s, E.O. Johnson and W.M. Webster developed a grid-controlled gas tube called the plasmatron. In this device, a plasma is generated by an auxiliary discharge and not by the anode current itself as is the case in thyratrons. Therefore, the grid can affect continuous control over the anode current (Johnson 1951 and Johnson & Webster 1952). Johnson and Webster (1952) describe the plasmatron as a high-current, low voltage, low-impedance, grid-controlled gas tube. Figure 3.4 is a schematic of a triode plasmatron circuit.

#### **3.5.1 Operating Characteristics**

Johnson and Webster (1952) give two different methods of affecting continuous control over the conduction current. The first method takes into account that the plasma conductivity (and conduction current) is dependent on the plasma density. In the plasmatron, the plasma density is dependent on the intensity of the auxiliary discharge, so conduction current is controlled by the auxiliary discharge creating the plasma.

The second method of affecting continuous conduction current control is by using the grid. During operation, the grid is surrounded by a positive-ion sheath which controls the effective cross-sectional area of the plasma and prevents the tube from realizing its full

current-carrying capability. Johnson and Webster describe the sheath as a region of positive ions transitioning to the grid wire. That is, the plasma is a positive ion emitter and the grid is the collector of those ions.

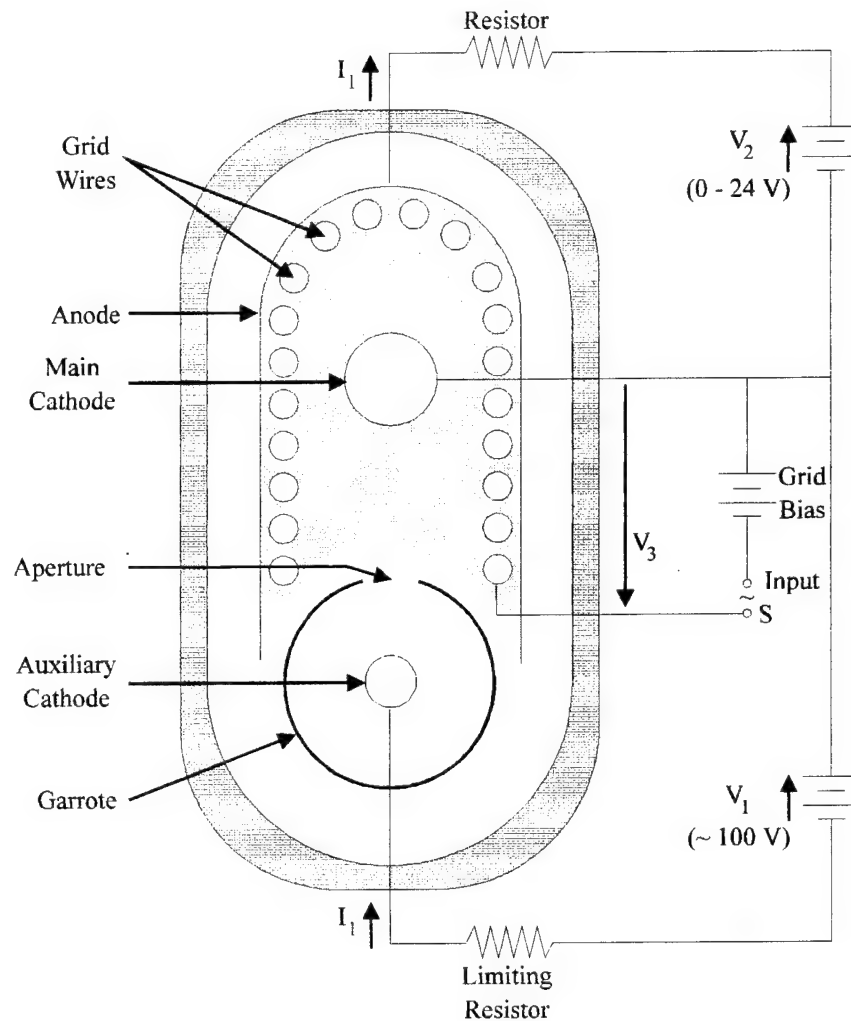


**Figure 3.4. Plasmatron Circuit Arrangement for Triode Operation. Adapted from Johnson & Webster (1952).**

The sheath thickness is a function of ion emission current and the grid voltage according to the "3/2 Power Law" discussed previously. As the negative grid bias voltage is increased, the sheaths around the grid wires grow until they overlap one another creating a barrier against the electrons en route to the anode - the conduction current is extinguished.

The auxiliary discharge in the triode plasmatron is created in the auxiliary cathode region that is surrounded by the garrote shown in Figure 3.4. The garrote aperture funnels and constricts the energy of the discharge electron beam such that ionization occurs in the main cathode-anode region of the tube. Conduction current is increased as the grid negative bias decreases to approximately -2 V, where the device ignites. The forward voltage drop of the device can be very low ( $< 1$  V) for the plasmatron, but additional power is necessary to create the auxiliary discharge. Despite this, the switching efficiency of the plasmatron is very high.

### **3.5.2 Applications**

Johnson and Webster (1952) state that, "... the principle of operation [of the plasmatron] puts no definite restrictions upon the size or geometry of a tube provided the basic features are retained." That is, the plasmatron should be scaleable according to the desired application. Because the plasmatron was a low-voltage, high-current device it was applicable for direct loudspeaker control, motor control, and efficient rectification and inversion.

### **3.5.3 Summary**

The plasmatron was similar to the thyatron operationally, but included continuous grid influence of the conduction current. The plasmatron's auxiliary discharge was unique during the time of its development and allowed for the first time a practicable means to have both low-impedance operation and continuous control in one hot-cathode gas electron tube. The forward voltage drop of the plasmatron was very low ( $< 0.3$  V), but could only conduct currents in the milliamperage range. Also, its hold-off voltage was less than 25 V. These disadvantages and the fact that control of the auxiliary discharge in the plasmatron complicated the device, led to efforts in developing a fully grid-controlled gas tube that could handle high currents while maintaining low forward voltage.

## **3.6 Tacitrons**

Brief descriptions of the various tacitrons that have been developed and their operating characteristics will be outlined. Because the emphasis of this thesis is the high-current Cs-Ba tacitron, a brief historic summary of the most recent work on Cs-Ba tacitrons will also be presented. For a more detailed outline of tacitron development and operational theory, see the work of Murray and El-Genk (1993).

### **3.6.1 Hydrogen Tacitron**

In 1954, E.O. Johnson, J. Olmstead, and W.M. Webster presented results of testing a new thyatron-type device called a tacitron. Their tacitron was similar in construction to the hydrogen thyatron but the conduction current was fully grid-controlled. This made the tacitron simple and more convenient for use in thyatron applications.

Also, the tacitron was different from plasmatrons in that ion generation occurred solely in the grid-anode region without the use of an auxiliary discharge. This method of ion generation was achieved by careful consideration of grid hole size, ionizing medium (hydrogen), gas pressure, and overall tube geometry (Johnson et al. 1954). The grid holes of the hydrogen tacitron were very small making the grid appear almost opaque while the operating hydrogen pressure was on the order of 50 - 300 mTorr (Operating pressure for the hydrogen thyatron was on the order of about 500 mTorr.) (Burkes 1987).

Turning the hydrogen tacitron device on was identical to that of the thyatron: a negative bias to the grid is removed and the device is on. The extinguishing mechanism for the hydrogen tacitron was similar to that of the plasmatron in that the positive ion sheath that forms around the grid holes halts the conduction current from cathode to anode. Murray and El-Genk give a definition of sheath thickness in terms of the grid voltage ( $V$ ), particle density ( $n_i$ ), and electron temperature ( $T_e$ ) as:

$$d = \sqrt{\frac{3.74 \cdot 10^9 \cdot V^{\frac{3}{2}}}{n_i \cdot (T_e)^{\frac{1}{2}}}} \quad (3.4)$$

This extinguishing method resulted in very small sheath thicknesses, necessitating grid apertures to be small, thereby causing grids for hydrogen tacitrons to be small, fragile, and requiring cooling. Also, because the ion density of the plasma is proportional to the conduction current of the device and since sheath thickness decreases with increasing ion density, maximum conduction currents were limited to less than 1 A. Forward voltage

drops for the hydrogen tacitrons were on the same order as early thyratrons ( $\sim 15 - 30$  V), which was somewhat large for low-voltage applications (Murray & El-Genk 1993).

#### **3.6.1.1 Applications**

The low conduction current limits of the early hydrogen tacitrons were overcome by the Soviets who designed and developed commercially available hydrogen tacitrons (Dvornikov et al. 1972 & 1974) at peak ratings of a few megawatts of switched power at voltages up to 20 kV and grid-controlled modulation frequencies up to 200 kHz. Forward voltage drops for these devices remained typically higher than an equivalent thyatron, making it ill-suited for low-voltage applications such as power conditioning for space nuclear power (Burkes 1987). However, the hydrogen tacitron is well suited for high power applications such as pulse forming networks for lasers, high power radars, etc..

#### **3.6.1.2 Summary**

By the 1970s, gas tube switching technology had come a long way. Typical hot-cathode gas tubes could conduct hundreds of amps, hold-off voltages of tens of kilovolts, and modulate at hundreds of kilohertz at forward voltage drops of less than 100 V (Murray & El-Genk 1993). The reduction of the forward voltage drop in these tubes was the next step in development for gas tubes. In the process of developing these tubes, it was discovered that a gas with a high affinity for ionization, cesium, could decrease the forward voltage to below 5 V.

### 3.6.2 Cs Tacitron

The use of cesium as the conduction medium in grid-controlled switches arose from the development of thermionic energy converters for space applications. Thermionic energy converters in the 1960s employed cesium as a conduction medium. By using cesium, with its low ionization potential, the forward voltage drop for grid-controlled switching devices could be significantly reduced. Table 3.1 gives the first ionization potentials for several gases.

**Table 3-1 First Ionization Potentials of Gases Used in Grid-Controlled Switches**

<b>Gas</b>	<b>First Ionization Potential (ev)</b>
Cesium, Cs	3.890
Mercury, Hg	10.437
Krypton, Kr	13.999
Xenon, Xe	12.130
Hydrogen, H	13.598

In the 1970s, the Soviets researched Cs tacitrons extensively (Kaplan et al. 1977a, Baksht et al. 1978a, 1978b). The Soviets did find that the forward voltage drop of these devices was significantly lower, but the conduction currents were not exceptionally high.

The low conduction currents of Cs tacitrons were attributed to the Schottky effect (Hemenway et al. 1962 and Baksht et al. 1978c). The Schottky effect is a result of increased emission current due to the effective electric field at the cathode surface that limits conduction due to voltage saturation. Cesium introduced into the tacitron interelectrode gap has a combined effect on the effective electric field at the cathode. First, a non-uniform layer of cesium can form on the surface of the cathode creating small

electric fields at the electrode surface which would increase the emission current. Second, ionized cesium in the gap creates an ion current flowing to the cathode surface, again increasing the emission current. Third, the sheath potential at the surface can increase the cathode emission current. Murray and El-Genk (1993) derived the increase in emission current due to the Schottky effect as:

$$j_{th} = j_s \cdot \exp \left[ \frac{612.7 \cdot (j_{iE})^{\frac{1}{4}} \cdot (V_e)^{\frac{1}{8}}}{T} \right] \quad (3.5)$$

where  $j_s$  is the thermal saturation current given in equation 3.1,  $j_{iE}$  is the ion current density at the cathode,  $V_e$  is the cathode sheath potential, and  $T$  is the cathode temperature.

Kaplan et al. (1977a) showed that the voltage hold-off of the Cs tacitron was a strong function of the Cs pressure. The hold-off voltage could be increased by applying a small negative bias to the grid during current conduction. This negative bias also controlled the electron emission from the grid into the grid-anode region. Excessive emission ( $> 0.5 - 1.5 \text{ A/cm}^2$ ) from the grid, resulting from cesium vapor decreasing the dielectric strength of the switch, could cause premature breakdown of the device.

The Cs tacitron device was put in the on-state by applying a positively-pulsed bias to the grid of several volts. Kaplan et al. (1977b) describe three extinguishing mechanisms: potential quenching, fast quenching, and slow quenching. Potential quenching is the same extinguishing mechanism as for the hydrogen tacitron or plasmatron. That is, the potential barrier sheath around the grid apertures overlap interrupting the flow of electrons into the grid-anode region. Potential quenching turn-off occurs in less than 1 microsecond. Fast

quenching occurs in about 1 microsecond and is the result of the grid sheaths not completely overlapping, but eventually extinguishing the discharge when the ion loss rate to the grid surface is greater than the ion production rate in the grid-anode region. If the loss rate is less than the production rate then the discharge will reignite (Murray & El-Genk 1993). Slow quenching occurs when a small negative bias is applied to the grid causing a slow increase in ion current. The discharge is extinguished when the anode current rapidly decreases after about  $5 \mu\text{s}$ , that is, when the ion loss rate overcomes the ion production rate.

Kaplan et al. (1977a) showed that the forward voltage drop in the Cs tacitron was a function of grid placement, grid thickness, and grid aperture size and ranged from 1.75 V to 2.75 V. These effects of the grid change the plasma density to increase or decrease the forward voltage drop. By moving the grid closer to the anode, ionization occurs near the anode surface (discharge volume decreases, thus increasing the plasma density) and the forward drop decreases. The opposite is true if the grid is closer to the cathode. A thicker grid means more surface area for ion leakage to the grid. This causes the plasma density to decrease and the forward drop to increase. Finally, as the grid aperture size is decreased (decreased transparency), electron movement is inhibited and the forward drop increases. A minimum forward voltage drop can be achieved by some combination of these grid attributes (Murray & El-Genk 1993).

### **3.6.2.1 Applications**

Kaplan et al. (1977a & 1977b) gives the switching frequencies of the Cs tacitron as 0.1 kHz to 1 kHz. The Cs tacitron was the first switching device best suited for thermionic

space nuclear power conditioning applications because of its potential high switching efficiency due to a low forward voltage drop and inherent radiation survivability. However, extinguishing the Cs tacitron is complicated due to the low ionization potential of Cs. Either the Cs pressure ( $< 10^{-2}$  Torr) (Kaibyshev et al. 1972) or the grid aperture size ( $10^{-4}$  to  $10^{-3}$  cm) needs to be small enough in order to extinguish the device. If the pressure is too low, the emission current from the cathode is significantly reduced. Also, if the aperture holes are too small the grid temperature increases causing higher emission from the grid. Higher emission from the grid causes temperature breakdown in the grid-anode region (Murray & El-Genk 1993).

#### **3.6.2.2 Summary**

The Cs tacitron's low forward voltage drop (1.75 - 2.75 V), switching frequency of up to 1 kHz, full grid control (up to 50 V of anode voltage), and inherent characteristics (high temperature, radiation hard) make this device better suited for space nuclear power applications than the previous gas tube switches. However, the Cs tacitron has low cathode emission currents associated with low operating Cs pressures and cathode temperature limitations. The Cs tacitron device needs to be modified in order to increase the emission current of the cathode while maintaining low grid emission and not sacrificing low forward voltage drops and grid controllability.

#### **3.6.3 Cs-Ba Tacitron**

The Soviets found that by adding barium to the interelectrode gap of the Cs tacitron emission currents could be increased at lower Cs pressures, and the dielectric strength of

the device could be increased. These improvements would make the tacitron the premier switching device for space nuclear power conditioning needs.

As before, the Cs vapor neutralizes the space charge effect in the interelectrode gap while the Ba decreases the cathode work function (relative to Cs alone) thereby increasing the current density of the device at a given cathode temperature. The reduced work function results from barium's higher heat of adsorption (as compared to Cs) causing higher Ba coverage on the cathode surface at a given temperature. Baksht et al. (1978c) report the heat of adsorption for Cs and Ba as 2.5 eV and 4.5 eV, respectfully. Murray and El-Genk (1993) include a comparison of work functions for several refractory metals under cesiated and bariated coatings. Murray and El-Genk (1993) also demonstrate the improvement of the emission current with the addition of Ba by the following example. By adding Ba at a reservoir temperature of 600 °C (0.4 mTorr) to a device with Cs pressure at  $10^{-1}$  Torr and tungsten cathode temperature of 1225 °C, the tungsten cathode work function could be reduced from 2.6 eV to 2.28 eV. This change in work function would increase the emission current density from 0.49 A/cm<sup>2</sup> to 5.84 A/cm<sup>2</sup> - an order of magnitude increase. Kaibyshev et al. (1972) and Kaplan et al. (1979) report current densities in excess of 15 A/cm<sup>2</sup> during their research of the Cs-Ba tacitron.

The addition of Ba to the Cs tacitron permits a higher operating temperature for the cathode at a given Cs pressure, resulting in a higher emission current. The higher cathode temperature is possible due to the fact that the work function of the grid is increased with the addition of the Ba vapor. The barium increases the grid's work function by displacing adsorbed Cs atoms from the grid surface. A higher grid work function translates to a

lower emission current density from the grid; therefore the cathode temperature, and necessarily the grid temperature, can be increased. This is significant because the tacitron thermal profile is such that the grid temperature is approximately the average of the emitter and collector temperatures; therefore, all else being equal, increasing the emitter temperature increases the grid temperature. Figure 3.5 shows the emission current density versus electrode temperature for different electrode work functions.

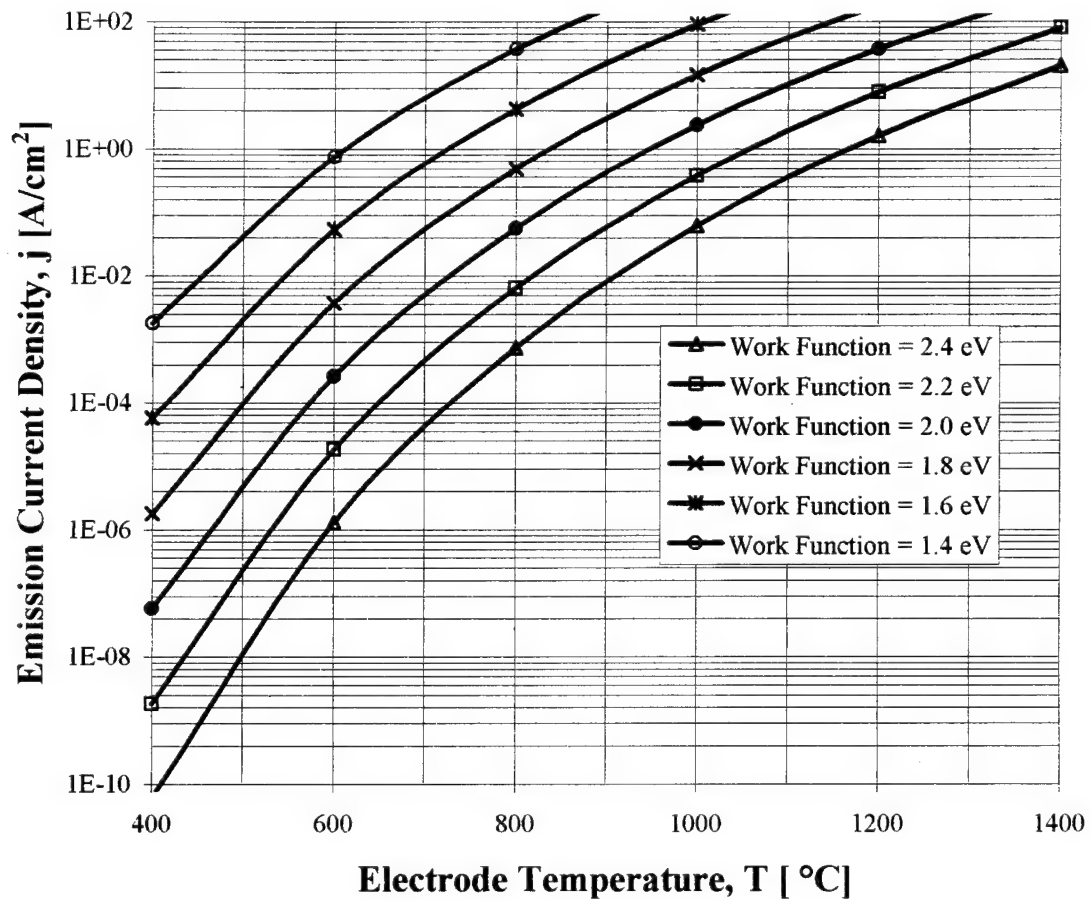


**Figure 3.5. Dependence of Emission Current Density on Electrode Temperature.**

With this assumption, Kaibyshev et al. (1972) and Kaibyshev and Kuzin (1975) reported voltage hold-offs of greater than 200 V. In addition, the hold-off voltage may be increased further by applying small negatively biased voltage pulses to the grid during current conduction as in the thyatron and Cs tacitron (Kaibyshev & Kuzin 1975 and Kaplan et al. 1977a).

Ignition, or turn-on characteristics, for the Cs-Ba tacitron are like those of the Cs tacitron: a positively pulsed bias is applied to the grid to initiate breakdown. Kaplan et al. (1977c & 1979) and Kaibyshev and Kuzin (1975) describe several extinguishing mechanisms for the Cs-Ba tacitron, dependent on the Cs pressure and grid design. The extinguishing mechanisms are similar to those of the hydrogen tacitron and plasmatron under potential and fast quenching where grid sheaths interrupt the conduction current as described by Kaplan et al. (1977b). Under these various extinguishing mechanisms, modulation frequencies of 1.65 kHz to 6 kHz were reported for different Cs-Ba tacitron arrangements (Kaplan et al. 1977c & 1979).

The forward voltage for the Cs-Ba tacitron is about the same as that for the Cs tacitron (1 - 2.5 V). The variations in grid placement, thickness, and grid aperture size effecting the plasma density in the Cs tacitron are applicable to the Cs-Ba tacitron.

#### **3.6.3.1 Recent Work**

The Institute for Space and Nuclear Power Studies (ISNPS) at the University of New Mexico has investigated the Cs-Ba tacitron under several situations for over five years. Their findings are too numerous to list here in their entirety, but some highlights specific to the operational characteristics of the high-current tacitron will be briefly discussed.

ISNPS has investigated two tacitron configurations: a cylindrical device with two triode sections and one diode section (Figure 3.6), and a planar device (Figure 3.7). Each configuration's grid has an effective area of about  $2 \text{ cm}^2$  with equal transparencies ( $\sim 34\%$ ). Also, the emitter-grid and grid-collector gaps for the two devices are the same ( $\sim 1 \text{ mm}$ ).

The cylindrical device has been operated as an inverter in two modes, the thyatron (forced commutation) mode and the tacitron (grid-controlled) mode. The cylindrical device was shown to modulate up to 10 kHz at a forward voltage drop as low as 2 V for the thyatron mode, and up to 20 kHz at voltage drops of 3 - 3.5 V for the tacitron mode corresponding to current densities of about  $3 \text{ A/cm}^2$ . In the inverter mode, the triode sections of the cylindrical device are operated in a push-pull sequence: one triode section is ignited while the other is extinguished. This process is repeated in reverse order, generating an alternating series of square pulses (Murray & El-Genk 1993 and El-Genk et al. 1994).

In the planar device, the electrode spacing can be changed easily by replacing insulating spacers or by interchanging the anode and cathode electrodes. Each electrode is separately heated and can therefore be used as either the emitter, or the collector while the grid remains stationary (See Figure 3.7). Also, this variable emitter arrangement allows for the investigation of Cs reservoir placement on device performance (Since the Cs inlet is located between the lower electrode and the grid.). The planar tacitron has exhibited conduction currents on the order of  $10 \text{ A/cm}^2$ , and in modulation of  $5 \text{ A/cm}^2$  at 22 kHz

(grid power supply limited), at a forward voltage drop of 2.2 V. Hold-off voltages of up to 200 V have also been attained (El-Genk et al. 1994 and Wernsman & El-Genk 1996).

### **3.6.3.2 Applications**

As with the Cs tacitron, the Cs-Ba tacitron is best suited for power conditioning in space nuclear power applications and could be a promising alternative to solid-state switching elements in high-temperature, high-radiation environments. However, the Cs-Ba tacitron could also be used in other commercial high-temperature switching applications such as electro-plating.

### **3.6.3.3 Summary**

Cesium-barium tacitrons are low-pressure, grid-controlled gas switching tubes that are inherently radiation and temperature hard. The main operational difference between the Cs-Ba tacitron and a conventional high-power gas switching tube, such as the hydrogen thyratron, is that the tacitron is completely grid-controlled, while the thyratron is grid-controlled only during the ignition mode. Cesium-barium tacitrons have demonstrated low forward voltage drops ( $< 3$  V), high current conduction densities ( $> 10$  A/cm<sup>2</sup>), switching frequencies up to 22 kHz, and voltage hold-offs of up to 200 V. At this time, the Cs-Ba tacitron is the best suited gas tube switching device for static energy converting (thermionic or thermoelectric), space nuclear power conditioning applications.

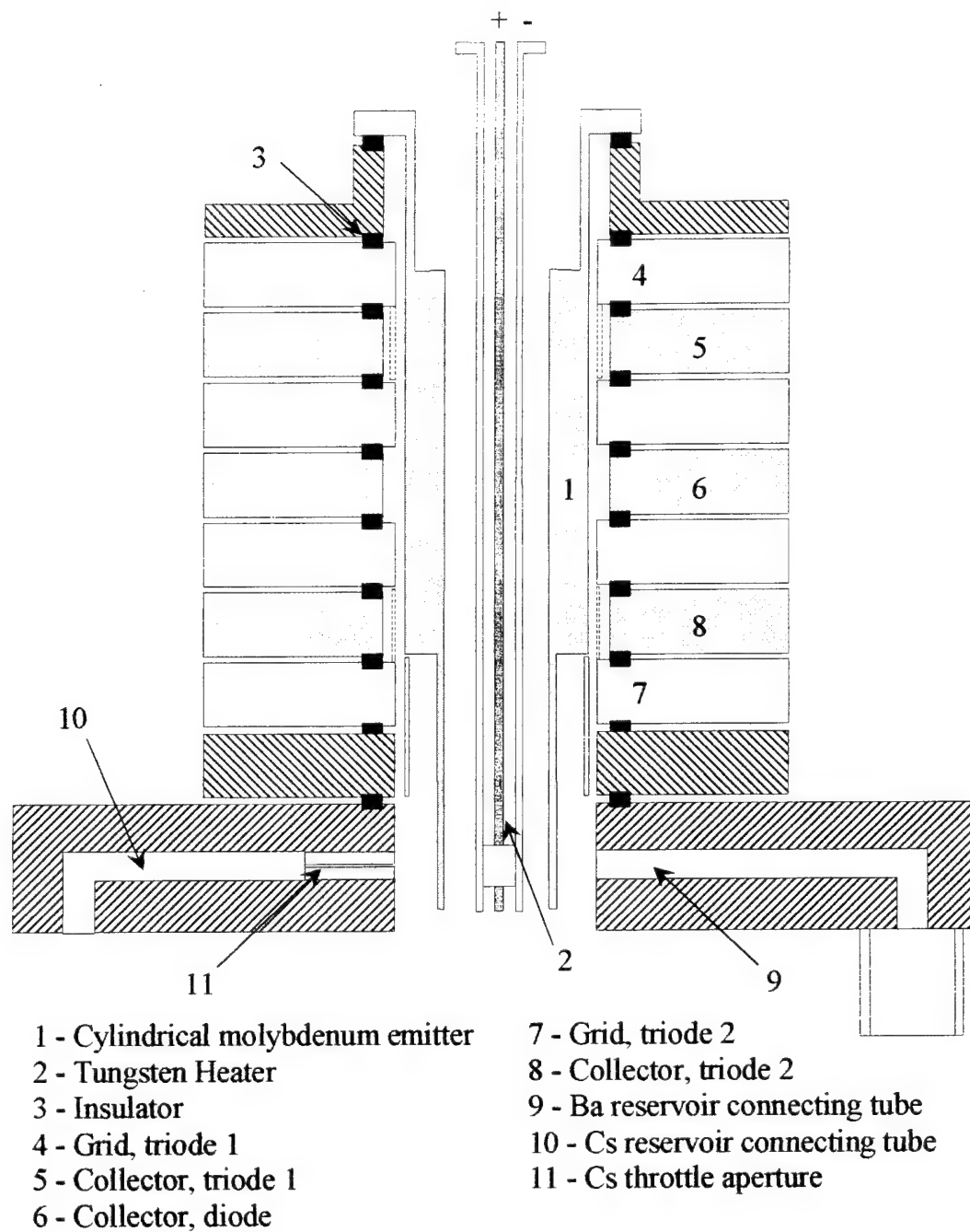


Figure 3.6. Cylindrical Cs-Ba Tacitron (Murray & El-Genk 1993).

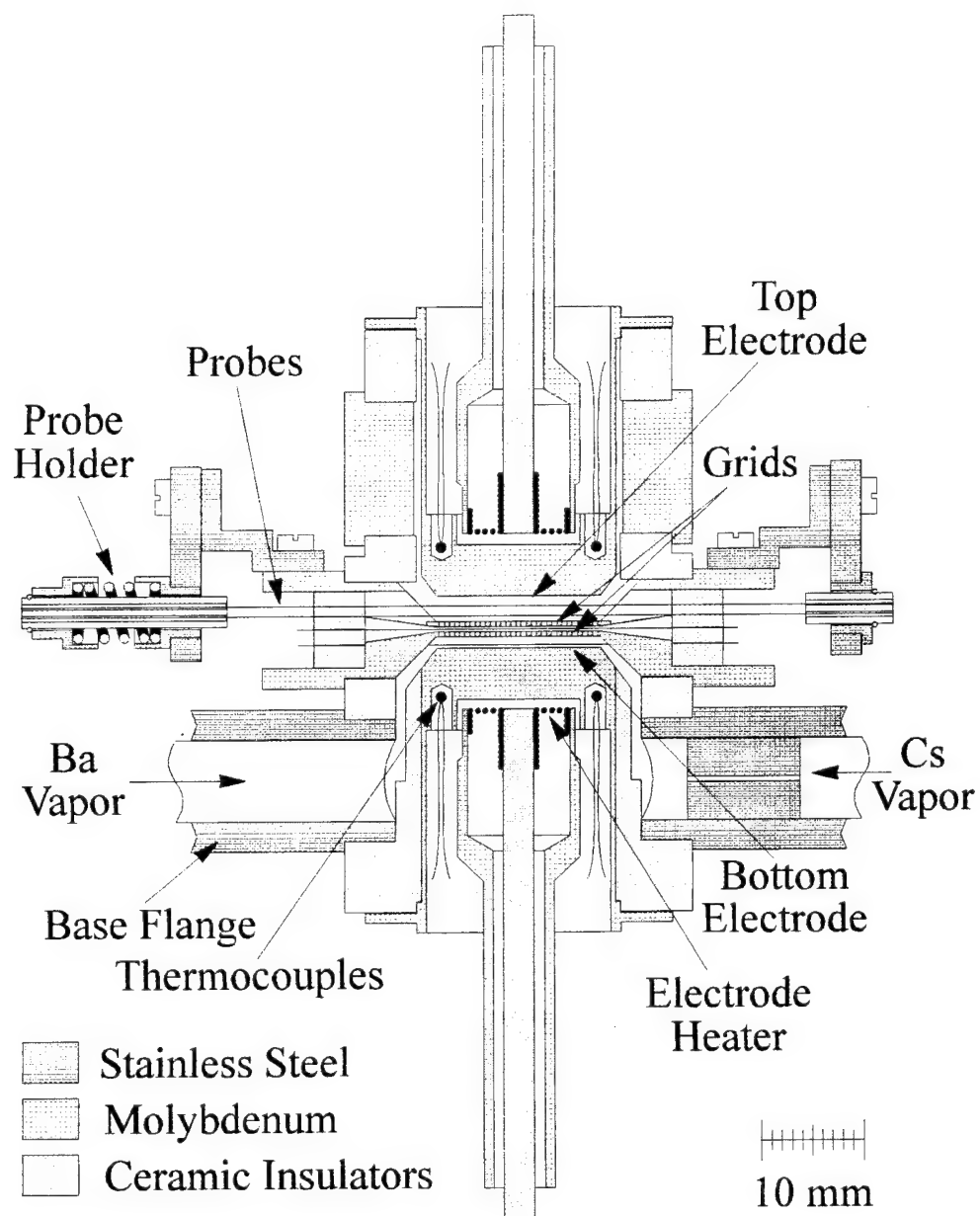


Figure 3.7. Planar Cs-Ba Tacitron (*Wernsman & El-Genk 1996*).

## **4. HIGH-CURRENT CESIUM-BARIUM TACITRON**

This chapter contains the test facility description, including the high-current tacitron device, experimental procedures, preliminary operational characteristics of the devices as diodes in the I-V mode, preliminary results of the operational characteristics under grid-controlled current modulation, and preliminary voltage hold-off measurements.

### **4.1 Test Facility Description**

The facility space for the high-current tacitron research consisted of a vacuum system, a power rack for each of the two high-current tacitrons, control rack, a shared cesium reservoir, separate barium reservoirs for each device, a computer data acquisition system, and the tacitrons. Figure 4.1 is a photograph of the test equipment.

#### **4.1.1 Vacuum System**

The vacuum system consists of a vacuum chamber, isolation gate valve, one roughing pump, a turbomolecular pump, and vacuum gauges. The vacuum chamber is of the bell-jar variety with a device mounting plate and flange providing feedthroughs for emitter, base flange, Ba reservoir, and Cs pipeline heater leads; thermocouples; emitter and collector bias power leads; grid control leads, Ba reservoir linear translation feedthroughs, internal Cs piping, and cooling water supply. Figure 4.2 shows a schematic of the main feedthroughs.

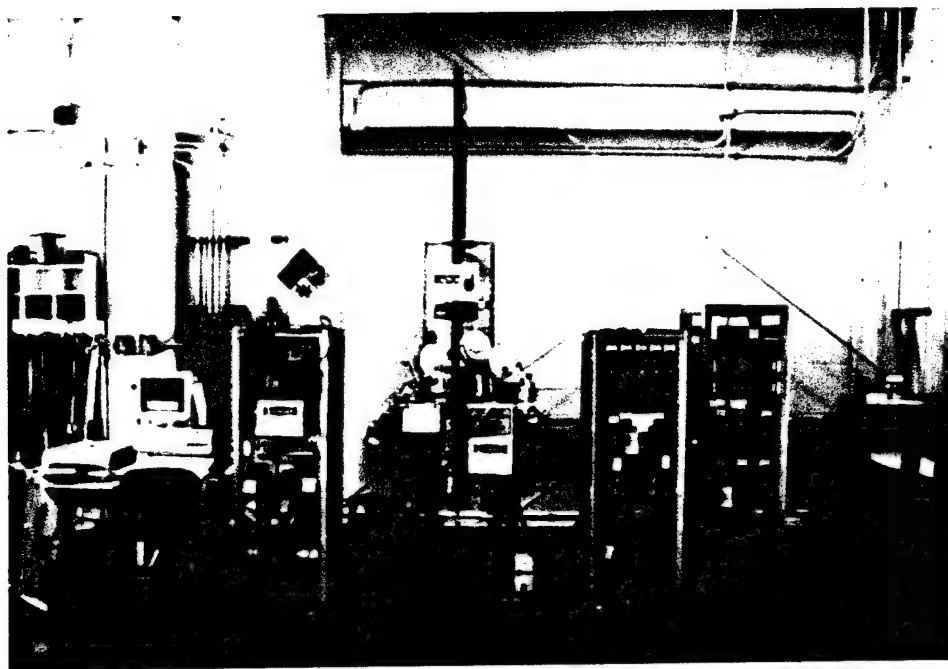


**Figure 4.1.** Photograph of the High-Current Cs-Ba Tacitron Facility (*From Left to Right: Data Acquisition System, Control Rack, Vacuum Stand, Power Rack 1, and Power Rack 2.*).

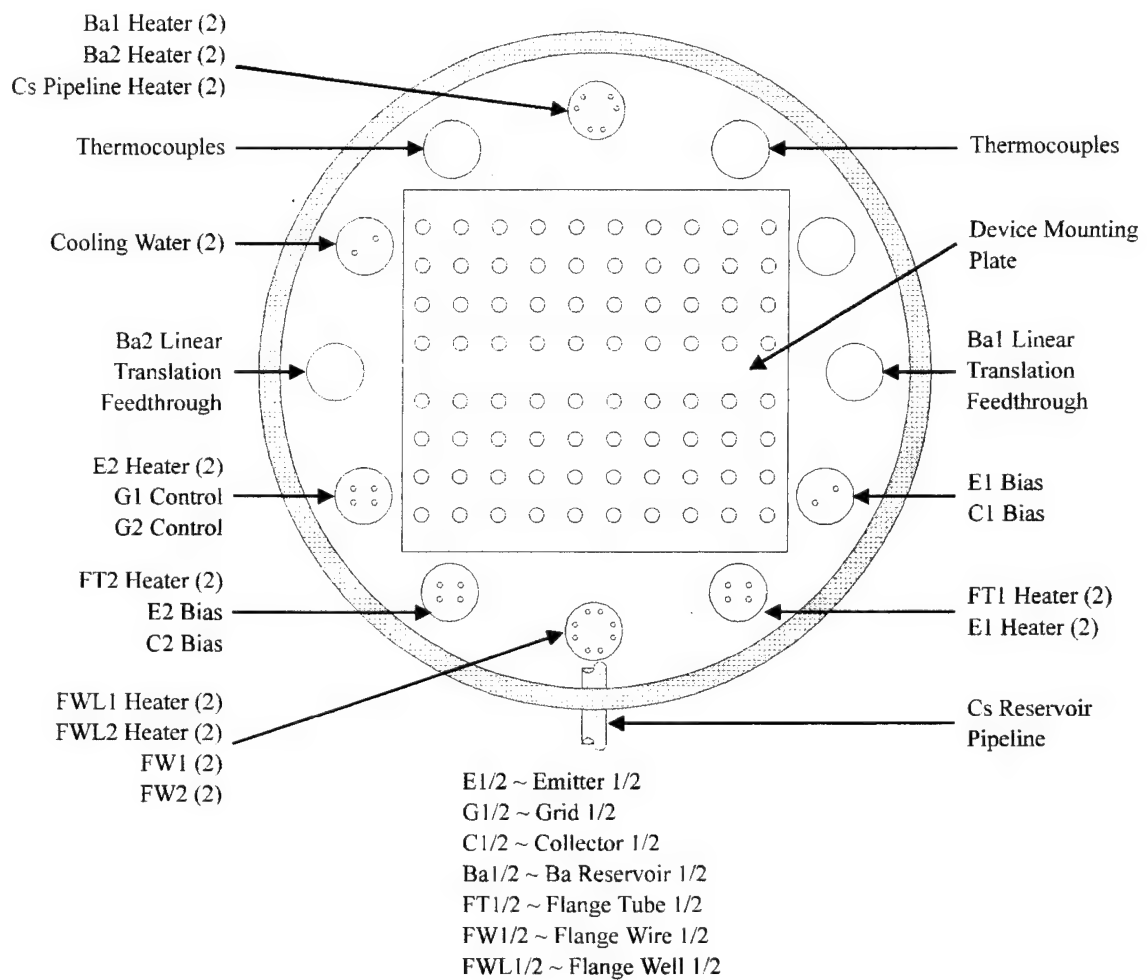


**Figure 4.2. Vacuum Chamber Feedthrough Designs.**

When the chamber is sealed, the roughing pump takes the chamber pressure to about  $10^{-3}$  Torr. At this point, the turbomolecular pump is activated and the chamber can be pumped down to  $10^{-8}$  Torr. The isolation gate valve is a pneumatic-driven solenoid valve pressurized with nitrogen and is used to isolate the vacuum chamber from the pumping system. The valve can either be closed manually or automatically. Automatic closure occurs if the solenoid is deenergized as in the case of loss of power. This isolates the chamber's contents from atmospheric pressure during a loss of power. The chamber pressure is monitored with two ionization gauges for high vacuum ( $10^{-3}$  -  $10^{-10}$  Torr), and two Pirani gauges for roughing ( $10^3$  -  $10^{-4}$  Torr).

#### **4.1.2 Control Rack**

The facility's control rack contains the I-V power supply for characterization of the devices. The I-V power supply consists of a half-wave rectified transformer energized by a variac. The supply provides a variable amplitude signal that sweeps from zero voltage up to a maximum value and then back to zero. An Electronics Measurement Inc. TCR 120T40 power supply, providing a dc collector bias of up to 120 V at 40 A is used during modulation tests. The control rack also houses the grid bias power supply, and the data acquisition and control system (DAS) interfacing components.

#### **4.1.3 Data Acquisition and Control System**

An external ADAC Corp. 5302EN I/O (with reference junctions for the thermocouples) monitors the devices temperatures and also contains analog and digital I/O terminals for signal control. The DAS records current, voltage, and temperature measurements and

provides I-V plots for data analyses. The DAS consists of an 80486 PC running a software application written in the National Instruments LabWindows development environment. The acquisition and control application is interfaced to a LeCroy 9304 (4-channel) 175 MHz digital oscilloscope for current and voltage measurements. Current measurements for I-V tests are accomplished through the use of current shunts while modulation currents are measured with current transformers.

The LabWindows data acquisition program enables the user to control the operation of either device and was developed by a visiting scientist from the Kurchatov Institute in Moscow, Russia.<sup>1</sup> The main screen that appears upon execution of the program is shown in Figure 4.3. The software is capable of monitoring collector and grid signals simultaneously. Several operations can be executed from the main menu screen, such as, trigger pulse initiation for I-V mode ('Mes/I-V'), waveform save ('Save'), and waveform recall ('Read'). There are three other control buttons that call up additional pop-up menus. The first labeled 'Sc9304', generates a screen to properly initialize the oscilloscope (i.e. attenuation, trigger delay, time scale, voltage scale, etc.) as shown in Figure 4.3. The second button labeled 'I-V', generates a current versus voltage curve for the signals from the collector. The third control button labeled 'T\_MAP' calls up a screen that maps, continuously at a user-defined interval, thermocouple temperature measurements for the emitter, collector, grid, and reservoirs.

---

<sup>1</sup> Djachiachvili, I. (1994), Software Programmer of the High-Current Cs-Ba Tacitron DAS. Contracted with the KIAE, Moscow, Russia through ORION International Technologies, Albuquerque, New Mexico.

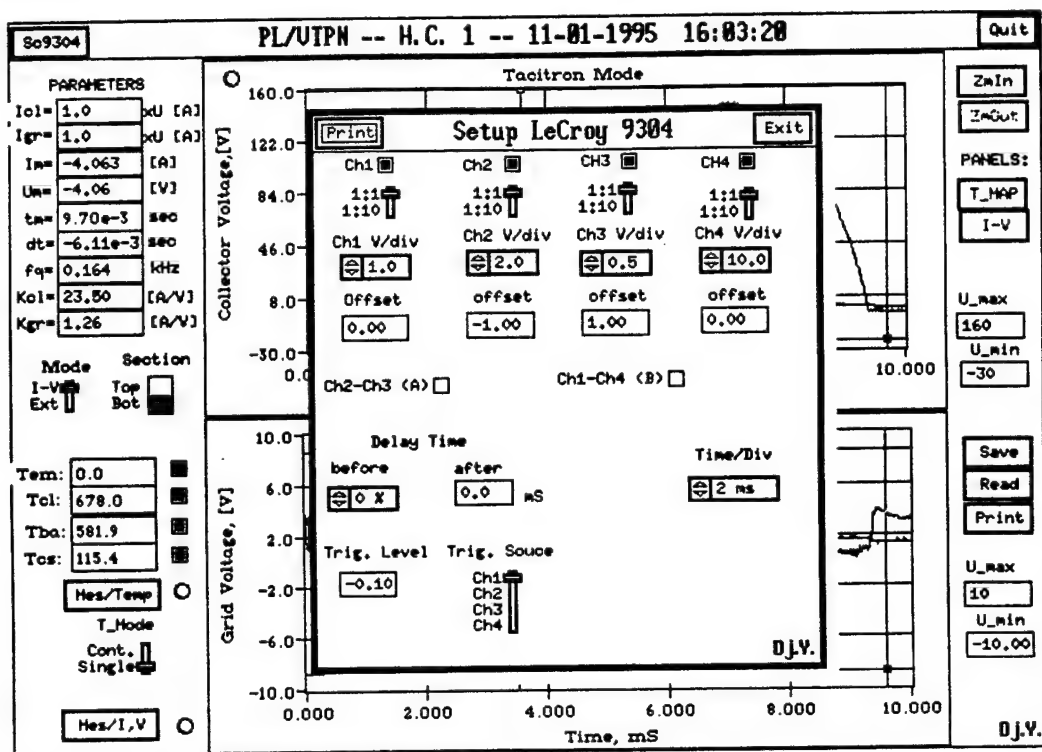


Figure 4.3. 'Main Menu' Screen of Data Acquisition & Control System.

#### **4.1.4 Instrumentation**

Each device is configured with two Type-B platinum-rhodium (Pt6%Rh-Pt30%Rh) and nine Type-K thermocouples. The Type-B thermocouples are placed in the emitter and on the collector. The Type-K thermocouples are allocated as follows: three on the grid, two of which are over the Cs and Ba reservoir inlets; two on the base flange, one on the base flange well, two in the barium reservoir, and one on the top plate near the emitter cup.

The internal Cs pipeline has two Type-K thermocouples. One is located at a 'tee' just inside the feedthrough for the Cs reservoir pipeline. The other is located on the Cs pipeline entering Device 1. These thermocouples monitor the temperature along the internal Cs pipeline. The thermocouples on the external pipeline and reservoirs are shown in Figure 4.4.

#### **4.1.5 Cs and Ba Reservoirs**

The Cs and Ba reservoirs are independently controlled. Prior to operation, liquid Cs (~ 5 g) is put into Reservoir 2 of the Cs external valve assembly. The valve assembly is used to precipitate Cs from one reservoir to the other, or from the reservoir (or reservoirs) to the devices. The entire valve assembly is surrounded by three separately controlled insulated wire heaters: one for the pipeline and valve closest to the chamber (Reservoir 1), one for Reservoir 1 itself, and one for the valve and reservoir furthest from the chamber (Reservoir 2). Precipitation of the Cs is accomplished by changing the heater current of these heaters, opening and closing the necessary valve(s), and varying the water flow near one or both reservoirs. The internal pipeline is surrounded by another separately controlled wire heater. One Cs pipeline feeds both devices from the external assembly.

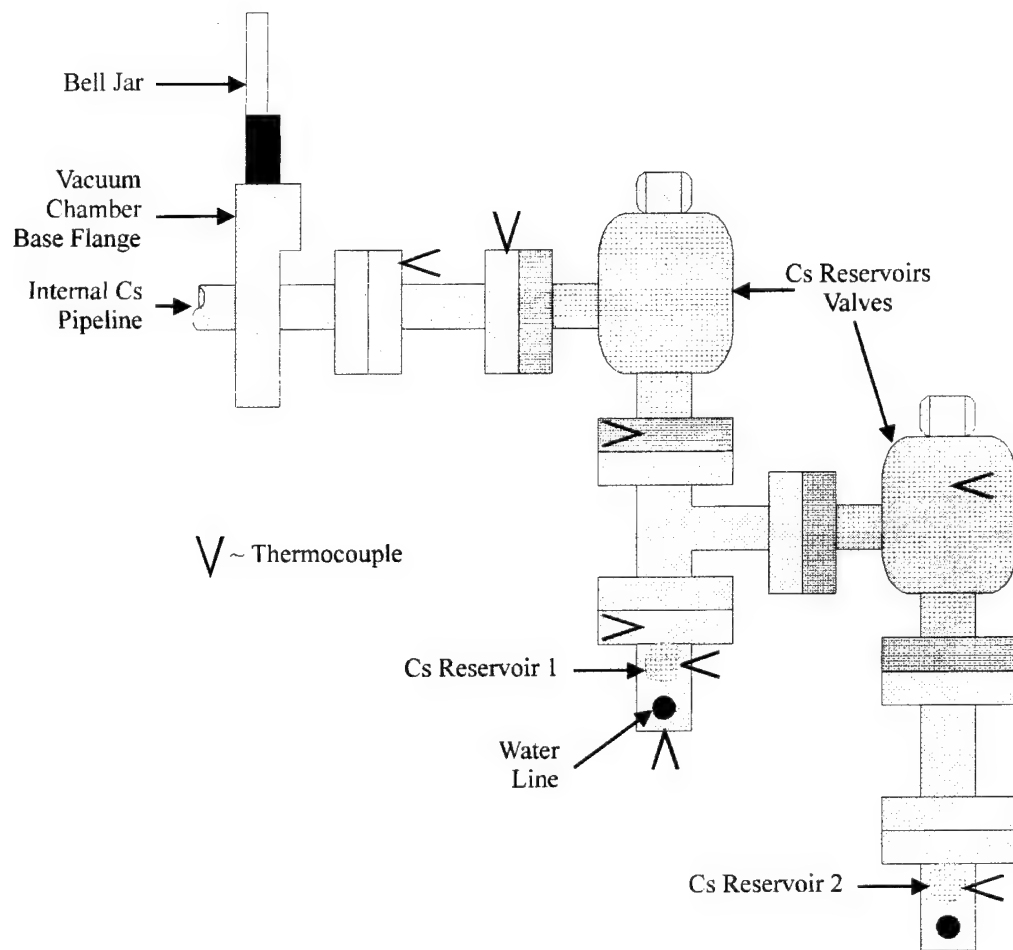


**Figure 4.4. External Cs Pipeline & Reservoirs with Thermocouples.**

Each device has its own Ba reservoir and heater. The reservoir and heater are located beneath the high-current device. Prior to sealing the vacuum chamber, Ba ( $\sim 1 \text{ cm}^3$  piece) is loaded into the devices' reservoirs.

#### **4.1.6 Power Racks**

All heater power units are located on the power racks. Power is supplied for outgassing the system after exposure to air and to provide power for tacitron device operation. Each device has its own controls for the Ba reservoir heater, emitter power, flange tube heater, flange well heater, and flange wire heater. The Cs pipeline heaters each have their own power unit and are located on Power Rack 1. As stated previously, the grid supply is located on the Control Rack. Only one device can be grid-biased at a time during the I-V mode of operation.

Initial device outgassing is performed when the vacuum chamber has reached  $5 \times 10^{-6}$  Torr or better. Device outgassing proceeds by applying heater current, waiting until the chamber pressure peaks and begins to decrease, then increasing the heater current once again. Chamber pressure is held below the heater damage threshold of  $1 \times 10^{-5}$  Torr. The 'heater damage threshold' limit is an operational limitation developed by the Russians in their concern for the specially designed tungsten emitter heaters. These heaters, once heated to operating temperature, are very fragile. Also, the heaters can be stressed if operated in low vacuum (oxidation) or their current is increased too rapidly (thermal expansion). This degrades the heater and their operational lifetime. At device temperatures below about  $400^\circ\text{C}$ , chamber pressure is generally the factor that limits the rate at which heater current can be increased. Outgassing will increase dramatically as

various parts of the device pass through the temperature range of 150 °C to 400 °C. The rate of outgassing at device temperatures above 400 °C is minimal.

There are a total of eight types of heaters used for the operation of the device (emitter, flange tube, flange wire, flange well, Cs internal pipeline, Cs system (external), Cs reservoirs, and Ba reservoir). The emitter heater is brought up to operating temperature first while maintaining the heater damage threshold. Then the other heaters are brought to operating temperature in sequence. See Table 4.2 for the sequence of heater operation and heater power limits at operating temperature.

**Table 4-1 Heater Operation Sequence and Current Limits**

HEATER	MAX OPERATING POWER
Emitter	~ 660 W
Flange Tube	~ 294 W
Flange Wire	~ 70 W
Flange Well	~ 68 W
Cs Internal Pipeline	~ 37 W
Cs External Pipeline	~ 124 W
Cs Reservoir	~ 60 W
Ba Reservoir	~ 120 W

Initial outgassing is complete when all heaters are to their operating current and the chamber pressure is below  $5 \times 10^{-6}$  Torr for at least one day. At this point, all heaters are slowly turned off, the system is opened, and Ba is loaded into the Ba reservoirs. Initial outgassing 'cleans' the devices and prevents the Ba from getting contaminated. Next the system is closed and outgassing begins again to operating temperature and pressure. Once

at operating temperature and pressure, the Ba can then be melted by raising the Ba reservoir temperature to about 700 °C (melting temperature for Ba is ~ 710 °C). After the Ba melts, the reservoir is raised (via the Ba translation feedthrough) to seal with the base flange of the device. At this point, Cs gas can be fed into the system and I-V operation can commence.

#### **4.1.7 High Current Cs-Ba Tacitron (Masten et al. 1995a, b)**

Figure 4.5 is a photograph of the device and Figure 4.6 shows a schematic of the high-current Cs-Ba tacitron. The emitter heater consists of a wound tungsten filament (~ 0.060" wire) placed within the molybdenum emitter cup. Two refractory metal heat shields are placed between the winding and the top plate (See Figure 4.7). A molybdenum spacer is used between the upper lip of the emitter cup and the boron-alumina nitride (B,Al)N ceramic insulator that isolates the emitter from the grid. The spacer also functions as a heat shield for the emitter cup. The grid is a honey-comb design in 6 sectors (Figure 4.9), constructed of 1-mm wide tantalum ribbon with a mean cell diameter of approximately 1 mm. The sectors are separated by 1 mm thick struts running radially outward from a 1.6-cm diameter hub. A tubular attachment extends downward from the hub of the grid, through an orifice in the collector electrode, into a cool well (base flange well) located in the base flange. The purpose of this tubular attachment is to radiate heat from the grid to the base flange. The molybdenum collector electrode is isolated from both the base flange and the grid electrode by (B,Al)N insulators. Figure 4.8 is a photograph of the tacitron electrode components.

Emitter and collector planar surface areas are  $28 \text{ cm}^2$  and  $27 \text{ cm}^2$ , respectfully. The grid has the same planar area as the emitter, with a transparency of approximately 65%, for a geometrically 'open' planar area of  $18 \text{ cm}^2$  (Total surface area of the grid 'cells' is about  $10 \text{ cm}^2$ , while the total grid area including cells, the spokes and hub (top and bottom) is about  $19 \text{ cm}^2$ ). The grid is located approximately in the center of the emitter-collector gap, with grid-collector and grid-emitter electrode separations of approximately 1.5 mm. The barium reservoir consists of a molybdenum cup mounted on an upright linear feedthrough below the base flange, while the Cs reservoirs are placed outside the vacuum chamber.

During device operation, the base flange is maintained at a temperature approximately 30 - 80 °C higher than the Ba reservoir to prevent Ba and Cs condensation within in the flange. The temperature gradient between the emitter and the base flange insures that the internal surfaces of the device are hot enough to remain free from excessive Cs or Ba condensation. The Cs orifice plug in the base flange Cs delivery line serves to minimize the diffusion of Ba into the Cs system.

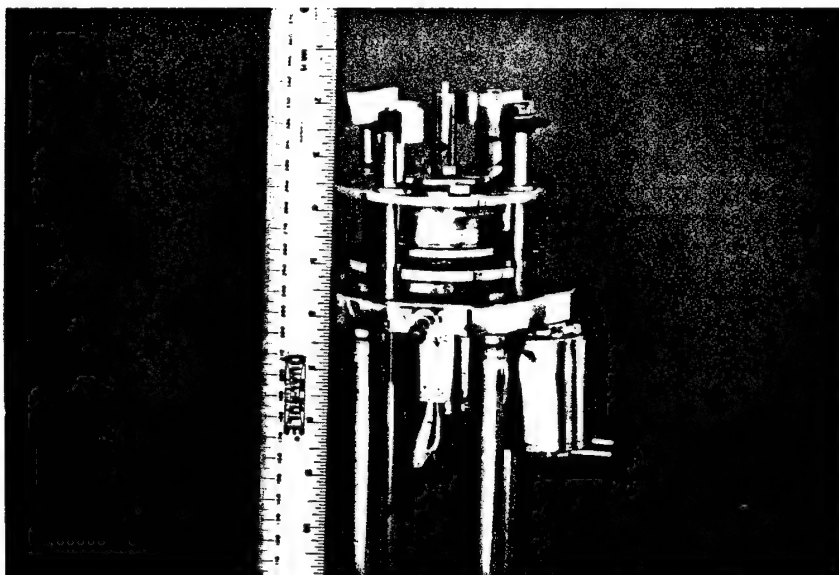


**Figure 4.5. Photograph of the High-Current Cs-Ba Tacitron.**

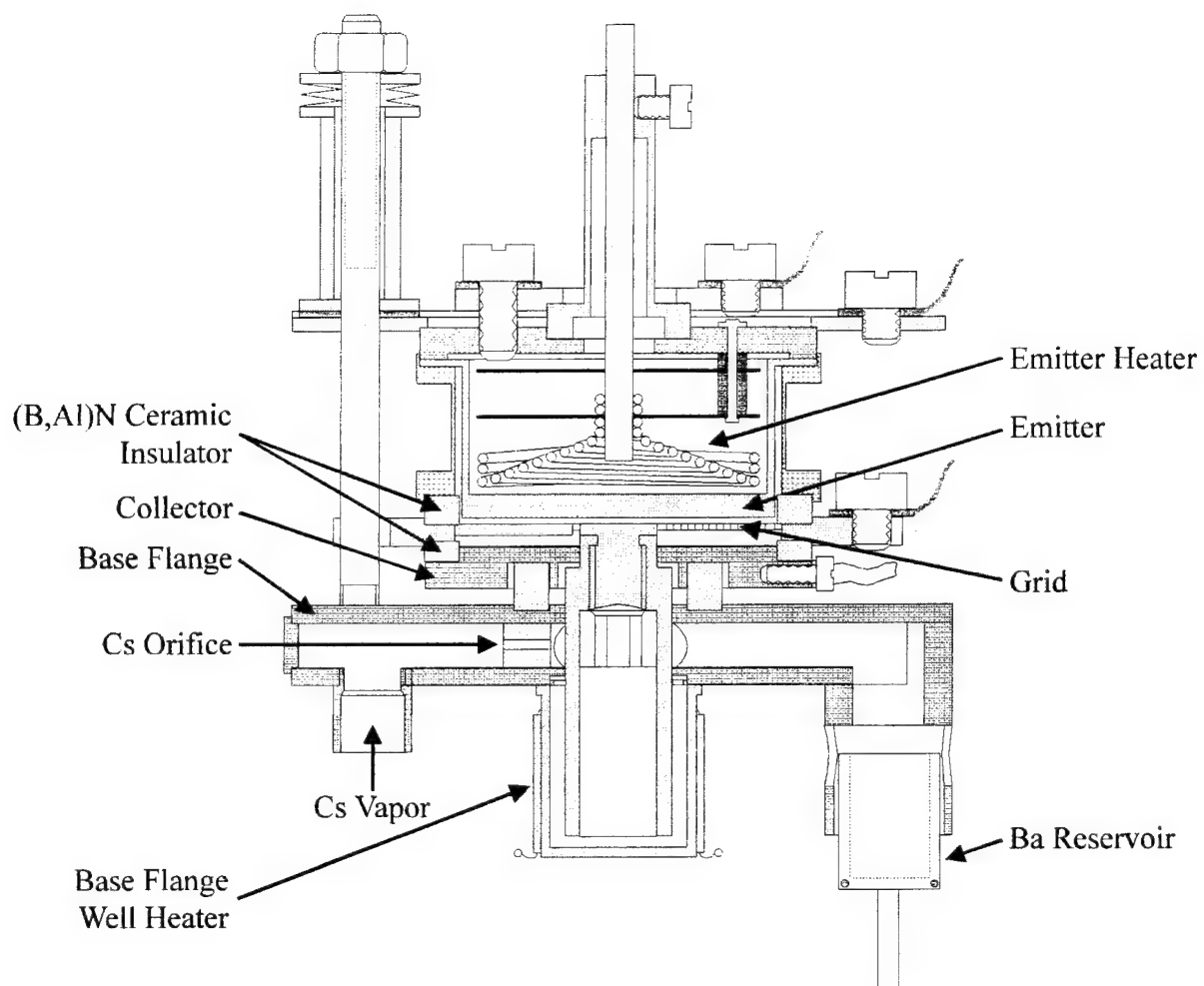


**Figure 4.6. Schematic of the High-Current Cs-Ba Tacitron.**

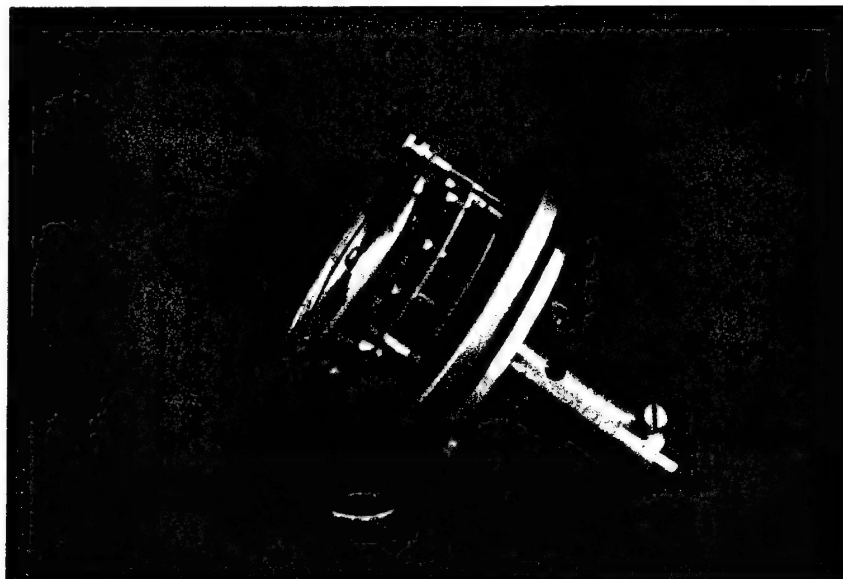


**Figure 4.7** Photograph of the tungsten emitter heater assembly.

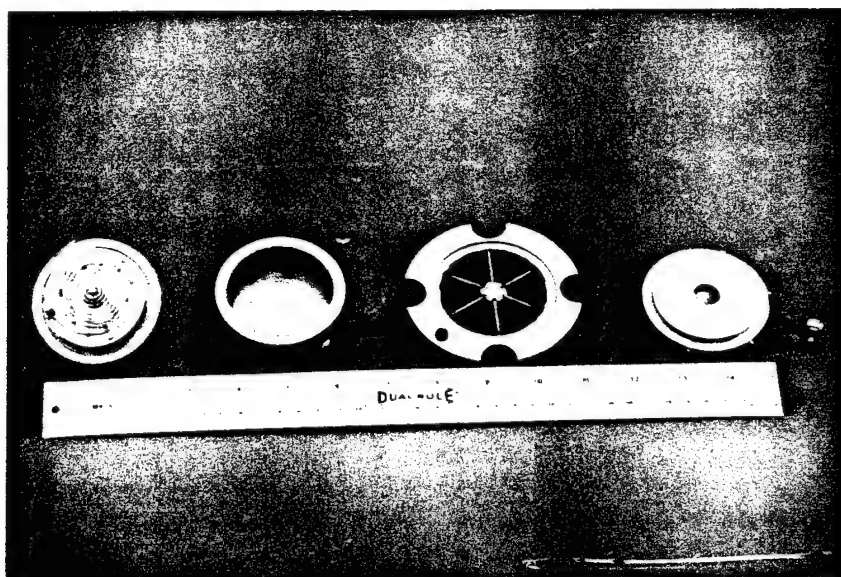


**Figure 4.8.** Photograph of Components of the High-Current Cs-Ba Tacitron (*From Left to Right: Emitter Heater, Emitter Cup, Grid, and Collector*).

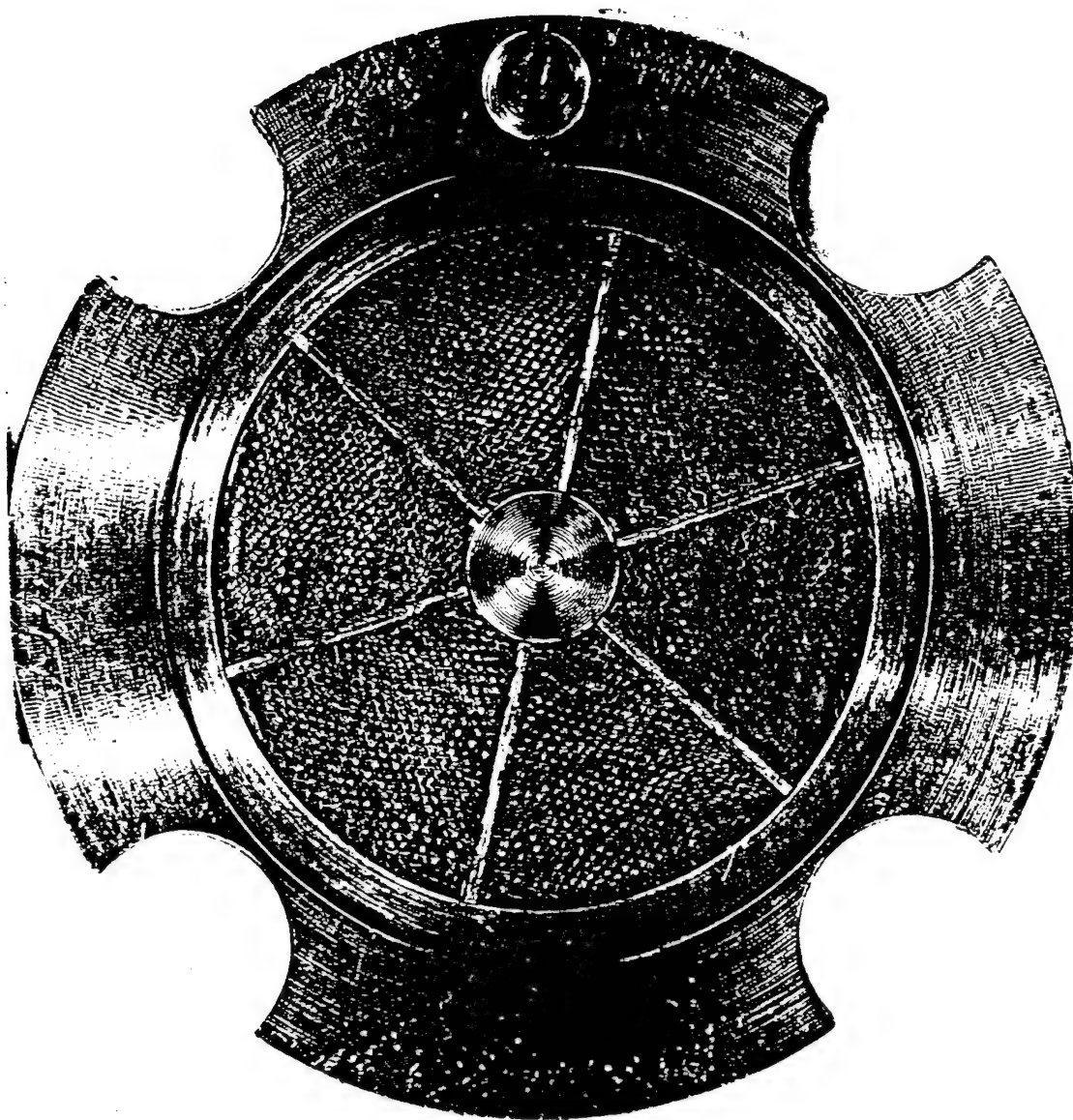


**Figure 4.9. Hexagonal Grid Geometry of the High-Current Cs-Ba Tacitron.**

## **4.2 Operational Characteristics**

Performance of a switch is defined by its forward voltage-drop, current modulation, and hold-off voltage characteristics. These attributes associated with the high-current Cs-Ba tacitron are examined in this section.

### **4.2.1 Experimental Procedures**

After outgassing and when the device and supplemental components are at operating temperature for approximately two hours, the system is assumed to have reached steady-state conditions (system temperatures and pressures have stabilized). Approximate operating temperature ranges are presented in Table 4.2. It should be noted that the collector is heated radiatively via the emitter and base flange. Also, because of the base flange design, the thermocouples measuring the operating temperatures in Table 4-2 could not be located at the hottest section of the base flange (the center).

**Table 4-2 System Operating Temperatures**

<b>COMPONENT</b>	<b>OPERATING TEMPERATURE</b>
Emitter	1100 - 1250 °C
Grid	600 - 800 °C
Collector	800 - 1000 °C
Base Flange	600 - 700 °C
Cs Pipeline	225 - 300 °C
Cs Reservoir	120 - 180 °C
Ba Reservoir	500 - 600 °C

Measurements are taken after the Cs and Ba reservoir temperatures and pressures have reached steady-state after changing one of the operating parameters (emitter temperature, Cs pressure, and Ba pressure). Once the system has reached steady-state, any changes in the operating parameters will require a short waiting period for the system to again reach steady-state conditions. This waiting period is on the order of 20 - 30 minutes.

Experiments in the I-V mode are conducted by incrementally applying a voltage to the collector ( $V_{cc}$ ). If ignition does not occur, then the collector bias is removed and the operating parameters are changed. When ignition is observed, the waveform is saved on the DAS. During the I-V mode, the device is operated as a diode, that is, no bias is applied to the grid. Operating parameters are varied as follows: emitter temperature of 1050 °C, 1150 °C, and 1250 °C; Ba reservoir temperature of 550 °C, 575 °C, and 600 °C; Cs reservoir temperature of 130 °C, 155 °C, and 180 °C. This schedule of operating parameters results in a matrix of 27 different experimental conditions (3 settings for 3 variables =  $3^3$  conditions) for the two identical high-current devices (Device 1 and Device 2, respectfully). The two devices are tested one after the other at the specific experimental conditions. Therefore, their performance compared to one another can be evaluated. In addition, the testing sequence for the devices at each experimental condition is alternated every other attempt. That is, Device 1 is tested first at condition 1 then Device 2, Device 2 is tested first at condition 2 then Device 1, Device 1 is tested first at condition 3 then Device 2, and so on.

Modulation experiments are conducted by applying a positive or negative grid voltage to ignite and extinguish the device, respectfully. Observations from the I-V mode are used

to determine the lowest plasma and electrode temperatures resulting in ignition. These are the conditions used during modulation experiments.

Voltage hold-off measurements of the high-current tacitron are taken with the grid electrode grounded to the emitter. The applied collector potential is a half-sine pulse with a 3.6 ms duration.

#### **4.2.2 Forward Voltage Drop**

The forward conduction voltage drop dictates the switching efficiency of the device and the range of input voltages for which the device could be useful. In order to maintain a switching efficiency of greater than 90% for power systems having an output voltage as low as 50 VDC (as envisioned in space nuclear power sources), the maximum voltage drop in the device should be less than 4 -5 V. In this section, the forward voltage drop will be examined by discussing the effects of the operating parameters. That is, the effects of the emitter temperature, Cs pressure, and Ba pressure on the forward voltage drop of the high current devices will be discussed.

##### **4.2.2.1 Effect of Emitter Temperature**

Thermionic emission is strongly dependent on the emitter work function and emitter temperature (as shown in the Richardson-Dushman equation (3.1)). The dependence of the I-V characteristic for the high-current Cs-Ba tacitron on the emitter temperature is shown in Figure 4.10 and Figure 4.11. As can be seen in the figures, the collector (conduction) current remains small and relatively constant until the device is ignited. The collector-emitter voltage then collapses to a stable conduction voltage - the forward voltage drop,  $V_f$ . The forward voltage drop remains constant regardless of increasing the

power supply voltage, until the conduction current reaches the thermal emission saturation current. As mentioned previously, the conduction current can only be increased beyond the thermal emission saturation point if the forward conduction drop increases. The increased conduction drop modifies the emitter work function, such that additional current can be gained via Schottky emission. This transition point at which significant Schottky emission (equation 3.5) begins to occur is referred to as the 'knee' of the I-V curve.

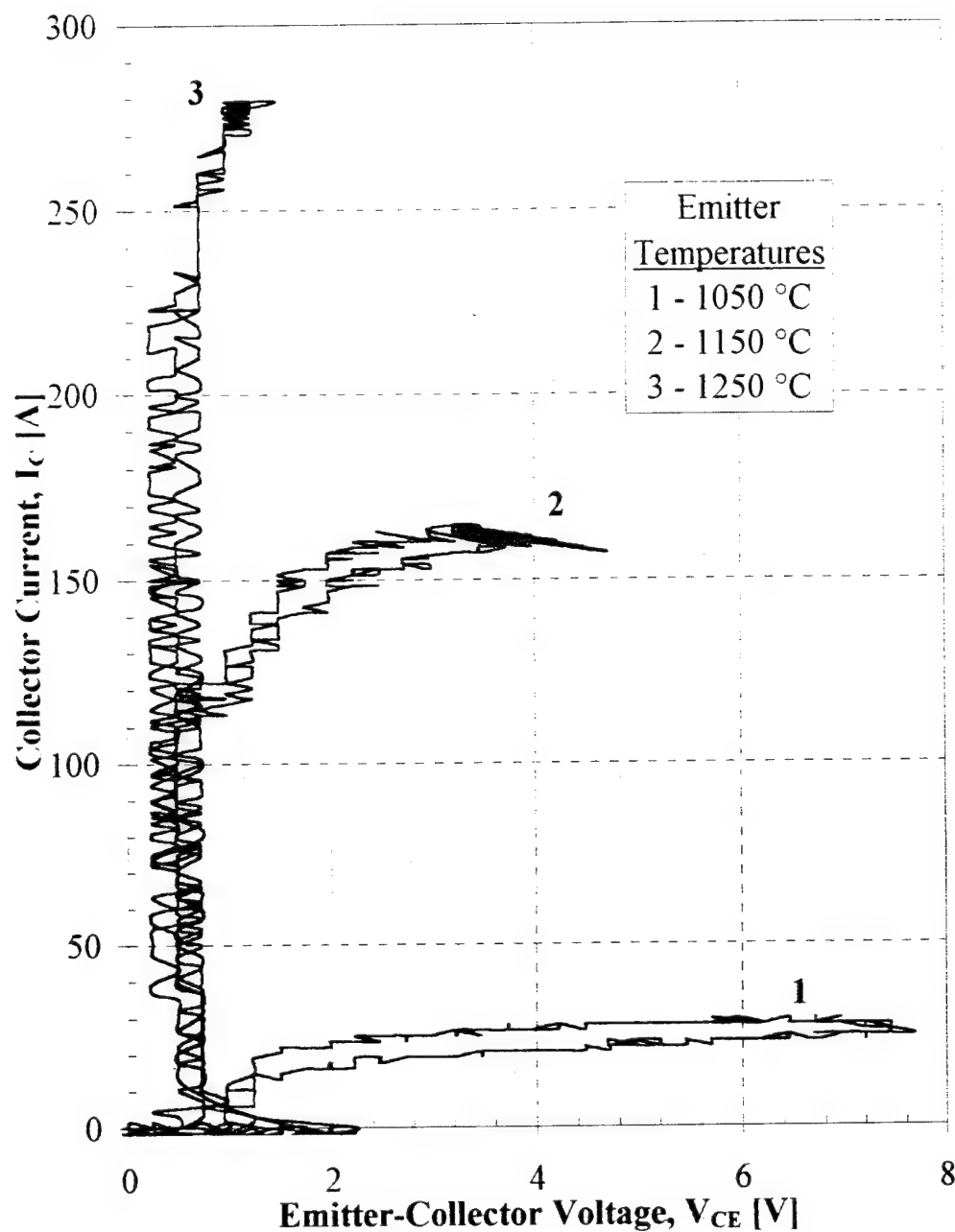
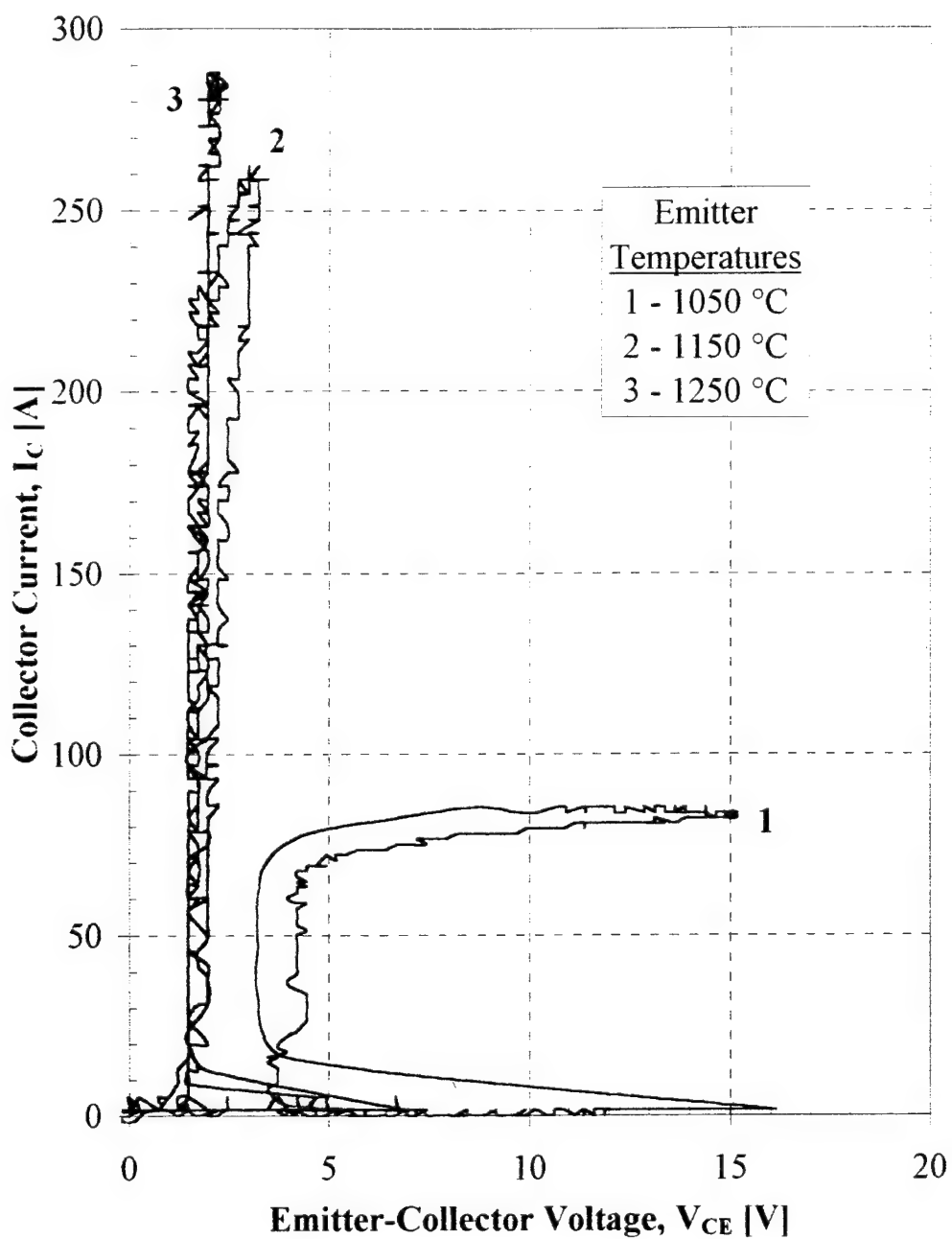


Figure 4.10. Effect of Emitter Temperature on the Forward Voltage Drop,  $V_{CE}$ , for Device 1 at  $T_G = 155\text{ °C}$  ( $P_G = 11\text{ mTorr}$ ),  $T_{Ba} = 575\text{ °C}$  ( $P_{Ba} = 1.4\text{ mTorr}$ ) (Data sweeps are h110114, h100329, and h110127 for curves 1, 2, and 3, respectfully.).



**Figure 4.11.** Effect of Emitter Temperature on the Forward Voltage Drop,  $V_{CE}$ , for Device 2 at  $T_{Cs} = 130\text{ °C}$  ( $P_{Cs} = 3.1\text{ mTorr}$ ),  $T_{Ba} = 600\text{ °C}$  ( $P_{Ba} = 2.9\text{ mTorr}$ ) (Data sweeps are h103056, h103053, and h110133 for curves 1, 2, and 3, respectfully.).

Previous tacitron studies show that the minimum forward voltage drop decreases with an increase in emitter temperature (at fixed Cs and Ba vapor pressure) near the ‘normal’ operating temperature. At the same time, the increase in emitter temperature raises the ‘knee’, corresponding to increased current conduction (Murray & El-Genk 1993 and Wernsman & El-Genk 1994).

As mentioned earlier, the emitter temperature ( $T_E$ ) of the devices was varied to three temperatures: 1050 °C, 1150 °C, and 1250 °C. Figure 4.10 illustrates the performance of the first high-current tacitron device (Device 1). The data were taken at constant cesium and barium temperatures of  $T_{Cs} = 155$  °C ( $P_{Cs} = 11$  mTorr) and  $T_{Ba} = 575$  °C ( $P_{Ba} = 1.4$  mTorr) while the emitter temperature was taken at the three designated temperatures. The forward voltage drop decreased from 1.2 V for the low emitter temperature to 0.5 V for the highest emitter temperature. Table 4.3 summarizes the effects of emitter temperature on the forward voltage drop of Device 1.

**Table 4-3 Effects of Emitter Temperature on Device 1 at  $T_{Cs} = 155$  °C ( $P_{Cs} = 11$  mTorr) and  $T_{Ba} = 575$  °C ( $P_{Ba} = 1.4$  mTorr)**

EMITTER TEMPERATURE	FORWARD VOLTAGE DROP	‘KNEE’ CURRENT
1050 °C	1.2 V	22 A
1150 °C	0.8 V	120 A
1250 °C	0.5 V	250 A

Figure 4.11 illustrates the performance of Device 2 at constant cesium and barium temperatures of  $T_{Cs} = 130$  °C ( $P_{Cs} = 3.1$  mTorr) and  $T_{Ba} = 600$  °C ( $P_{Ba} = 2.9$  mTorr).

Increasing  $T_E$ , for Device 2 lowered the forward voltage drop from 3.8 V to 1.6 V. Table 4.4 summarizes the effects of emitter temperature on Device 2.

**Table 4-4 Effects of Emitter Temperature on Device 2 at  $T_{Cs} = 130\text{ }^{\circ}\text{C}$  ( $P_{Cs} = 3.1\text{ mTorr}$ ) and  $T_{Ba} = 600\text{ }^{\circ}\text{C}$  ( $P_{Ba} = 2.9\text{ mTorr}$ )**

EMITTER TEMPERATURE	FORWARD VOLTAGE DROP	'KNEE' CURRENT
1050 $^{\circ}\text{C}$	3.8 V	75 A
1150 $^{\circ}\text{C}$	1.8 V	215 A
1250 $^{\circ}\text{C}$	1.6 V	285 A

#### 4.2.2.2 Effect of Cs Pressure

The Cs and Ba pressures listed throughout this text are those related to the particular reservoir. These reservoir pressures are not the interelectrode gap pressures. Since there is a temperature gradient that exists between the reservoir and interelectrode gap, the reservoir and gap pressures are different, but related. Appendix A gives the relationships of the reservoir pressures to the gap pressures for both Cs and Ba. Throughout the text, for simplicity, only the reservoir pressures (via measured temperatures) are given.

As shown in Figure 4.12, the Cs pressure has some effect on the forward voltage drop. The decrease in forward voltage drop is due to the plasma density increase associated with higher Cs temperatures. From the figure, the forward voltage drop decreases from 3.8 V to 1.6 V for  $T_{Cs} = 130\text{ }^{\circ}\text{C}$  (3.1 mTorr) and  $T_{Cs} = 180\text{ }^{\circ}\text{C}$  (33 mTorr), respectfully. Decreasing the forward voltage drop by increasing the Cs pressure can result in an

increase in the switching efficiency. However, modulation performance of the device is also strongly dependent on the Cs vapor pressure. Cesium reservoir temperatures greater than 140 °C (> 5 mTorr) significantly decrease grid control over discharge extinction (Wernsman & El-Genk 1994).

#### 4.2.2.3 Effect of Ba Pressure

Previous publications have stated that the Ba pressure does not affect the forward voltage drop, but does affect the thermal emission, that is, the thermal saturation current, or 'knee' (Wernsman & El-Genk 1994, Murray & El-Genk 1993, and El-Genk et al. 1994). However, as can be seen in Figure 4.13, the voltage drop of the high-current device is affected by the Ba pressure. The lower  $P_{Ba}$  data, corresponding to curve 1, have a significantly larger forward voltage drop than the curves at higher  $P_{Ba}$ .<sup>2</sup> Luke (1994) suggests that this higher drop at lower Ba pressure could be due to changes in the electrode work functions (relative to Cs alone), and are partly due to the oscillations in the I-V curve at lower  $P_{Ba}$ . The oscillations increase electron temperature (and ion leakage) and reduce the Cs pressure in the gap, increasing the forward voltage drop. As shown in Figure 4.13, increasing the Ba pressure reduces the oscillations and forward voltage drop, while increasing the conduction current. Table 4.5 summarizes the effects of Ba pressure on the forward voltage drop of Device 2.

---

<sup>2</sup> Curve 1 represents a drastic increase in  $V_f$  relative to the other curves in the figure and is atypical for observed changes of  $P_{Ba}$  alone. The data for curve 1 were chosen to illustrate the oscillation effects associated with lower  $P_{Ba}$ . Typical fractional increases in  $V_f$  associated with lower  $P_{Ba}$  were on the order of < 10% for the temperature changes indicated in the figure and are indicative to what Luke (1994) observed.

**Table 4-5** Effects of Barium Pressure on Device 2 at  $T_E = 1250\text{ }^\circ\text{C}$  and  $T_{Cs} = 130\text{ }^\circ\text{C}$   
( $P_{Cs} = 3.1\text{ mTorr}$ )

<b>Ba RESERVOIR TEMPERATURE</b>	<b>FORWARD VOLTAGE DROP</b>	<b>'KNEE' CURRENT</b>
550 $^\circ\text{C}$	5.4 V	125 A
575 $^\circ\text{C}$	2.0 V	$\sim 240\text{ A}$
600 $^\circ\text{C}$	1.8 V	$\sim 270\text{ A}$

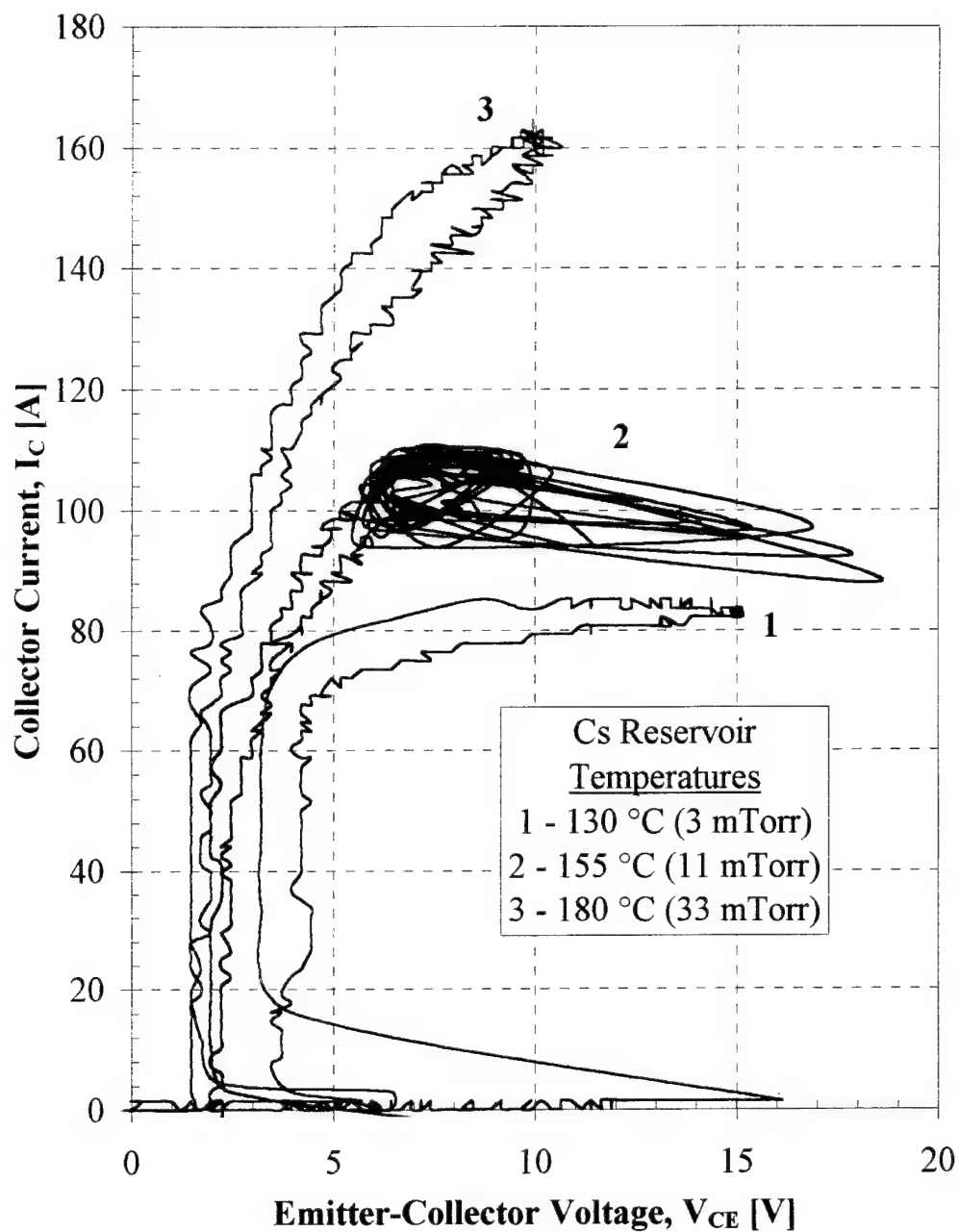


**Figure 4.12.** Effect of Cesium Pressure on the Forward Voltage Drop,  $V_{CE}$ , for Device 2 at  $T_E = 1050$  °C,  $T_{Ba} = 600$  °C ( $P_{Ba} = 2.9$  mTorr) (Data sweeps are h103056, h110119, and h103019 for curves 1, 2, and 3, respectively.).

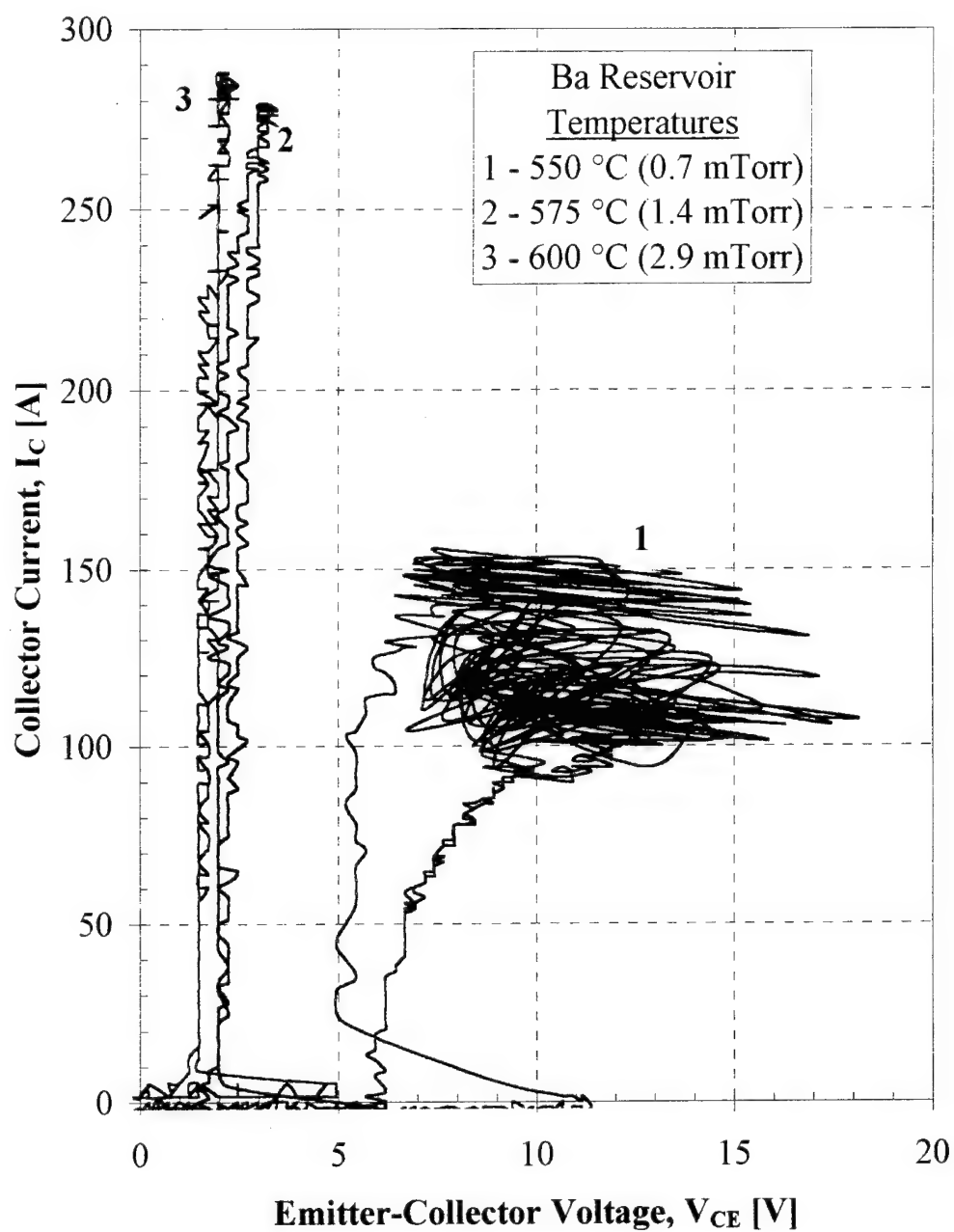


Figure 4.13. Effect of Barium Pressure on the Forward Voltage Drop,  $V_{CE}$ , for Device 2 at  $T_E = 1250$  °C,  $T_{Cs} = 130$  °C ( $P_{Cs} = 3.1$  mTorr) (Data sweeps are h110140, h110133, and h103044 for curves 1, 2, and 3, respectively.).

These results, similar to what Luke (1994) found, suggest that the low pressure barium vapor does contribute to the plasma density in some fashion. Luke states that it could be argued that this phenomena is caused by a relative Ba coverage on the electrode surfaces. Changes in this coverage affect the desorption of Cs from the electrodes, and therefore affect the discharge. There could also be an effect related to low emission, that is, fewer electrons are emitted from the cathode resulting in decreased Cs ionization.

#### **4.2.2.4 Effect of the Grid**

Murray and El-Genk (1993) found that the presence of a grid contributed to a higher forward voltage drop as compared to the diode version of their device. They compared the I-V operational characteristics of their device both as a diode and triode. The increase in voltage drop is attributed to the grid sheaths that form when the device is operating.

Wernsman and El-Genk (1996) have extensively studied grid structure on a demountable planar tacitron. They found that the forward voltage drop decreased with increasing grid transparency. Also, they found that the forward voltage drop decreased with increasing grid-anode spacing in the range of 1 - 2.5 mm, but was insensitive to cathode-grid spacing over the same range. Above 40% grid transparency, the relative decrease in forward voltage drop with increasing grid transparency is small (at constant Cs pressure). However, grid control over the discharge current decreased with decreased transparency and/or increased aperture size. Lowering the grid transparency made the device easier to extinguish, but harder to ignite.

Although the relatively large thick grid of the high-current tacitron was not used during I-V mode testing, its presence and large surface area could modify the desorption rate of

Cs and the plasma in general, affecting, though it is not precisely known to what extent, the forward voltage drop.

#### **4.2.2.5 High-Current Devices Comparison**

It should be noted that Device 1 had been operated previous to the experiments covered in this paper (Masten et al. 1995a, b) and that Device 2 had not. Although the two devices are identical in construction, their operating performance differed significantly. Device 2 consistently performed better, in that its performance was predictable, reliable, and produced better conduction currents at low forward voltage drops. The performance of Device 1 changed from the experiments conducted by Masten et al. (1995a) to the experiments covered in this report. At the beginning of testing, Device 1 performed predictably and results similar to what Masten et al. (1995a, b). had obtained were reproducible. However, the performance of Device 1 became very erratic, unpredictable, and non-reproducible by the end of the testing. The reason for this performance deterioration could not be found, other than it may be attributed to effects incurred during its first operation. It seems that the performance of Device 1 got progressively worse throughout the experiments. Toward the end of the experiments, Device 1 appeared to have very small forward voltage drops and ignition voltages as if the entire I-V curve for Device 1 had been shifted to the left. This would indicate that there was some sort of inherent electric field buildup within the device that was disrupting its operation. Tests were conducted to try and measure a 'ghost' voltage, but failed. The true origin of this phenomenon and the reason for the device's deterioration are not known. Figure 4.14 illustrates the shifting of the forward voltage drop and ignition

voltage for Device 1 over the experimental cycle. The average forward drop decreased from 1.69 V to 0.91 V over the three-day period - a 46% decrease. The average ignition voltage decreased from 4.17 V to 2.82 V - a 32% decrease.

This work does not attempt to discuss further the performance change and presumed failure of Device 1, nor does it expand upon the operating performance difference between Device 1 and Device 2. These differences are simply noted, but are not elaborated upon in the context of this thesis. Characterization of the devices only encompasses the generalized effects of the operating parameters under certain conditions and, to some extent, the operating limitations. Throughout the rest of the text, only the performance data for Device 2 is reported unless indicated otherwise.

#### **4.2.2.6 Optimal Performance Parameters**

Figure 4.15 shows the optimal I-V performance for each device under the stated experimental parameters. Device 1 had a maximum conduction current,  $I_C$ , of about 275 A ( $V_f = 0.5$  V at thermal emission current density of 8.6 A/cm<sup>2</sup>) while Device 2 had a maximum  $I_C$  of 280 A ( $V_f = 1.5$  V at thermal emission current density of 9.0 A/cm<sup>2</sup>).

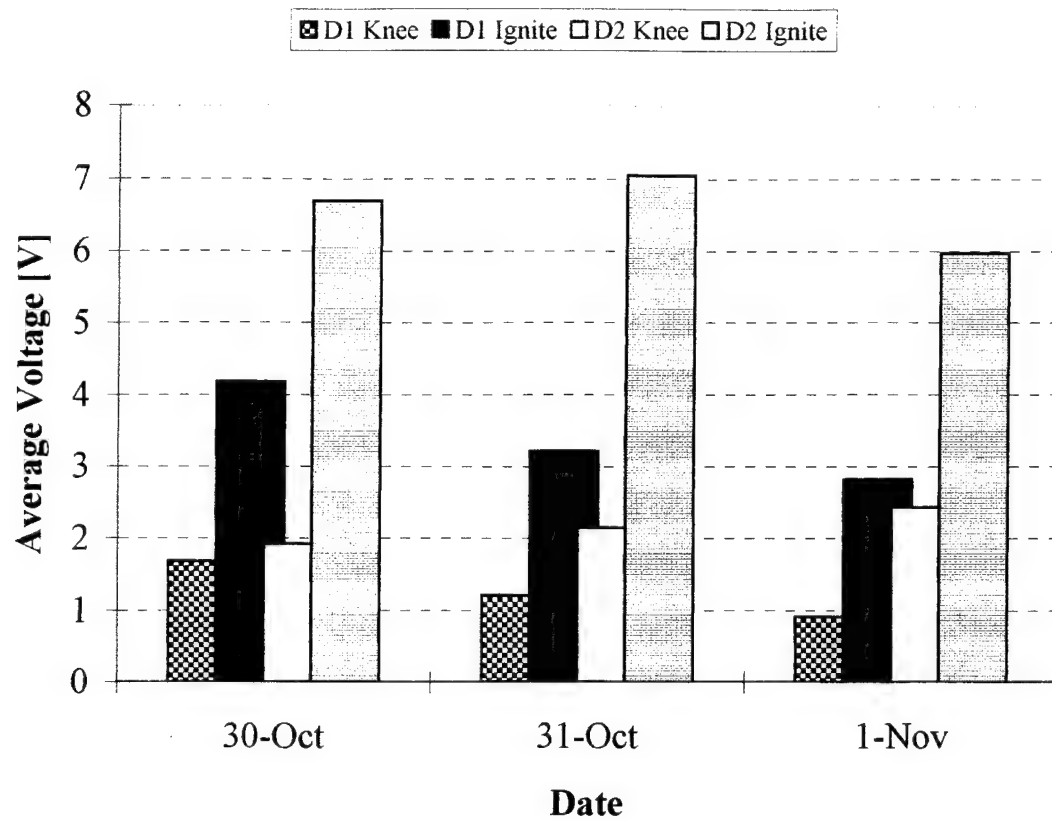


**Figure 4.14. Average Forward Voltage Drop and Ignition Voltages for the High-Current Cs-Ba Tacitrons as Diodes Over Experiment Duration (Each Device Under Identical Conditions.).**

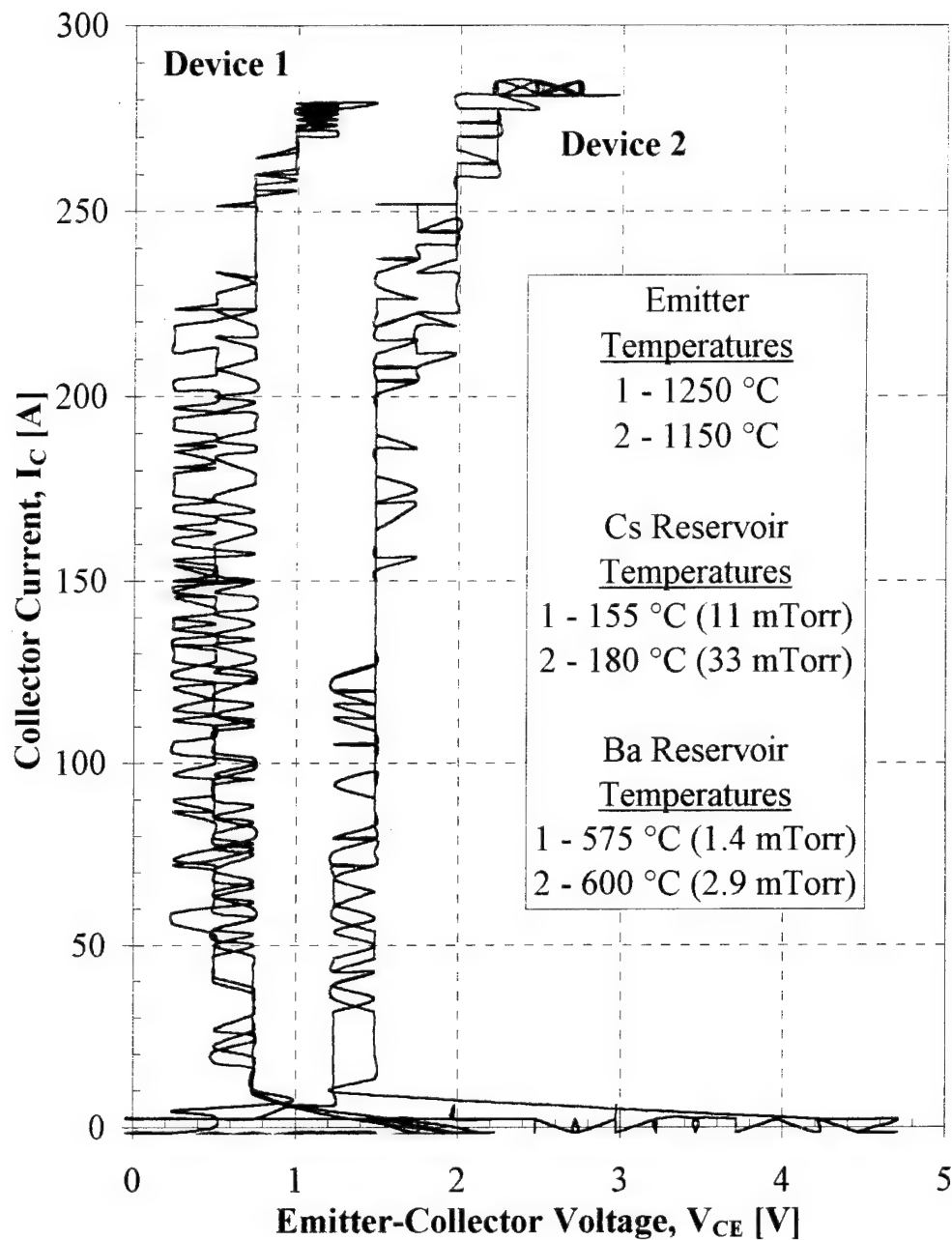


Figure 4.15. Optimal I-V Performance of the High-Current Cs-Ba Tacitrons as Diodes (Data sweeps are h110127 for Device 1 & h103029 for Device 2.).

### 4.2.3 Current Modulation

During current modulation, the grid is biased in order to control the ignition (turn on) and extinguishing (turn off) of the device. In the current modulation mode, once ignited by a positive grid bias, the device will either shut off without the application of a negative bias (self-extinguishing); the device will extinguish randomly with an applied grid bias (unstable modulation); or the device will turn on and off with the application of a positive or negative grid bias, respectfully (stable modulation). Stable modulation is a function of the Cs pressure, current density, grid structure, and the thermal emission current density.

A grid trigger unit for each of the high-current devices was designed and constructed by a visiting Russian scientist from the Kurchatov Institute, Moscow.<sup>3</sup> The grid trigger was designed to provide ignition and extinguishing grid pulses ( $V_{g+}$  and  $V_{g-}$ , respectfully) of up to 85 V in amplitude at peak currents of 50 A. Modulation frequency can be varied in the range of  $f_m = 2 - 10$  kHz, and a grid pulse risetime of  $t_{rg+} = 100$  ns into a non-reactive load. Grid pulse duration can be varied in the range of  $t_{g+} = 10 - 50$   $\mu$ sec, and pulse duration and amplitude can be set independently for both the ignition pulse and the extinguishing pulse (Masten et al. 1995b).

#### 4.2.3.1 Extinguishing

In most of the devices described in Chapter 3, current interruption was accomplished by removing the collector bias or by sufficient sheath build-up around the grid. Kaibyshev

---

<sup>3</sup> Djachiachvili, I. (1995). Designer and Developer of the High-Current Cs-Ba Tacitron Grid Trigger Unit, Contracted with the KIAE, Moscow, Russia through ORION International Technologies, Albuquerque, New Mexico.

and Kuzin (1975) suggest that the extinguishing mechanism for the 'thick-grid' tacitron is different. For thick-grid tacitrons with relatively large apertures, such as the high-current Cs-Ba tacitron, they attribute the dominant extinguishing mechanism to a plasma instability induced by the removal of heavy components (atoms and ions) from the discharge region.

#### 4.2.3.2 Modulation Performance

Masten et al. (1995b) conducted preliminary modulation experiments on one of the high-current tacitrons (Device 1). During those experiments a serious limitation in the data not indicative of the fundamental limitations of the high-current tacitron performance was observed: low collector bias,  $V_{cc}$  ( $< 15$  V). They found that the low collector bias was necessary to prevent self-ignition of the device because the trigger circuit allowed the grid to float at near collector potential. In turn, this limited the magnitude of the discharge current (20 - 55 A).

Masten et al. were able to modulate at frequencies in the range of 3 - 12 kHz for  $T_{Cs} = 130 - 145$  °C (3.1 - 6.7 mTorr). They found that the device was more difficult to ignite and easier to extinguish at higher frequencies, and the forward voltage drop is greater at higher frequencies. They attributed these effects to lower effective plasma density in the discharge region at the higher frequency which could be mitigated by higher Cs pressures at higher modulation frequencies. In fact, they found that a higher  $T_{Cs}$  (141 °C) required a lower grid ignition voltage,  $V_{g+}$  (+40 V) and collector bias  $V_{cc}$  (7.4 V), to prevent self-ignition with the floating grid, which resulted in a lower forward voltage drop,  $V_f$  (3.1 V), and a larger conduction current fall time  $t_{fc}$  (28  $\mu$ s). The lower required

ignition voltage resulted in a larger ignition delay time,  $t_{d+}$  (20  $\mu$ s), and a lower ignition current,  $I_{g+}$  (11 A).

New modulation experiments for the high-current tacitron were also intended as preliminary tests in order to increase the collector bias and optimize frequency. Table 4.6 summarizes the modulation parameters from the previous modulation.

**Table 4-6 Modulation Parameters From Preliminary Tests of the High-Current Demountable Cs-Ba Tacitron (Device 1 Only)**

Parameter	Symbol	SC623-03	SC623-12	SC623-19	SC623-25
Emitter temperature	$T_E$	1038 °C	1033 °C	1033 °C	1030 °C
Barium reservoir temperature	$T_{Ba}$	554 °C	554 °C	554 °C	552 °C
Cesium reservoir temperature	$T_{Cs}$	134 °C	134 °C	134 °C	141 °C
Modulation frequency	$f_m$	3.7 kHz	12 kHz	12 kHz	4.0 kHz
Grid ignition pulse voltage	$V_{g+}$	+68 V	+86 V	+86 V	+40 V
Grid extinguishing pulse voltage	$V_{g-}$	-83 V	-83 V	-85 V	-85 V
Grid ignition pulse duration	$t_{g+}$	52 $\mu$ s	15 $\mu$ s	35 $\mu$ s	52 $\mu$ s
Grid extinguishing pulse duration	$t_{g-}$	44 $\mu$ s	9 $\mu$ s	28 $\mu$ s	47 $\mu$ s
Grid ignition pulse current	$I_{g+}$	21 A	25 A	44 A	11 A
Grid extinguishing pulse current	$I_{g-}$	6.0 A	2.7 A	2.1 A	2.1 A
Grid ignition pulse current risetime	$t_{rg+}$	16 $\mu$ s	13 $\mu$ s	14 $\mu$ s	22 $\mu$ s
Collector bias voltage	$V_{cc}$	14.5 V	13.8 V	12.6 V	7.24 V
Conduction voltage drop	$V_f$	4.1 V	3.7 V	4.4 V	3.1 V
Conduction current, peak/mean	$I_c$	54 A/41A	53 A/29 A	47 A/27 A	21 A/5 A
Collector current risetime	$t_{rc}$	37 $\mu$ s	24 $\mu$ s	26 $\mu$ s	38 $\mu$ s
Collector current fall time	$t_{fc}$	20 $\mu$ s	0.7 $\mu$ s	1.5 $\mu$ s	28 $\mu$ s
Ignition delay time	$t_{d+}$	9.3 $\mu$ s	8.6 $\mu$ s	9.5 $\mu$ s	20 $\mu$ s
Extinguishing delay time	$t_{d-}$	3.0 $\mu$ s	1.2 $\mu$ s	1.2 $\mu$ s	1.3 $\mu$ s

The cesium reservoir temperature for the new current modulation tests was in the range  $T_{Cs} = 126 - 132$  °C ( $P_{Cs} = 2.5 - 3.4$  mTorr) while barium reservoir temperature ranged  $T_{Ba}$

= 548 - 553 °C ( $P_{Ba}$  = 0.6 - 0.8 mTorr). The emitter temperature ranged  $T_E$  = 1050 - 1100 °C. Under these operating parameters, conduction currents of up to 80 A and modulation frequencies up to 12 kHz were observed. Collector bias voltages,  $V_{cc}$ , of up to 30 V were also achieved - this being an improvement to the previous modulation data for the high-current device. Shut-off of the device was demonstrated to be very fast. Collector current fall times,  $t_{fc}$ , averaged less than 2  $\mu$ s. Table 4.7 summarizes the modulation parameters for several tests at similar operating parameters. Figures 4.16 through 4.19 illustrate the modulation performance under the operating parameters in Table 4.7.

**Table 4-7 Modulation Parameters From Preliminary Tests of the High-Current Demountable Cs-Ba Tacitron**

Parameter	Symbol	1108-005	1108-006	1117-010	1117-012
Emitter temperature	$T_E$	1050 °C	1050 °C	1050 °C	1050 °C
Barium reservoir temperature	$T_{Ba}$	553 °C	553 °C	548 °C	548 °C
Cesium reservoir temperature	$T_{Cs}$	132 °C	132 °C	126 °C	126 °C
Modulation frequency	$f_m$	3.8 kHz	7 kHz	4.7 kHz	6.6 kHz
Grid ignition pulse voltage	$V_{g+}$	+45 V	+45 V	+30 V	+30 V
Grid extinguishing pulse voltage	$V_{g-}$	-80 V	-80 V	-70 V	-70 V
Grid ignition pulse duration	$t_{g+}$	45 $\mu$ s	40 $\mu$ s	57 $\mu$ s	53 $\mu$ s
Grid extinguishing pulse duration	$t_{g-}$	34 $\mu$ s	37 $\mu$ s	40 $\mu$ s	46 $\mu$ s
Grid ignition pulse current	$I_{g+}$	14 A	14 A	14 A	17 A
Grid extinguishing pulse current	$I_{g-}$	7 A	4 A	8.3 A	10.6 A
Grid ignition pulse current risetime	$t_{rg+}$	13 $\mu$ s	13 $\mu$ s	6 $\mu$ s	15 $\mu$ s
Collector bias voltage	$V_{cc}$	18 V	18 V	12.6 V	7.24 V
Conduction voltage drop	$V_f$	4.8 V	5.3 V	5.6 V	1.9 V
Conduction current, peak/mean	$I_c$	66 A/42 A	65 A/35 A	60 A/27 A	59 A/12 A
Collector current risetime	$t_{rc}$	36 $\mu$ s	35 $\mu$ s	45 $\mu$ s	36 $\mu$ s
Collector current fall time	$t_{fc}$	0.4 $\mu$ s	1.8 $\mu$ s	0.6 $\mu$ s	2.1 $\mu$ s
Ignition delay time	$t_{d+}$	2.7 $\mu$ s	9.7 $\mu$ s	14.5 $\mu$ s	12 $\mu$ s
Extinguishing delay time	$t_{d-}$	1.0 $\mu$ s	1.2 $\mu$ s	0.5 $\mu$ s	2.2 $\mu$ s

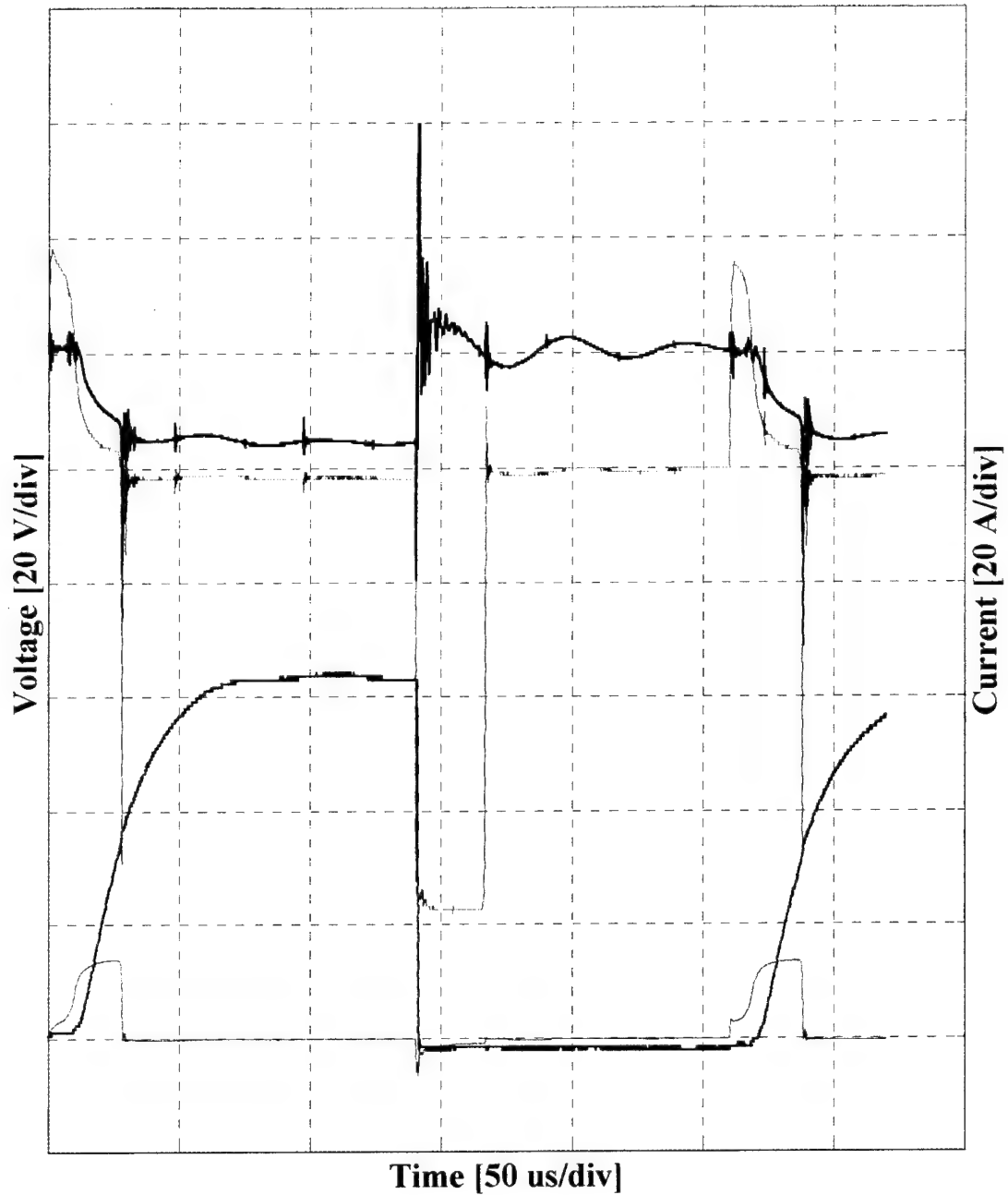


**Figure 4.16. Modulation Test 1108-005 of the High-Current Cs-Ba Tacitron (Grid (Fine) and Collector (Bold) Voltage Waveforms are at the Top of the Figure, While Grid (Fine) and Collector (Bold) Current Waveforms are at the Bottom.).**

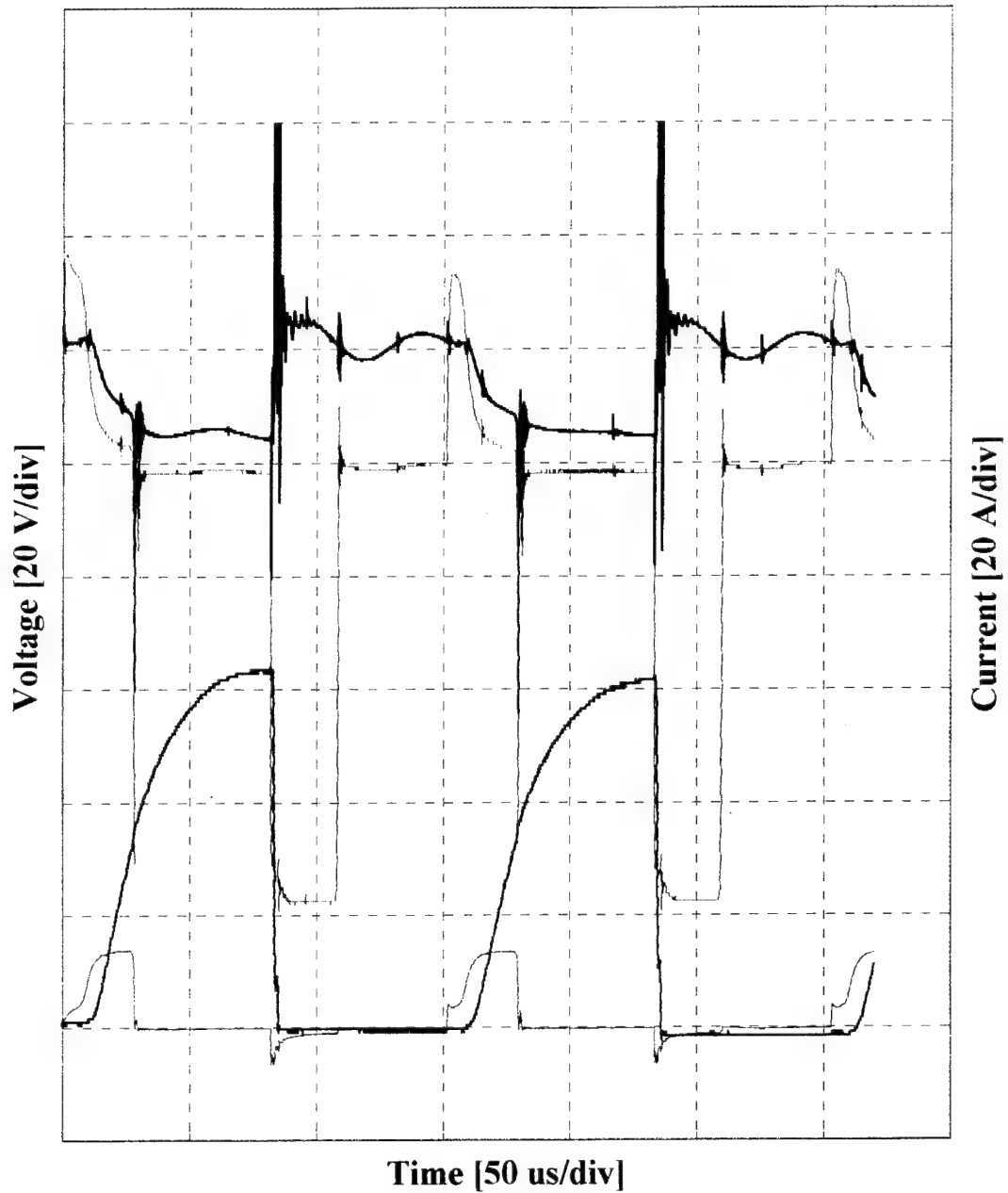


**Figure 4.17. Modulation Test 1108-006 of the High-Current Cs-Ba Tacitron (*Grid (Fine) and Collector (Bold) Voltage Waveforms are at the Top of the Figure, While Grid (Fine) and Collector (Bold) Current Waveforms are at the Bottom.*).**

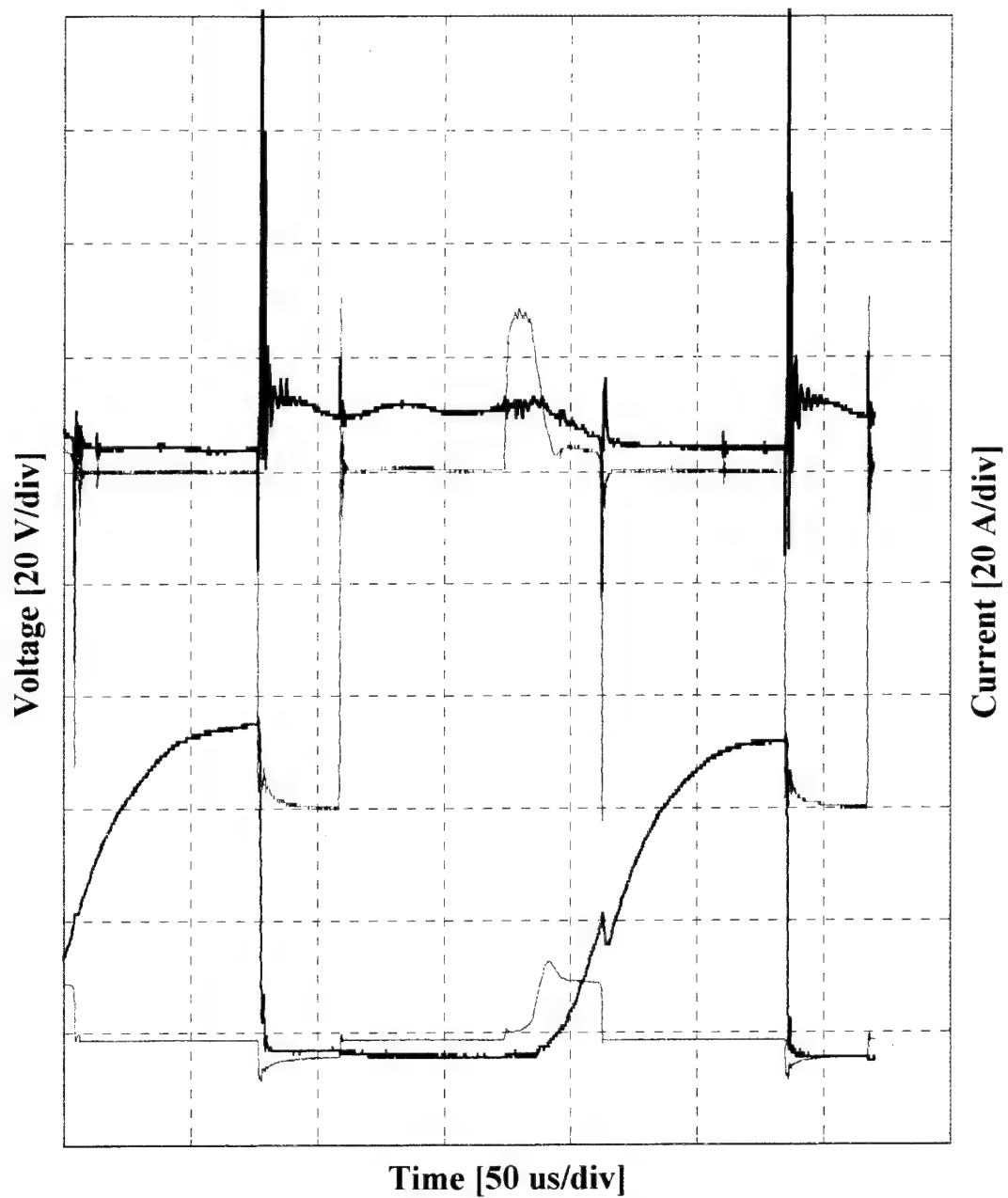


**Figure 4.18. Modulation Test 1117-010 of the High-Current Cs-Ba Tacitron (Grid (Fine) and Collector (Bold) Voltage Waveforms are at the Top of the Figure, While Grid (Fine) and Collector (Bold) Current Waveforms are at the Bottom.).**

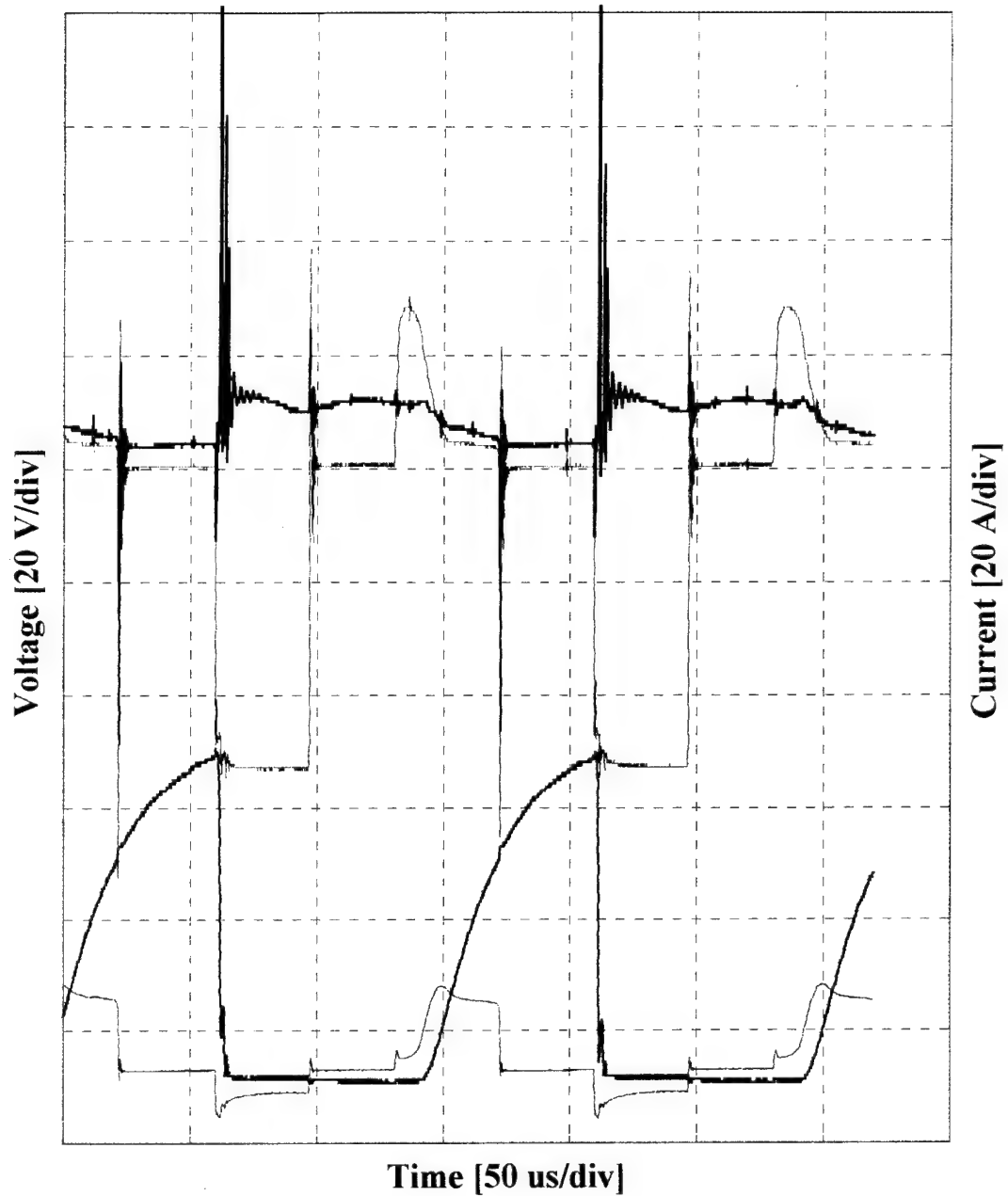


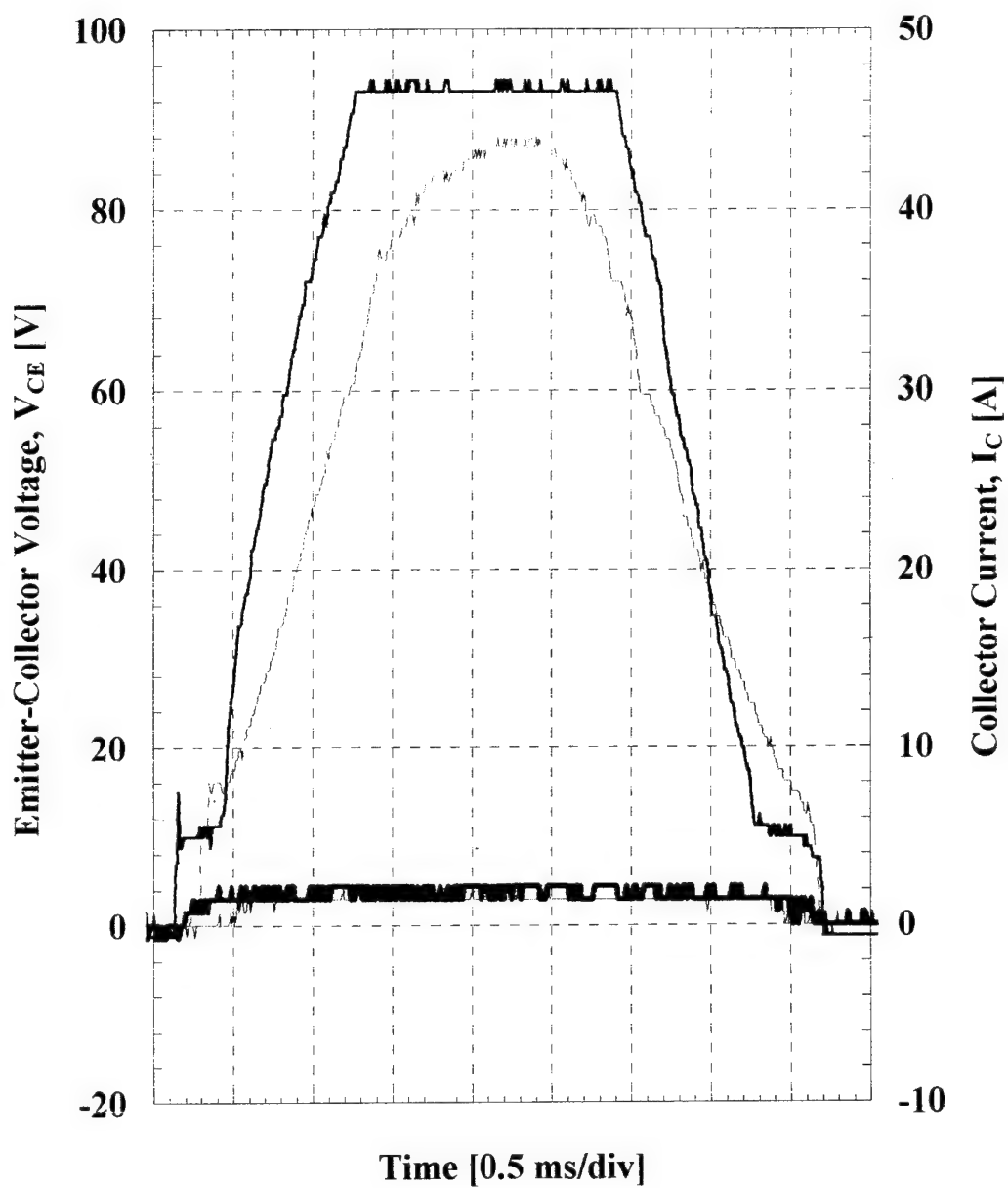
**Figure 4.19. Modulation Test 1117-012 of the High-Current Cs-Ba Tacitron (Grid (Fine) and Collector (Bold) Voltage Waveforms are at the Top of the Figure, While Grid (Fine) and Collector (Bold) Current Waveforms are at the Bottom.).**

The high-current Cs-Ba tacitron has demonstrated reduced-power current modulation. The physical size of the device does not appear to limit the extinguishing time. The collector current risetimes of  $t_{rc} = 32 - 60 \mu\text{s}$ , for collector bias of  $V_{cc} = 7 - 18 \text{ V}$  are relatively longer than those of Murray and El-Genk's (1993) cylindrical device. The differences are probably due to the low collector bias voltages associated with the high-current tacitron modulation tests. The cesium reservoir temperatures in the range  $T_{Cs} = 126 - 145 \text{ }^\circ\text{C}$  (2.5 - 6.7 mTorr) necessary to achieve current modulation are similar to those of a triangular aperture grid device tested by Djachiachvili and El-Genk (1993) ( $T_{Cs} = 140 - 154 \text{ }^\circ\text{C}$  (5.2 - 10 mTorr)). The triangular grid was similar in construction and size to the large, thick grid of the high-current device. The high grid transparency of the high-current tacitron (65%) requires a relatively low cesium pressure to achieve reliable discharge extinction and to prevent self-ignition at a collector bias greater than approximately  $V_{cc} = 10 - 20 \text{ V}$ .

#### 4.2.4 Voltage Hold-Off

The only voltage hold-off experiments conducted with the high-current tacitron were done by Masten et al. (1995a) and were preliminary at best. The voltage hold-off measurements of the device were taken with the grid electrode grounded to the emitter. The applied collector potential was a half-sine of 3.6 ms duration. Masten et al. found that voltage hold-off exceeded 125 V at  $T_E = 1070 \text{ }^\circ\text{C}$ ,  $T_{Ba} = 560 \text{ }^\circ\text{C}$  ( $P_{Ba} = 0.9 \text{ mTorr}$ ), and  $T_{Cs} = 135 \text{ }^\circ\text{C}$  (4 mTorr) at less than 2 A leakage current. Figure 4.19 illustrates these preliminary voltage hold-off measurements. The plateau at 93 V in the 125 V pulse of

Figure 4.20 was caused by saturation of a measurement buffer amplifier in the data acquisition system.



## 5. SUMMARY AND CONCLUSIONS

The high-current Cs-Ba tacitron is a planar device similar in construction to the planar Cs-Ba device most recently tested by the ISNPS. However, the electrode surface areas of the high-current device are nearly 15 times that of the planar Cs-Ba tacitron ( $\sim 28 \text{ cm}^2$  vs.  $\sim 2 \text{ cm}^2$ ). Also, the grid structure and transparency differ from that of the planar device. The high-current device is considered a thick grid ( $\sim 1 \text{ mm}$ ) device and has a hexagonal ribbon-hole ( $\sim 1 \text{ mm}$  in diameter) grid geometry while the planar device has a circular hole geometry ( $\sim 0.4 \text{ mm}$  in diameter). The grid transparency of the high-current device is nearly twice that of the planar device ( $\sim 65\%$  vs.  $\sim 34\%$ ) as is the grid thickness ( $\sim 1 \text{ mm}$ ) (El-Genk et al. 1994).

Preliminary operational characterization of the high-current Cs-Ba tacitron has been completed. The device's performance under various operating parameters of emitter temperature, cesium pressure, and barium pressure in the I-V mode has been presented. In addition, preliminary modulation and voltage hold-off performance were investigated and presented.

Effects of the emitter temperature were investigated at three temperatures:  $T_E = 1050^\circ\text{C}$ ,  $1150^\circ\text{C}$ , and  $1250^\circ\text{C}$  while maintaining constant pressures in the Cs and Ba reservoirs. As with previous tacitrons, an increase in emitter temperature decreased the forward voltage drop,  $V_f$ , of the device while at the same time, raised the 'knee' current,  $I_k$ . Emitter temperature primarily affects emission current, but also affects  $V_f$ . Increased emitter temperature increases thermionic emission of the emitter yielding higher thermal emission currents ('knee' current). Also, increased emitter temperatures (and

emission) have the effect of increasing the external load impedance which, in turn, increases the external voltage drop allowing the drop of the device to decrease (lower switch impedance). The forward voltage drops for the cylindrical, planar, and high-current Cs-Ba tacitrons (in the I-V mode) are in the range of  $V_f = 1.2 - 2.0$  V at emitter operating temperatures of  $T_E = 1050 - 1250$  °C (Murray & El-Genk 1993, Wernsman & El-Genk 1994, and Luke 1994).

As with previous Cs-Ba tacitrons, changes in Cs pressure also affect the forward voltage drop of the high-current device. Changing the Cs pressure, changes the plasma density and therefore changes the stable conduction voltage. It was found, as with the other Cs-Ba tacitrons, that increased Cs pressure lowered the forward voltage drop of the high-current device. The forward voltage drop was more than halved by increasing the Cs pressure by an order of magnitude. For example, by increasing the Cs pressure from  $P_{Cs} = 3.1$  mTorr to 33 mTorr, the forward voltage drop of the high-current device was decreased from  $V_f = 3.8$  V to 1.6 V, respectfully.

The effects of Ba pressure were found to be similar to those associated with emitter temperature. Higher Ba pressures increased the conduction current and decreased the forward voltage drop of the high-current device. The latter is contrary to most previous Cs-Ba tacitron research, except that of Luke (1994). Higher conduction currents are expected with increased Ba pressure because the function of the Ba is to reduce the electrode work function (relative to Cs alone), thereby, increasing the conduction current of the device for a given cathode temperature. Experiments with the high-current device also demonstrated that lower Ba pressures resulted in I-V oscillations and higher voltage

drops. It is assumed that these oscillations increase the forward voltage drop by reducing the Cs plasma pressure. By increasing the Ba pressure from  $P_{Ba} = 1.4$  mTorr to 2.9 mTorr, the forward voltage drop decreased from  $V_f = 2.0$  V to 1.8 V, respectfully, while the 'knee' current increased from  $I_k = 240$  A to 270 A, respectfully.

The high-current Cs-Ba tacitron was shown to be able to conduct up to nearly 10 A/cm<sup>2</sup> with forward voltage drops below 2 V in the I-V mode. These results are comparable to those of the cylindrical and planar Cs-Ba tacitrons (Murray & El-Genk 1993, Wernsman & El-Genk 1994, and Luke 1994). However, as expected, much greater conduction currents were achieved with the high-current device than the previously tested cylindrical and planar devices. Maximum conduction currents in the I-V mode were more than an order of magnitude greater in the high current device ( $\sim 280$  A) than that of the planar device ( $\sim 10 - 15$  A) (Wernsman & El-Genk 1994). The maximum conduction currents were due to the much larger electrode surface areas resulting in increased emitter emission currents of the high-current device and higher operating pressures of the Cs and Ba reservoirs ( $P_{Cs} = 11 - 33$  mTorr,  $P_{Ba} = 1.4 - 2.9$  mTorr). These results indicate that the previously tested Cs-Ba tacitrons and the high-current Cs-Ba tacitron operate in similar fashion in the I-V mode. Also, this indicates that the combined increase in grid transparency and thickness of the high-current device, compared to the planar device, is sufficient to achieve the current densities and voltage drops of its precursor. Further, these results may indicate a scaling relationship: a magnitude increase in electrode surface area yields a magnitude increase in maximum conduction current. However, further

analysis is necessary to examine device performance related to electrode area and conduction current in conjunction with grid size and geometry.

Preliminary modulation performance of the high-current Cs-Ba tacitron was investigated for Cs reservoir pressures in the range of  $P_{Cs} = 2.5 - 6.7$  mTorr. Stable modulation frequencies of up to  $f_m = 12$  kHz were observed with very low collector bias at voltage drops of less than  $V_f = 5$  V and current densities of  $> 2$  A/cm<sup>2</sup>. These frequencies and densities are slightly lower than that achieved with the cylindrical and planar Cs-Ba tacitrons. The planar tacitron was shown to modulate up to 5 A/cm<sup>2</sup> at  $f_m = 22$  kHz, at a forward voltage drop of  $V_f = 2.2$  V (El-Genk et al. 1994). A potential scaling factor could be argued here as well because the grid of the high-current device is twice as thick as that of the other Cs-Ba tacitrons and modulates at about half the frequency. Again, further analysis of grid size and geometry is necessary to substantiate a 'scaling' hypothesis. Low collector bias was necessary to prevent self-ignition of the device because the prototype trigger circuit allowed the grid to float at near collector potential. The low discharge current during modulation of the high-current device is limited by the collector bias.

Preliminary voltage hold-off experiments for the high-current device showed that hold-off exceeds 125 V at  $T_E = 1070$  °C,  $P_{Ba} = 0.9$  mTorr, and  $P_{Cs} = 4$  mTorr. El-Genk et al. (1991) report a voltage hold-off of the cylindrical device as 170 V at  $T_E = 1170$  °C,  $P_{Ba} = 0.2$  mTorr, and  $P_{Cs} = 11$  mTorr. Wernsman and El-Genk (1996) report voltage hold-offs exceeding 200 V for the planar device. Voltage hold-off for the high-current tacitron was limited by the circuit power supply.

The high-current Cs-Ba tacitron has demonstrated it performs similarly to previous Cs-Ba tacitrons, indicating that device scaling does not strongly affect performance. Its

operation characteristics during I-V mode and current modulation indicate that the Cs-Ba tacitron does possess some scaling attributes that deserve further study. These, with the preliminary performance parameters above, indicate that the high-current tacitron switch is comparable to conventional solid-state devices at average potential power switching densities in excess of 1 kW/cm<sup>2</sup>. In addition, because the tacitron is inherently temperature and radiation hard, it is well-suited to be used in conjunction with a space nuclear power system or in terrestrial applications of extreme temperature and/or radiation.

## 6. FUTURE WORK

The research up to now on the high-current Cs-Ba tacitron has consisted of a preliminary performance characterization. Further characterization of the device under I-V and current modulation modes of operation is needed to fully comprehend the operating parameters of the device and for analysis on the possible scaling attributes of the high-current device compared to the cylindrical and planar Cs-Ba tacitrons. With this in mind, further characterization should include analyses on electrode size and conduction current in conjunction with grid size and geometry.

A transient model has been developed by the ISNPS for operation of low-pressure Cs-Ba diodes (Luke 1994). The model has been benchmarked with tacitron data collected by the ISNPS. This model could be modified to examine theoretical predicted performance of the high-current device against actual experimental results - further detailing the operating parameters of the device. Modifications would have to account for the much larger planar surface areas of the high-current electrodes, total surface area of the grid (for ion balance equations), and, in general, the thick hexagonal grid design.

The high-current device has demonstrated controlled modulation at reduced power, but further characterization is needed in order to place the device in a high-power inverter circuit. The grid trigger circuit for inverter operation must reliably ignite the discharge in one tacitron while extinguishing the discharge in a second. This grid trigger circuit has already been developed and tested and was used during modulation experiments presented in this work. The goal of inverter operation using two high-current Cs-Ba tacitrons is to determine the feasibility of constructing a 6 kWe continuous power inverter (Masten et al.

1995) for use in a power conditioning unit (PCU) (Appendix B lists the approximate tacitron circuit design parameters for a PCU). Once inverter operation is demonstrated at this power rating, an applicability experiment could be performed on a TOPAZ-II thermionic space nuclear power system.

Efforts to date have focused on fully grid-controlled devices. However, conventional power supply technology relies heavily on switches such as silicon-controlled rectifiers (SCRs) that can be triggered 'on,' but require external commutation to turn 'off.' A Cs-Ba gas switch designed in the same manner as a conventional high-performance hydrogen thyatron could deliver high switching efficiency at the cost of full grid control (See Appendix C). Thyatron mode operation has not been reported for a planar tacitron, but it is expected (based on cylindrical device performance in thyatron mode) that higher conduction current densities can be achieved at lower forward voltage drops (due to higher operating Cs pressures), at the expense of a lower operating frequency than in the tacitron mode case. Unlike the tacitron, less grid energy is needed in the thyatron mode because the device only needs to be turned 'on' via the grid. The maximum steady-state conduction current density during modulation reported by Wernsman and El-Genk (1996) is 5 A/cm<sup>2</sup> and the maximum voltage hold-off is 200 V yielding an average switching power density for the planar Cs-Ba tacitron of 1 kW/cm<sup>2</sup>. High radiation or high temperature applications could greatly benefit from the use of such a Cs-Ba thyatron.

## 7. REFERENCES

- Alcock, C.B., V.P. Itkin, and M.K. Horrigan (1984), "*Vapor Pressure Equations for the Metallic Elements*," Canadian Metallurgical Quarterly, **23**, No. 3, 309-313.
- Ambrus, J. W. Wright, and D. Bunch (1984), "*Review of the Tri-Agency Space Nuclear Reactor Power System Technology Program*," 19th Intersociety Energy Conversion Engineering Conference.
- Angelo, J.A. and D. Buden (1985), *Space Nuclear Power*, Orbit Book Co., Malabar, FL.
- Baksht, F.G., V.B. Kaplan, A.A. Koskin, A.M. Martsinovskii, F.N. Rasulov, N.N. Sveshnikova, V.I. Serbin, and V.G. Yur'ev (1978a), "*Stationary Conducting State of A Grid-Controlled Switching Element: I*," Sov. Phys. Tech. Phys., **23**, 1301.
- Baksht, F.G., V.B. Kaplan, A.A. Koskin, A.M. Martsinovskii, F.N. Rasulov, N.N. Sveshnikova, V.I. Serbin, and V.G. Yur'ev (1978b), "*Stationary Conducting State of A Grid-Controlled Switching Element: II*," Sov. Phys. Tech. Phys., **23**, 1308.
- Baksht, F.G., G.A. Dyuzhev, A.M. Martsinovskii, B.Ya. Moyzhes, G.Ye. Pikus, E.B. Sonin, V.G. Yur'ev (1978c), *Thermionic Converters and Low-Temperature Plasmas*, English edition edited by L.K. Hansen, Rasor Associates, Inc., Published by Technical Information Center/U.S. Department of Energy.
- Booz-Allen & Hamilton, Inc. (1995), "*TOPAZ International Program: Lessons Learned in Technology Cooperation With Russia*," produced, designed, & researched under BMDO Contract #SDI1084-93-C-0010, Stephenson Printing, Springfield, VA.
- Burkes, T.R. (1987), "*A Critical Analysis and Assessment of High Power Switches: 1987*," Final Report for subcontract DAAK21-82-C-0011, submitted to Naval Surface Weapons Center, Dahlgren, VA 22448-5000.
- Chen, F.F. (1984), *Introduction to Plasma Physics and Controlled Fusion*, Plenum Press, New York, NY.
- Child, C.D. (1911), "*Discharge from Hot CaO*," Physical Review, **32**, 492.
- Cobine, J.D. (1958), *Gaseous Conductors: Theory and Engineering Applications*, Dover Publications, Inc., New York.
- Djachiachvili, I. and M.S. El-Genk (1994), "*Investigation of Triangular Aperture Grid for Plasma Switch Devices*," 21st International Power Modulation Symposium, June 28-30, Costa Mesa, CA, 1994.

- Dvornikov, V.D., S.T. Latushkin, V.A. Krestov, L.M. Tikhomirov, and L.I. Yudin (1972), "*Powerful Tacitrons and Certain of Their Characteristics in the Nanosecond Range*," (Translated from Priory I Tekhnika Eksperimenta, No. 4, 108), Plenum Publishing Corporation, New York, NY (1973).
- Dvornikov, V.D., S.T. Latushkin, L.I. Yudin, and V.M. Komarov (1974), "*A Pulse Generator Based on Tacitrons*," (Translated from Priory I Tekhnika Eksperimenta, No. 2, 107), Plenum Publishing Corporation, New York, NY (1975).
- El-Genk, M.S., C.S. Murray, and S. Chaudhuri of ISNPS; V. Kaibyshev, A. Borovskikh, I. Djachiachvili, and Y. Taldonov of KIAE (1991), "*Experimental Evaluation of Cs-Ba Thermionic Switch/Inverter -- Tacitron*," Proceedings of the IECEC, Boston, MA, 4-9 August.
- El-Genk, M.S., B. Wernsman, and J. Luke (1994), "*Recent Advances In Cs-Ba Tacitron Technology*," University of New Mexico, NM.
- Fry, T.C. (1921), "*The Thermionic Current Between Parallel Plane Electrodes: Velocities of Emission Distributed According to Maxwell's Law*," Physical Review, **17**, 441.
- Goldberg, S. & J. Rothstein (1961), "*Hydrogen Thyatrons*," Advance in Electronics and Electron Physics, **14**, Academic Press.
- Hatsopoulos, G.N. and E.P. Gyftopoulos (1973), *Thermionic Energy Conversion-Volume I: Processes and Devices*, MIT Press, Boston, MA.
- Henderson, B.W. (1992), "*Tacitron Research Upgrades Under Way*," Aviation Week and Space Technology, **136**, No. 20, p. 26.
- Hemenway, C.L. R.W. Henry, and M. Caulton (1962), *Physical Electronics*, John Wiley & Sons, Inc., New York.
- Hull, A.W. (1929), "*Hot-Emitter Thyatrons*," General Electric Review, **32**, 213.
- Johnson, E.O. (1951), "*Controllable Gas Diode*," Electronics, 107.
- Johnson, E.O. & W.M. Webster (1952), "*The Plasmatron, A Continuously Controllable Gas-Discharge Developmental Tube*," Proc. Inst. Rad. Eng., 645.
- Johnson, E.O., J. Olmstead, and W.M. Webster (1954), "*The Tacitron, A Low-Noise Thyatron Capable of Current Interruption by Grid Action*," Proc. Inst. Rad. Eng., 1350.

- Kaibyshev, V.Z., G.A. Kuzin, and M.V. Mel'nikov (1972), "*Use of the Thermionic Converter for Regulation of Current in Electric Circuits*," Sov. Phys. Tech. Phys., **17**, 1006.
- Kaibyshev, V.Z. and G.A. Kuzin (1975) "*Effect of a Third Electrode on a Low-Voltage Arc*," Sov. Phys. Tech. Phys., **20**, 203.
- Kaplan, V.B., A.N. Makarov, A.M. Martsinovskii, A.V. Novikov, V.I. Serbin, B.I. Tsirkel, and V.G. Yur'ev (1977a), "*Novel Low-Voltage High-Temperature Switching Element for DC-to-AC Conversion I: Effect of Grid on a Low-Voltage Cesium Arc*," Sov. Phys. Tech. Phys., **22**, 159.
- Kaplan, V.B., A.N. Makarov, A.M. Martsinovskii, A.V. Novikov, V.I. Serbin, B.I. Tsirkel, and V.G. Yur'ev (1977b), "*Novel Low-Voltage High-Temperature Switching Element for DC-to-AC Conversion II: Kinetics of the Quenching of the Discharge and Modulation in a Three-Electrode System*," Sov. Phys. Tech. Phys., **22**, 166.
- Kaplan, V.B., A.M. Martsinovskii, A.S. Mustafaev, V.I. Sitnov, A.Ya. Ender, and V.G. Yur'ev (1979), "*Spontaneous Current Cutoff in a High-Current Low Pressure Cesium-Barium Discharge*," Sov. Phys. Tech. Phys., **24**, 325.
- King, R.W. (1923), "*Thermionic Vacuum Tubes and Their Applications*," Bell System Technical Journal, **1**, 31.
- Langmuir, I. (1913), "*The Effect of Space Charge and Residual Gases on Thermionic Currents in High Vacuum*," Physical Review (2), **2**, 450.
- Luke, J.R. (1994), "*A Transient Model of a Cesium-Barium Diode*," Masters Thesis, Chemical & Nuclear Engineering Department of the University of New Mexico, Albuquerque, NM.
- Masten, G.B., I. Djachiachvili, D.B. Morris, and J.M. Gahl (1995a), "*Operating Characteristics of a High-Current Demountable Cs-Ba Tacitron*," 10th IEEE Pulsed Power Conference, Albuquerque, NM, 10-13 July, 1995.
- Masten, G.B., I. Djachiachvili, D.B. Morris, and J.M. Gahl (1995b), "*Preliminary Performance Results of a High-Current Cs-Ba Tacitron in a Simple Inverter*," 10th IEEE Pulsed Power Conference, Albuquerque, NM, 10-13 July, 1995.
- Murray, C.S. and M.S. El-Genk (1993), "*Experimental and Theoretical Studies of a High-Temperature Cesium-Barium Tacitron, with Application to Low Voltage-High Current Inversion*," Dissertation and Final Report No. UNM-ISBNPS-1-1994, Institute for Space & Nuclear Power Studies, University of New Mexico, NM.

ORION (1994), "*Development of High-Current Discharge Gas-Emission Additive Tacitron Power Conditioning Unit*," Task Area II of Subcontract S94-013, ORION International Technologies, Albuquerque, NM.

Pirrie, C.A., P.D. Culling, H. Menown, and N.S. Nicholls (1988), "*Performance of a Compact Four Gap Thyatron in a High Voltage Repetition Rate Circuit*," IEEE Power Modulation Symposium, Hilton Head Island, SC, 141.

PL/VTPP (1995), "*Space Power System Component Testing: High-Current Tacitron Characterization*," SubTask Statement 09/00, Contract #F29601-94-C-0139, Phillips Laboratory Space & Missiles Technology Directorate, Power and Thermal Management Division (PL/VTP), Kirtland AFB, NM.

Preece, W.H. (1885), "*On Peculiar Behavior of Glow-Lamps When Raised to High Incandescence*," Proc. Roy. Soc. (London), Ser. A, **38**, 219.

Prince, D.C. (1925), "*The Inverter*," General Electric Review, **28**, 676.

Sarjeant, W.J. and R.E. Dollinger (1989), *High-Power Electronics*, TAB Professional and Reference Books, Blue Ridge Summit, PA.

U.S. Congress (1986), "*Space Nuclear Power, Conversion, and Energy Storage for the Nineties and Beyond*," Hearings Before the Subcommittee on Energy Research and Production of the Committee on Science and Technology, U.S. House of Representatives, Ninety-Ninth Congress, First Session, Government Publications Office, Washington, D.C..

Wernsman, B. and M.S. El-Genk (1996), Private Communication on "Cs-Ba Tacitron: Effects of Control Grid Design on Tube Switching Performance," Final Draft Report of work sponsored by the Ballistic Missile Defense Organization, the U.S. Air Force Phillips Laboratory, and the Department of Energy's University Research Program under research contracts #F29601-C-91-0031 and #DEFG02-92ER75708, respectfully (*To be published as an U.S. Air Force Phillips Laboratory Technical Report*).

Wernsman, B. and M.S. El-Genk (1994), "*Operation Characteristics of a Planar Cs-Ba Tacitron*," *Review of Scientific Instruments*, April 1994.

## APPENDIX A - CESIUM AND BARIUM VAPOR PRESSURES IN THE RESERVOIR AND GAP

Throughout the text, only the Cs and Ba reservoir vapor pressures are given because these pressures can be directly obtained from known relationships based on the temperature at these locations. Those relationships of pressure to temperature are given. The relationship between the Cs vapor pressure and temperature is given by Hatsopoulos and Gyftopoulos (1973) as:

$$P_{Cs} = \frac{2.45 \cdot 10^8 \cdot \exp\left(-\frac{8910}{T_{Cs}}\right)}{\sqrt{T_{Cs}}} \quad (\text{A.1})$$

This is the vapor pressure in the reservoir. Because there is a temperature gradient between the reservoir and the interelectrode gap, the Cs pressure in the gap is not equal to the pressure in the reservoir. A correlation between the reservoir pressure and gap pressure can be obtained by using the flux leaving the reservoir and the flux entering the gap (assuming molecular flow). The flux relationship between gap and reservoir is:

$$\frac{1}{4} \cdot N_{gap} \cdot v_{gap} = \frac{1}{4} \cdot N_{Cs} \cdot v_{Cs} \quad (\text{A.2})$$

$$\frac{1}{4} \cdot N_{gap} \cdot \sqrt{\frac{8 \cdot k \cdot T_{gap}}{\pi \cdot M_i}} = \frac{1}{4} \cdot N_{Cs} \cdot \sqrt{\frac{8 \cdot k \cdot T_{Cs}}{\pi \cdot M_i}} \quad (\text{A.3})$$

where  $N$  is the particle density,  $v$  is the average particle velocity,  $k$  is Boltzmann's Constant, and  $M_i$  is the ion molecular weight. From the ideal gas law, the pressure is:

$$p = N \cdot k \cdot T \quad (\text{A.4})$$

Now, the densities in equation A.3 can be replaced by the pressures, obtaining:

$$P_{gap} = P_{Cs} \cdot \sqrt{\frac{T_{gap}}{T_{Cs}}} \quad (A.5)$$

This equation relates the pressure in the gap to the pressure in the reservoir, given the temperatures of the gap and reservoir. The temperature of the gap,  $T_{gap}$ , is taken as the average temperature between emitter and collector:

$$T_{gap} = \frac{1}{2} (T_E + T_C) \quad (A.6)$$

The Cs pressure in the gap and reservoir as a function of  $T_{Cs}$  are plotted in Figure A.1.

Similarly, the relationship for Ba reservoir pressure to Ba reservoir temperature is given as (Alcock et al. 1984):

$$\log(P_{Ba}) = \left( 12.405 - \frac{9690}{T_{Ba}} - 2.289 \cdot \log(T_{Ba}) \right) \quad (A.7)$$

Using equation A.5, the Ba pressure in the gap and reservoir as a function of  $T_{Ba}$  is obtained and illustrated in Figure A.2.

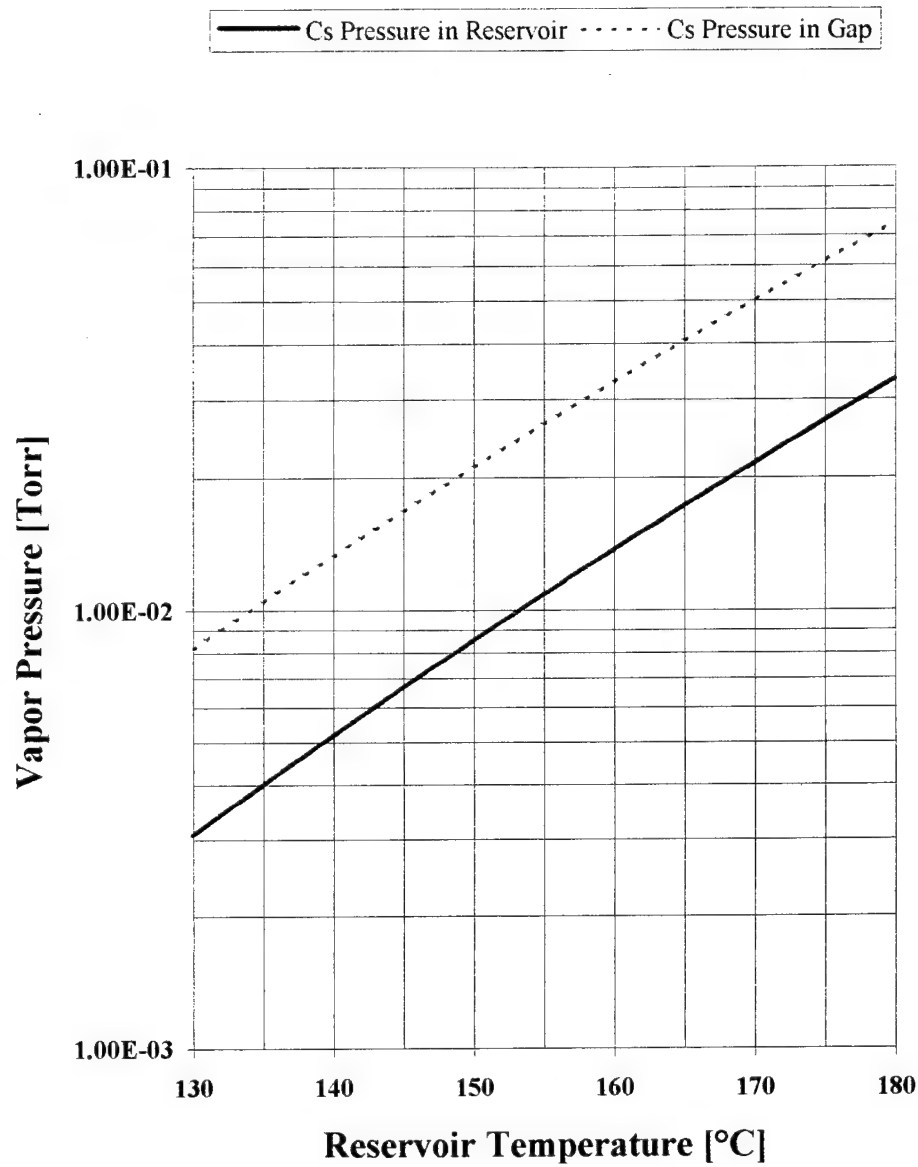


**Figure A.1.** Cs Pressure in the Reservoir and Interelectrode Gap with  $T_E = 1150$  °C,  $T_C = 675$  °C, and  $T_G \approx 913$  °C.

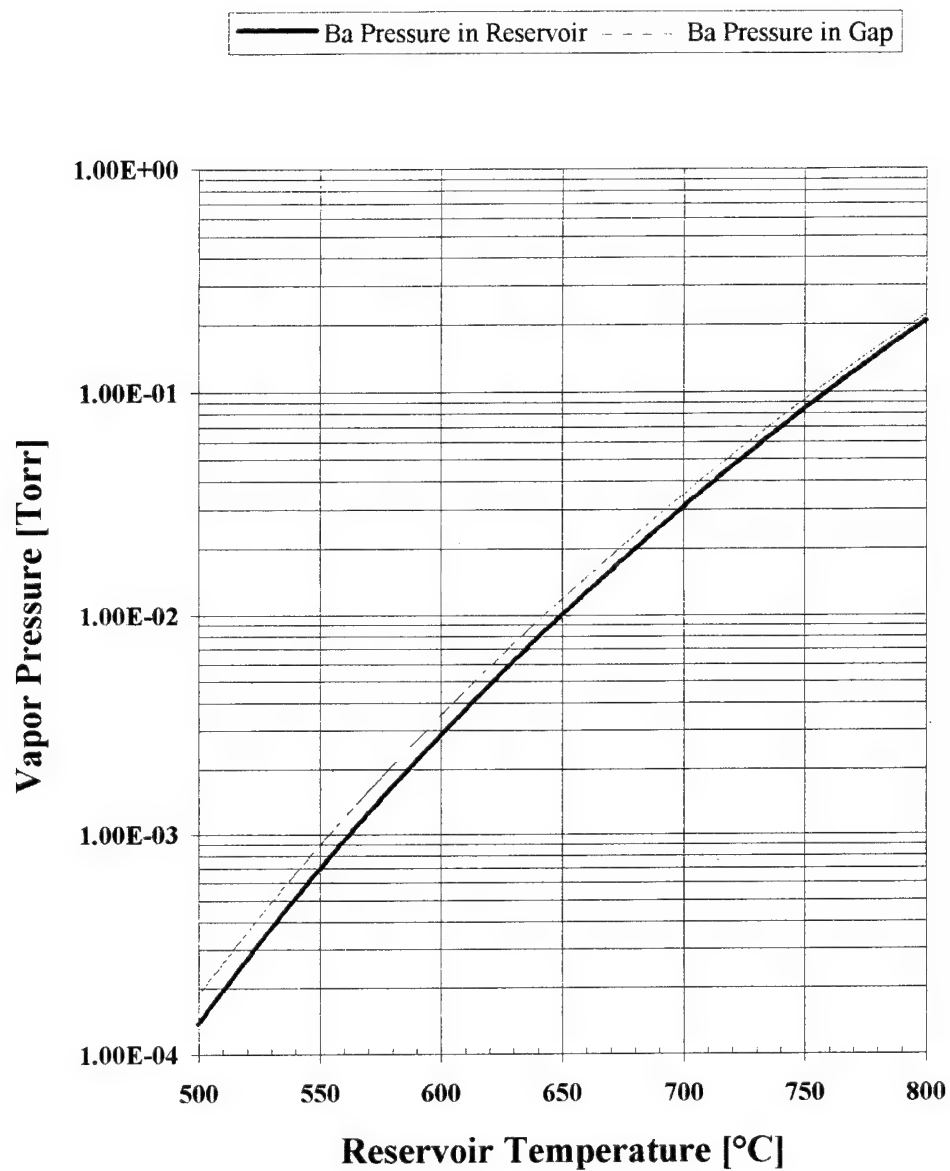


**Figure A.2.** Ba Pressure in the Reservoir and Interelectrode Gap with  $T_E = 1150$  °C,  $T_C = 675$  °C, and  $T_G \approx 913$  °C.

## APPENDIX B - APPROXIMATE TACITRON CIRCUIT DESIGN

### PARAMETERS\*

Parameter	Symbol	Value	
Forward breakdown voltage	$V_{(br)F}$	100-200 V	(Note 1)
Reverse breakdown voltage	$V_{(br)R}$		(Note 2)
On-state voltage	$V_F$	1 - 4 V	(Note 3)
On-state current	$I_F$	$\sim 10 \text{ A/cm}^2 \text{ max}$	(Note 4)
Holding current	$I_H$	$< 1 \text{ A/cm}^2$	(Note 5)
Gate trigger current	$I_{GT}$	$\sim 1.8 \text{ A/cm}^2 \text{ max}$	(Note 6)
Gate trigger voltage	$V_{GT}$	$\sim 10 - 50 \text{ V}$	(Note 6)
Gate turn-on time	$t_{on}$	$\sim 10 - 20 \mu\text{s}$	(Note 7)
Commutated turn-off time	$t_{off}$	$\sim 0.1 - 3.0 \mu\text{s}$	(Note 8)
Input capacitance	$C_{iss}$	$\sim 0.5 \text{ pF/cm}^2$	(Note 9)
Rise time	$t_r$	$\sim 15 - 40 \mu\text{s}$	(Note 10)
Fall time	$t_f$	$\sim 1 - 20 \mu\text{s}$	(Note 11)
Device dissipation	$P_D$	$\sim 20 \text{ W/cm}^2$	(Note 12)
Average grid dissipation	$P_G$	$\sim 2 \text{ W/cm}^2$	(Note 13)
Voltage rate-of-rise	$dv/dt$	$\sim 7.5 - 22 \text{ V}/\mu\text{s}$	
Current rate-of-rise	$di/dt$	$\sim 3 - 9 \text{ A}/\mu\text{s}$	
Max switching frequency	$f_T$	$> 20 \text{ kHz}$	(Note 14)

Note 1: Depends on the grid voltage. If the grid voltage is held to some negative voltage, a higher forward voltage can be applied between collector and emitter. The reported 200 V maximum is a limitation of the test rig. B. Wernsman estimates that the actual maximum hold-off is approximately 1 kV.

Note 2: Unknown, but since the collector does not emit appreciably in normal operation,  $V_{(br)R}$  should be greater than  $V_{(br)F}$ .

Note 3: This value is a function of grid transparency and thickness, and Cs pressure. The 1-V value is from a thin grid device the Soviets developed in the mid-1970s. The 4-V value is for fully grid-controlled modulation at frequencies of 15 - 20 kHz.

Note 4: Stable current modulation has been demonstrated at  $2.5 \text{ A/cm}^2$  with full grid control, and at  $5 \text{ A/cm}^2$  with grid control over ignition only (thyatron mode).

Note 5: Unknown, but like an SCR there will be a required minimum current (necessary to keep the discharge ionized). It is known that this minimum current is less than  $1 \text{ A/cm}^2$ .

---

\* This table comes from an internal memo from Dr. Gordon Masten, Chief Scientist of Tacitron research for the US Phillips Laboratory (PL/VTP) 1994-1995 and is based on the cylindrical & planar devices tested by ISNPS.

- Note 6: Minimum value is unknown. Since the grid is placed within one mean-free-path of the emitter, the grid intercepts approximately half the full emission current during ignition.
- Note 7: Depends on grid transparency and thickness, Cs pressure, and applied collector-emitter voltage.
- Note 8: Commutated turn-off time refers to external commutation. The tacitron will also have a grid turn-off time associated with a grid extinguishing pulse. The grid turn-off time is approximately the same as the commutated turn-off time.
- Note 9: This is an FET parameter. The tacitron will exhibit a small input capacitance due to the grid-emitter gap and the grid-collector gap. The  $0.5 \text{ pF/cm}^2$  is an estimate based on physical dimensions of the existing lab devices.
- Note 10: Rise time is dependent on cesium density and applied voltage at the beginning of the conduction cycle. The higher the applied voltage and the greater the gas density, the shorter the rise time.
- Note 11: Fall time is dependent on plasma density at the end of the conduction cycle. The lower the plasma density, the shorter the fall time. Plasma density can be depleted via large conduction currents or long conduction times.
- Note 12: For solid-state devices, this is normally given at an ambient temperature of  $20^\circ\text{C}$  and represents a device limitation. In the case of the tacitron, additional heating will probably be required to maintain the emitter at  $\sim 1100^\circ\text{C}$ .
- Note 13: The maximum grid dissipation will be a function of the temperature at which the grid begins to emit strongly enough to affect the hold-off voltage of the device (i.e., strongly dependent on grid design). This will also depend on the external cooling provided.
- Note 14: Limitations in the existing grid drive circuit prevent testing above about 20 kHz. However, the rise and fall times associated with thick-grid tacitron performance imply a maximum switching frequency of a few tens of kilohertz. It is known that the Soviets tested a thin-grid tacitron to 100 kHz in the mid 1970s, but it is expected that the thick-grid tacitron may have a lower frequency limit as a result of the differences in device extinguishing characteristics.

## APPENDIX C - TACITRON AND THYRATRON SWITCHING EFFICIENCIES

Wernsman and El-Genk (1995)\* have formulated an expression to estimate grid drive power requirements for a 2 cm<sup>2</sup> demountable planar tacitron based on the grid current provided by their laboratory grid trigger circuit, the modulation frequency, and the grid voltages used. The power switching efficiency for a two-switch tacitron inverter can be estimated by modifying this expression to account for the cross-sectional area of the tacitron, the emission current density, and the forward voltage drop:

$$\eta(\text{tacitron}) = 1 - \frac{2 \cdot P_{\text{loss}}}{P_{\text{switched}}} = 1 - \left( \frac{V_f}{V_{cc}} \right) - \frac{f_m}{10^6 \cdot (\text{sec}^{-1})} \cdot \frac{5.3 (A \cdot \text{cm}^{-2})}{J_c} \quad (\text{C.1})$$

where  $V_f$  is the conduction drop,  $V_{cc}$  is the collector bias,  $f_m$  is the modulation frequency,  $J_c$  is the conduction current density, and it is assumed that the magnitudes of the grid ignition and extinction pulses are equal to  $V_{cc}$ .

The constant factor of  $10^6 \text{ sec}^{-1}$  depends on the duration of the grid ignition and extinguishing pulses. Based on the approach used by Wernsman and El-Genk, the following expression has been derived for a Cs-Ba switch operating in thyatron mode:

$$\eta(\text{thyatron}) = 1 - \frac{2 \cdot P_{\text{loss}}}{P_{\text{switched}}} = 1 - \left( \frac{V_f}{V_{cc}} \right) - \frac{f_m}{10^7 \cdot (\text{sec}^{-1})} \cdot \frac{5.3 (A \cdot \text{cm}^{-2})}{J_c} \quad (\text{C.2})$$

---

\* Wernsman, B. and M.S. El-Genk (1995) "Effect of Grid Design on Cs-Ba Tacitron Operation and its Application to Space Nuclear Power Systems," 12th Symposium on Space Nuclear Power and Propulsion, Albuquerque, NM.

The principal difference between equations (C.1) and (C.2) is the constant factor in the denominator. The constant factor differs because the thyatron-mode switch does not require an extinguishing pulse, and its ignition pulse can be a fraction of the duration of the tacitron-mode switch (due to higher operating  $P_{Cs}$ ).

Cylindrical Cs-Ba tacitron conduction drop, (similar to that of the high-current Cs-Ba tacitron),  $V_f$  is estimated as

$$V_f = 3.97 \cdot 10^{-4} \cdot (T_{Cs})^2 - 0.362 \cdot T_{Cs} - 0.00218 \cdot T_E + 87.2 \quad (C.3)$$

where  $T_{Cs}$  is the cesium reservoir temperature in degrees K and  $T_E$  is the emitter temperature in degrees K. The Cs reservoir temperature governs the cesium gas pressure in the tacitron, and the emitter temperature governs thermionic emission current. This relationship is depicted in Figure C.1. The thyatron-mode operation results in significantly higher switching efficiencies than the tacitron-mode operation.

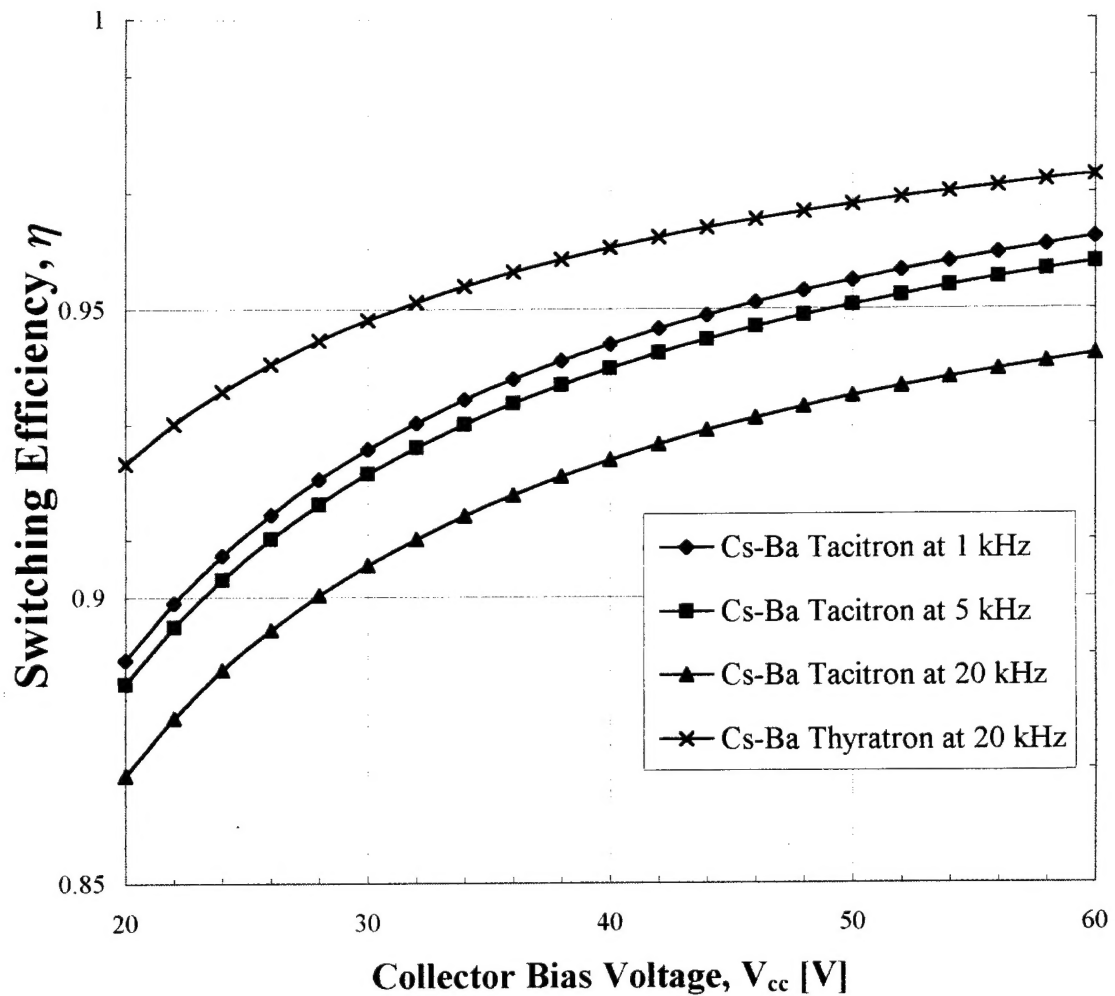


**Figure C.1. Switching Efficiency versus Collector Bias Voltage. Tacitron Operating Parameters are  $J_c = 5 \text{ A/cm}^2$ ,  $T_{Cs} = 140 \text{ }^\circ\text{C}$  ( $\sim 5 \text{ mTorr}$ ), and  $T_E = 1200 \text{ }^\circ\text{C}$ . Cs-Ba Thyatron Operating Parameters are the same, except  $T_{Cs} = 175 \text{ }^\circ\text{C}$  ( $\sim 27 \text{ mTorr}$ ).**